Invisible axion search methods

Pierre Sikivie[ORCID]

Department of Physics and Institute for Fundamental Theory, University of Florida, Gainesville, Florida 32611, USA

(published 18 February 2021)

In the late 1970s, the axion was proposed as a solution to the strong CP problem, i.e., the puzzle why the strong interactions conserve parity P and the product CP of charge conjugation and parity in spite of the fact that the standard model of elementary particles as a whole violates those symmetries. The original axion was soon ruled out by laboratory experiments and astrophysical considerations, but a new version was invented that is much more weakly coupled and that evades the laboratory and astrophysical constraints. It was named the "invisible" axion. However, the axion cannot be arbitrarily weakly coupled because it is overproduced in the early Universe by vacuum realignment in the limit of vanishing coupling. The axions produced by vacuum realignment are a form of cold dark matter today. The axion provides a solution then not only to the strong CP problem but also to the dark matter problem. Various methods have been proposed to search for dark matter axions and for axions emitted by the Sun. Their implementation and improvement has led to significant constraints on the notion of an invisible axion. Even purely laboratory methods may place significant constraints on invisible axions or axionlike particles. This review discusses the various methods that have been proposed and provides theoretical derivations of their signals.

CONTENTS

I. INTRODUCTION

During the 1970s, the standard model (SM) of elementary particles (Cheng and Li, 1984; Donoghue, Golowich, and Holstein, 2014) came to the fore as a correct description of all fundamental interactions other than gravity. It has proved since to be tremendously successful, explaining practically all relevant data in terms of a small number of parameters. Already in its early days, however, it was seen to present a puzzle: one would not expect within the SM that the strong interactions conserve parity P or the product CP of charge conjugation C with parity. The strong interactions and the electromagnetic interactions are observed to conserve P and CP. The weak interactions, on the other hand, violate P, C, and CP. The trouble with the SM is that the P and CP violation of the weak interactions produces P and CP violation in the strong interactions unless an unexpected cancellation occurs. This is commonly referred to as the strong CP problem.

The amount of P and CP violation in the strong interactions is controlled by a parameter, θ_{QCD}, which appears as the coefficient of a P and CP odd term in the action density

$$\mathcal{L}_{\text{SM}} = \cdots + \theta_{\text{QCD}} \frac{g_s^2}{32\pi^2} G_{\mu\nu}^a \tilde{G}^{a\mu\nu}, \quad (1)$$

where $G_{\mu\nu}^a$, $a = 1, 2, \ldots, 8$, are the field strengths of quantum chromodynamics (QCD), $\tilde{G}^{a\mu\nu} \equiv (1/2)\epsilon^{\mu\nu\alpha\beta}G_{\alpha\beta}^a$, and g_s is the QCD coupling constant. Unless otherwise stated, we use units[1] in which $\hbar = c = 1$ and conventions in which the Minkowski metric $(\eta_{\mu\nu}) = \text{diag}(+1,-1,-1,-1)$ and $\epsilon^{0123} = +1$. The dots represent all other terms in the SM action density, i.e., the terms that led to its numerous successes. Equation (1) shows the one term that is not a success. θ_{QCD} is an angle, i.e., it is cyclic with period 2π. QCD depends on θ_{QCD} because of the existence in that theory of quantum tunneling events ('t Hooft, 1976a; 't Hooft, 1976b), called "instantons," which violate P and CP if θ_{QCD} is not zero or π. Since in actuality the strong interactions obey P and CP, as well as can be observed, θ_{QCD} must be close to one of its CP conserving values. The best constraint derives from the experimental upper limit on the neutron electric dipole moment $|d_n| < 3 \times 10^{-26}$ e cm (90% C.L.) (Pendlebury et $al.$, 2015). For small θ_{QCD} the contribution of the term shown in Eq. (1) to the neutron electric dipole moment is of the order of (Baluni, 1979; Crewther et $al.$, 1979)

$$d_n \sim \theta_{\text{QCD}} \frac{m_u m_d}{m_u + m_d} \frac{1}{\Lambda_{\text{QCD}}} \frac{e}{m_n} \sim 3 \times 10^{-16}\theta_{\text{QCD}} \ e \ \text{cm}, \quad (2)$$

where m_u and m_d are the up and down quark masses, m_n is the neutron mass, and Λ_{QCD} is the QCD scale. θ_{QCD} should therefore be less than of the order of 10^{-10} (mod π). $\theta_{\text{QCD}} = 0$ or π is unexpected in the SM because P and CP are violated by the weak interactions. CP violation is introduced by giving apparently random phases to the Yukawa couplings that give rise to the quark masses. The overall phase of the quark mass matrix feeds into θ_{QCD}, which is therefore generically of the order of 1. The puzzle why θ_{QCD}, expected to be of the order of 1, is in fact less than 10^{-10} is the strong CP problem.

Soon after the strong CP problem was recognized, Peccei and Quinn (PQ) proposed a modification of the SM that offers a solution (Peccei and Quinn, 1977a, 1977b). They postulated a $U_{\text{PQ}}(1)$ symmetry that (1) is an exact symmetry of the classical action, (2) is spontaneously broken, and (3) has a color anomaly; i.e., it is explicitly broken by the nonperturbative QCD instanton effects that make physics depend on the value of θ_{QCD}. When this recipe is followed, the parameter θ_{QCD} is replaced by $a(x)/f_a$, where $a(x)$ is a dynamical pseudoscalar field and f_a is a quantity with dimension of energy, called the axion decay constant. f_a is of the order of the vacuum expectation value that spontaneously breaks $U_{\text{PQ}}(1)$ symmetry.[2] $a(x)$ is the associated Nambu-Goldstone boson. Weinberg and Wilczek (WW) pointed out that the nonperturbative instanton effects that make physics depend on θ_{QCD} introduce an effective potential for $a(x)$

(Weinberg, 1978; Wilczek, 1978). The minimum of this effective potential was later shown to be at $a(x) = 0$ (Vafa and Witten, 1984). The strong CP problem is solved after the $a(x)$ field settles there.

The PQ mechanism modifies the low energy effective theory of the SM with the addition of a light pseudoscalar particle, called the "axion," the quantum of the $a(x)$ field. The properties of the axion depend mainly on the value of the axion decay constant f_a; see Sec. II. The axion mass m_a and all its interaction strengths are inversely proportional to f_a. In the original PQWW model, f_a is of the order of the electroweak scale, implying an axion that is relatively strongly coupled and heavy, i.e., m_a of the order of 100 keV. The PQWW model was soon ruled out by a variety of laboratory experiments, including unsuccessful searches for axions in beam dumps and in rare particle decays such as $K^+ \to \pi^+ + a$ (Kim, 1987), and by stellar evolution constraints (Raffelt, 1990; Turner, 1990). The latter arise because stars emit the weakly coupled axions from their cores, whereas they emit photons only from their surfaces. If axions exist, stars have an additional energy loss mechanism, causing them to evolve faster. When the negative results from accelerator based axion searches are combined with the stellar evolution constraints, axion models with $f_a \lesssim 10^9$ GeV are generically ruled out.

Although the original PQWW model is untenable, the general idea of Peccei-Quinn symmetry and its concomitant axion are not. Kim and others showed that $U_{\text{PQ}}(1)$ need not be broken at the electroweak scale (Kim, 1979; Shifman, Vainshtein, and Zakharov, 1980; Zhitnitsky, 1980; Dine, Fischler, and Srednicki, 1981). It may be broken at an arbitrarily high energy, e.g., the hypothetical "grand unification scale" of 10^{15} GeV. When f_a is that large, the axion is light ($m_a \simeq 6 \times 10^{-9}$ eV for $f_a = 10^{15}$ GeV) and extremely weakly coupled: all axion production and interaction rates are suppressed by approximately 25 orders of magnitude relative to those of the PQWW axion. Thus was born the idea of the "invisible axion," a solution to the strong CP problem that conveniently avoids all constraints from laboratory searches and stellar evolution by making f_a arbitrarily large.

Fortunately, cosmology came to the rescue. Indeed, for $a(x)$ to relax to zero, the axion field oscillations must have commenced sufficiently early in the history of the Universe (today is too late), and for this the axion must be sufficiently heavy (Abbott and Sikivie, 1983; Dine and Fischler, 1983; Preskill, Wise, and Wilczek, 1983) since the oscillation period is $2\pi/m_a$. The finite age of the Universe implies a limit on how small m_a, or equivalently how large f_a, can be.

Unlike most other particles, relic axions are produced in the early Universe in two different populations, which we call "hot" and "cold." The hot axions are thermally produced in the primordial plasma. Like relic photons and neutrinos, they have a temperature of the order of a couple of kelvins today. Hot axions move too fast to gather in galactic halos and, for this reason, are not a good candidate for the dark matter observed in galactic halos and in clusters of galaxies. Like relic SM neutrinos they are a form of "hot dark matter." There is no known technique to detect hot relic axions in the laboratory.

The cold axion population is produced in the process of axion field relaxation, usually referred to as "vacuum

---

[1] appendix on units and conventions is included.

[2] The expression "decay constant" has a different meaning in nuclear physics than in particle physics. In nuclear physics, this term means what particle physicists refer to as "decay rate." Equation (202) gives the decay rate of the axion to two photons in terms of the axion mass and the axion decay constant.

realignment," mentioned in the paragraph previous to last. The vacuum realignment process is specific to Bose fields, such as axions or axionlike particles, that are both light and weakly coupled. The key point is that when the axion mass becomes larger than the inverse age of the Universe at that time, the axion field is not initially at the minimum of its effective potential (because it has no reason to be). It begins to oscillate then and, because the axion is very weakly coupled, these oscillations do not dissipate into other forms of energy. The energy density in relic axion field oscillations is a form of cold dark matter (Ipser and Sikivie, 1983). Indeed, among all the widely considered dark matter candidates, axions are the coldest.

As implied earlier, the cold axion cosmological energy density is an increasing function of f_a, and therefore a decreasing function of the axion mass. The axion mass for which, in the simplest scenarios, the cold axion density equals that of dark matter is of the order of 10^{-5} eV. There are, however, large uncertainties. The largest source of uncertainty is whether inflation homogenizes the axion field. If inflation takes place after the phase transition in which $U_{PQ}(1)$ is spontaneously broken, the value of $a(x)/f_a$ before the axion field oscillations begin, called the initial misalignment angle θ_{in}, is the same throughout the observable Universe (Pi, 1984). Because the cold axion cosmological energy density is proportional to θ_{in}^2 (for small θ_{in}), there is a 10% chance that the axion density is suppressed by a factor of the order of 10^{-2}, in which case the axion mass for which the axion density equals that of cold dark matter is approximately 100 times smaller, 10^{-7} instead of 10^{-5} eV. Likewise, there is a 1% chance that it is suppressed by a factor of 10^{-4}, with the cosmologically interesting axion mass most likely near 10^{-9} eV, etc. There are additional sources of uncertainty, including the contribution to the cold axion energy density from the decay of topological defects (axion strings and domain walls), the precise temperature dependence of the axion mass, and the amount of entropy produced during the QCD phase transition. Finally, we do not know what fraction of dark matter is axions if dark matter is composed of several species. These and other topics in axion cosmology were reviewed by Sikivie (2008) and Marsh (2016).

Various methods have been proposed to detect invisible axions. Most methods do not attempt to produce and detect axions but instead attempt to detect axions that are already in the laboratory either as dark matter or as particles emitted by the Sun. Indeed experiments that attempt to both produce and detect axions pay twice the price of very weak coupling and for this reason have extremely low event rates. On the other hand, such experiments make fewer assumptions and have better control over experimental variables. The goal of this review is to discuss the various methods that have been proposed and to provide theoretical derivations of their signal strengths. In a number of cases, noise and backgrounds are discussed as well. Previous reviews, with greater emphasis on experimental techniques, were given by Rosenberg and van Bibber (2000), Bradley et al. (2003), Asztalos et al. (2006), and Irastorza and Redondo (2018).

QCD axions are well motivated because they solve the strong CP problem and they are a good dark matter candidate. Their allowed mass range is $10^{-13} - 10^{-2}$ eV, where the lower bound is from the assumption that the scale of PQ symmetry breaking is smaller than the Planck scale and the upper bound is from stellar evolution arguments. For QCD axions there is a definite relationship between mass and interaction strength. They are proportional to each other. The residual model dependence is relatively small, except perhaps for the coupling of the axion to the electron. See Sec. II. QCD axions appear in many theories of physics beyond the SM, including supersymmetric extensions and string theory (Arias et al., 2012; Svrcek and Witten, 2006). In fact such theories often predict additional axionlike particles (ALPs), distinct from the QCD axion but with similar properties. We define an ALP as a light pseudoscalar particle with couplings to ordinary particles like those of the QCD axion but without an a priori relationship between coupling strength and mass. Many QCD axion search techniques are relevant to ALPs as well. In such cases it will be natural to include ALPs in the discussion. For definiteness, ALPs outside the allowed mass range of QCD axions ($10^{-13} - 10^{-2}$ eV) are not considered.

Finally, we mention that an argument has been made that the dark matter is axions, or ALPs, at least in part. The argument is based on the observation that cold dark matter axions thermalize through their gravitational self-interactions and, as a result, form a Bose-Einstein condensate (Sikivie and Yang, 2009). A thermalizing or rethermalizing Bose-Einstein condensate has properties different from ordinary cold dark matter (Erken et al., 2012), and it has been found that observations support the hypothesis that the dark matter is a rethermalizing Bose-Einstein condensate (Sikivie, 2011).

II. AXION PROPERTIES

This section provides basic information on axions, including formulas for the axion mass and for its couplings to ordinary particles, limits on axion properties from astrophysics and cosmology, an estimate of the flux of axions from the Sun, and two proposals for the local distribution of dark matter axions. Axion models were reviewed by Di Luzio et al. (2020).

A. Axion mass

In terms of the decay constant f_a, the axion mass is given by (Weinberg, 1978)

$$m_a \simeq \frac{\sqrt{m_u m_d}}{m_u + m_d} \frac{f_\pi m_\pi}{f_a} \simeq 6 \times 10^{-6} \text{ eV} \left(\frac{10^{12} \text{ GeV}}{f_a} \right), \quad (3)$$

where m_π is the pion mass and $f_\pi \simeq 93$ MeV is the pion decay constant.

Formulas for the axion couplings in the PQWW model were derived by Bardeen and Tye (1978), Donnelly et al. (1978), Ellis and Gaillard (1978), Goldman and Hoffman (1978), Kandaswamy, Salomonson, and Schechter (1978), Treiman and Wilczek (1978), and Weinberg (1978). The relevant formulas for the invisible axion models were originally given by Kim (1979), Shifman, Vainshtein, and Zakharov (1980), Zhitnitsky (1980), and Dine, Fischler, and Srednicki (1981). More general discussions of the axion couplings were given by Kaplan (1985), Srednicki (1985), and Sikivie (1986).

B. Electromagnetic coupling

The axion coupling to two photons is

$$\mathcal{L}_{a\gamma\gamma} = -g_\gamma \frac{\alpha}{\pi} \frac{1}{f_a} a(x) \vec{E}(x) \cdot \vec{B}(x), \qquad (4)$$

where α is the fine structure constant and

$$g_\gamma = \frac{1}{2}\left(\frac{N_e}{N} - \frac{5}{3} - \frac{m_d - m_u}{m_d + m_u}\right). \qquad (5)$$

N and N_e are, respectively, the color anomaly and electromagnetic anomaly of the PQ charge. They are given by

$$N\delta^{ab} = \mathrm{Tr}(Q_{\mathrm{PQ}} Q^a Q^b), \qquad N_e = \mathrm{Tr}(Q_{\mathrm{PQ}} Q_e Q_e), \quad (6)$$

where the trace symbol indicates a sum over all left-handed Weyl fermions in the model, Q_{PQ} is the PQ charge, Q^a ($a = 1, 2, \ldots, 8$) are the color charges, and Q_e is electric charge. In the original PQWW model and in the Dine-Fisher-Srednicki-Zhitnisky (DFSZ) invisible axion model, $N = 6$, $N_e = 16$, and therefore $g_\gamma \simeq 0.36$. In the Kim-Shifman-Vainshtein-Zakharov (KSVZ) invisible axion model, $N = 1$, $N_e = 0$, and therefore $g_\gamma \simeq -0.97$. In any grand unified model, $N/N_e = \sin^2\theta_W^0$, where θ_W^0 is the value of the electroweak angle at the grand unification scale. A favored value is $\sin^2\theta_W^0 = 3/8$ since this is consistent with the measured value of $\sin^2\theta_W$ at the electroweak scale (Georgi, Quinn, and Weinberg, 1974). For $N_e/N = 8/3$

$$g_\gamma = \frac{m_u}{m_u + m_d} \simeq 0.36, \qquad (7)$$

the same as in the PQWW and DFSZ models because these models are grand unifiable with $\sin^2\theta_W^0 = 3/8$. Because the axion mixes with the neutral pion, Eq. (5) has contributions both from the PQ charges of quarks and leptons and from the two photon coupling of the neutral pion. As a result g_γ can vanish only if there is a cancellation between unrelated contributions. The electromagnetic coupling is relevant to many approaches to invisible axion detection.

C. Coupling to nucleons and electrons

The coupling of the axion to a Dirac fermion $f(x)$ has the general form

$$\mathcal{L}_{a\bar{f}f} = \frac{1}{f_a}\left[-\frac{g_f}{2}\partial_\mu a(x)\bar{f}(x)\gamma^\mu\gamma^5 f(x) + \theta_f m_f a(x)\bar{f}(x)f(x)\right], \qquad (8)$$

where g_f are model dependent numbers that are generically of the order of 1, whereas θ_f are generically of the order of 10^{-17}, assuming that SM weak interactions are the only source of CP violation. The θ_f term would vanish if CP were conserved. The known CP violation of the weak interactions induces, through loop diagrams, small values for θ_{QCD} and for θ_f that are generically of the order of 10^{-17} (Ellis and Gaillard, 1979;

Georgi and Randall, 1986). In the nonrelativistic limit, Eq. (8) implies the interaction energy

$$H_{a\bar{f}f} = \frac{1}{f_a}\left[\frac{g_f}{2}\left(\vec{\sigma}\cdot\vec{\nabla}a(\vec{x},t) + \frac{\vec{p}\cdot\vec{\sigma}}{m_f}\partial_t a(\vec{x},t)\right) - \theta_f m_f a(\vec{x},t)\right], \qquad (9)$$

where $\vec{x}$, $\vec{p}$, m_f, and $(1/2)\vec{\sigma}$ are, respectively, the position, momentum, mass, and spin of the fermion. For axion searches, the most relevant fermions are the proton, the neutron, and the electron.

For nucleons ($f = p, n$), the coefficients g_f that appear in Eqs. (8) and (9) are given by

$$g_n^p = -\frac{1}{2}\left[\pm g_{A3}\left(\frac{m_d - m_u}{m_d + m_u} - \frac{g_u - g_d}{N}\right) + g_{A0}\left(1 - \frac{g_u + g_d}{N}\right)\right], \qquad (10)$$

where $g_{A3} = 1.25$ is the isotriplet axial vector coupling. The isosinglet axial vector coupling g_{A0} has not been measured directly. It was estimated by Adler et al. (1975) to be 0.74 using the quark model, and 0.65 using the MIT bag model. The g_u and g_d coefficients are related to the PQ charges of the up and down quarks in a way that depends on whether or not the PQ field spontaneously breaks SM gauge symmetries in addition to $U_{\mathrm{PQ}}(1)$. In the KSVZ model, $g_u = g_d = 0$. In the PQWW and DSVZ models,

$$g_u = \frac{v_2^2}{3(v_1^2 + v_2^2)}, \qquad g_d = \frac{v_1^2}{3(v_1^2 + v_2^2)}, \qquad (11)$$

where v_1 (v_2) is the vacuum expectation value of the Higgs field that gives mass to the up (down) quarks. Because the axion mixes with the neutral pion, g_p and g_n receive contributions from the pion-nucleon coupling as well as from the PQ charges of the up and down quarks. Each may vanish only if there is a fortuitous cancellation between unrelated contributions.

The coupling to the electron ($f = e$) is more model dependent than the others. In the PQWW and DFSZ models, $g_e = g_d$ given in Eq. (11). In the KSVZ model, $g_e = 0$ at tree level. However, a one loop correction yields a contribution of the order of $g_e \sim 10^{-3}$ (Srednicki, 1985).

D. Stellar evolution constraints

Stellar evolution arguments constrain the axion couplings. The two photon coupling causes axions to be produced in stellar cores by the Primakoff process, the conversion of a photon to an axion in the Coulomb field of a nucleus ($\gamma + N \to N + a$). The lifetime of horizontal branch stars in globular clusters implies the constraint (Raffelt, 2008)

$$g_{a\gamma\gamma} \equiv g_\gamma \frac{\alpha}{\pi} \frac{1}{f_a} < 10^{-10} \text{ GeV}^{-1}. \qquad (12)$$

The coupling to electrons causes stars to emit axions through the Compton-like process $\gamma + e^- \to e^- + a$ and through

axion bremsstrahlung $e^- + (Z, A) \rightarrow (Z, A) + e^- + a$. The resulting energy losses excessively delay the onset of helium burning in globular cluster stars unless (Raffelt and Weiss, 1995; Catelan, Freitas Pacheco, and Horvath, 1996)

$$g_{a\bar{e}e} \equiv \frac{g_e}{f_a} < 5 \times 10^{-10} \text{ GeV}^{-1}. \tag{13}$$

The increase in the cooling rate of white dwarfs resulting from these processes produces a similar bound (Raffelt, 1986; Blinnikov and Dunina-Barkovskaya, 1994). The coupling to nucleons causes axions to be radiated by the collapsed stellar core produced in a supernova explosion. The requirement that the observed neutrino pulse from SN1987a not be quenched by axion emission implies that (Ellis and Olive, 1987; Raffelt and Seckel, 1988; Turner, 1988; Raffelt, 2008).

$$f_a > 4 \times 10^8 \text{ GeV} \tag{14}$$

or $m_a < 1.6 \times 10^{-2}$ eV.

Extremely light axions ($6 \times 10^{-13} < m_a < 2 \times 10^{-11}$ eV) are constrained by stellar mass black hole superradiance, as discussed by Arvanitaki *et al.* (2010), Arvanitaki and Dubovsky (2011), and Arvanitaki, Baryakhtar, and Huang (2015).

Updates on the bounds of Eqs. (12) and (13) were given by Viaux *et al.* (2013) and Ayala *et al.* (2014).

E. Solar axion flux

The solar axion flux on Earth was calculated by Raffelt (2008) as

$$\frac{d\Phi_a}{dE} = \frac{6.0 \times 10^{10}}{\text{cm}^2 \text{ s keV}} \left(\frac{g_{a\gamma\gamma}}{10^{-10} \text{ GeV}^{-1}} \right)^2 \left(\frac{E}{\text{keV}} \right)^{2.481}$$
$$\times \exp \left(-\frac{E}{1.205 \text{ keV}} \right). \tag{15}$$

The integrated flux is

$$\Phi_a = \frac{3.75 \times 10^{11}}{\text{cm}^2 \text{ s}} \left(\frac{g_{a\gamma\gamma}}{10^{-10} \text{ GeV}^{-1}} \right)^2. \tag{16}$$

The energy spectrum in Eq. (15) is nearly isothermal with a temperature that of the solar core, approximately 1.3 keV. Equation (15) includes only solar axions produced by the Primakoff process. There may be additional axions from processes involving the electron coupling (Redondo, 2013). In addition, axions with specific energies are emitted in nuclear deexcitations in the solar core (Avignone *et al.*, 2018).

F. Cold axion cosmological energy density

The present cosmological energy density in cold axions, as a fraction of the critical energy density, may be written

$$\Omega_a \equiv \rho_a \frac{8\pi G}{3H_0^2} = 0.3 X \left(\frac{f_a}{10^{12} \text{ GeV}} \right)^{7/6}, \tag{17}$$

where X is a poorly known fudge factor reflecting cosmological uncertainties. According to the discussion given by Sikivie (2008), X is of the order of 2 if the axion field does not get homogenized by inflation and the string decay contribution is of the same order of magnitude as that from vacuum realignment. If the string decay contribution dominates, X may be as large as 10. If inflation homogenizes the axion field, X is of the order of $(1/2)\theta_{\text{in}}^2$, where θ_{in} is the initial misalignment angle. Lattice QCD simulations may help remove uncertainties associated with the dependence of the axion mass on temperature. For a discussion and list of references see Dine *et al.* (2017).

G. Galactic halo models

When discussing axion dark matter detection, we consider two contrasting proposals for the local density and velocity distribution of dark matter axions. Proposal A assumes that galactic halos are in thermal equilibrium. By fitting the isothermal model to the Milky Way rotation curve, one finds that (Turner, 1986)

$$\rho_{\text{dm}} \simeq 300 \text{ MeV/cm}^3 \tag{18}$$

for the local dark matter density. The velocity distribution is a Maxwell-Boltzmann one with dispersion $\sqrt{\langle \vec{v} \cdot \vec{v} \rangle} \simeq 270$ km/s at any location in the halo.

Proposal B is based on the observation that dark matter particles accreting onto a galactic halo do not, as a result of their gravitational interactions, thermalize over the age of the Universe (Sikivie and Ipser, 1992). A galactic halo is then a set of overlapping cold flows with sharp features, called "caustics," in the physical density. The caustic ring model (Duffy and Sikivie, 2008) is a particular realization motivated by observation. According to the model, we on Earth are located close to a caustic. As a result our local dark matter velocity distribution is dominated by the flows that form this caustic. Most prominent among these is the "big flow" (Sikivie, 2003). It has velocity vector (Duffy and Sikivie, 2008; Chakrabarty *et al.*, 2020)

$$\vec{v}_{\text{BF}} \simeq [509\hat{\phi} - 104\hat{r} + 6\hat{z}] \text{ km/s} \tag{19}$$

in a nonrotating galactic reference frame. $\hat{\phi}$ is the unit vector in the direction of galactic rotation, $\hat{r}$ in the direction away from the Galactic Center, and $\hat{z}$ in the direction of the north galactic pole. The big flow has velocity dispersion less than 71 m/s (Banik and Sikivie, 2016). The uncertainty in the speed (520 km/s) of the big flow is of the order of 9%. It is due mainly to the uncertainty in the galactic rotation velocity. The uncertainty in its direction is of the order of 1°. The density of the big flow on Earth depends sharply on our distance to a cusp in the nearby caustic and is poorly constrained for this reason. According to Chakrabarty *et al.* (2020), it is at least 6 GeV/cm³.

III. AXION TO PHOTON CONVERSION IN A MAGNETIC FIELD

This section discusses the conversion of axions to photons in a static magnetic field in the absence of cavity or reflecting walls for the photons (Sikivie, 1983, 1985; Anselm, 1985; Maiani, Petronzio, and Zavattini, 1986; Van Bibber *et al.*, 1987; Raffelt and Stodolsky, 1988; van Bibber *et al.*, 1989). We allow the presence of a homogeneous and static dielectric constant ϵ and magnetic susceptibility μ.

A. Axion electrodynamics

Consider the action density for the electromagnetic and axion fields:

$$\mathcal{L}_{\text{e.m.}+a} = \frac{1}{2}\left(\epsilon \vec{E}\cdot\vec{E} - \frac{1}{\mu}\vec{B}\cdot\vec{B}\right) - \rho_{\text{el}}\Phi + \vec{j}_{\text{el}}\cdot\vec{A}$$
$$+ \frac{1}{2}[(\partial_t a)^2 - (\vec{\nabla}a)^2] - \frac{1}{2}m_a^2 a^2 - ga\vec{E}\cdot\vec{B}, \quad (20)$$

where $\vec{E} = -\vec{\nabla}\Phi - \partial_t\vec{A}$, $\vec{B} = \vec{\nabla}\times\vec{A}$, and $g \equiv g_{a\gamma\gamma} = g_\gamma(\alpha/\pi)(1/f_a)$. ρ_{el} and $\vec{j}_{\text{el}}$ are the charge and current densities due to ordinary charged particles. Equation (20) implies the modified Maxwell's equations (Sikivie, 1983, 1984)

$$\vec{\nabla}\cdot(\epsilon\vec{E} - ga\vec{B}) = \rho_{\text{el}},$$
$$\vec{\nabla}\times\left(\frac{1}{\mu}\vec{B} + ga\vec{E}\right) - \partial_t(\epsilon\vec{E} - ga\vec{B}) = \vec{j}_{\text{el}},$$
$$\vec{\nabla}\times\vec{E} + \partial_t\vec{B} = 0,$$
$$\vec{\nabla}\cdot\vec{B} = 0, \quad (21)$$

and

$$\partial_t^2 a - \nabla^2 a + m_a^2 a = -g\vec{E}\cdot\vec{B}. \quad (22)$$

The set of equations (21) and (22) are referred to as "axion electrodynamics."

The first two equations (21) may be rewritten as

$$\vec{\nabla}\cdot(\epsilon\vec{E}) = g\vec{B}\cdot\vec{\nabla}a + \rho_{\text{el}},$$
$$\vec{\nabla}\times\left(\frac{1}{\mu}\vec{B}\right) - \partial_t(\epsilon\vec{E}) = g(\vec{E}\times\vec{\nabla}a - \vec{B}\partial_t a) + \vec{j}_{\text{el}}, \quad (23)$$

showing that in background magnetic $\vec{B}_0(\vec{x},t)$ and electric $\vec{E}_0(\vec{x},t)$ fields the axion is a source of electric charge and current density

$$\rho_a = g\vec{B}_0\cdot\vec{\nabla}a, \qquad \vec{j}_a = g(\vec{E}_0\times\vec{\nabla}a - \vec{B}_0\partial_t a). \quad (24)$$

In covariant form, $j_a^\mu = -g\tilde{F}^{\mu\nu}\partial_\nu a$. The axion induced electric current is separately conserved: $\partial_\mu j_a^\mu \equiv 0$.

j_a^μ is a source of electromagnetic waves, implying the conversion of energy from the axion to the electromagnetic field. For practical reasons, it is magnetic rather than electric fields that are used to cause the conversion. Hence, for

simplicity, we set $\vec{E}_0 = 0$ in the following. We assume furthermore that $\vec{B}_0$ is static and, henceforth in this section, that ϵ and μ are constant in space and time.

We set $\rho_{\text{el}} = \vec{j}_{\text{el}} = 0$ and consider an axion plane wave

$$a(\vec{x},t) = \text{Re}(Ae^{i(\vec{k}_a\cdot\vec{x}-\omega t)}), \quad (25)$$

where $\omega = \sqrt{m_a^2 + \vec{k}\cdot\vec{k}}$. We choose the gauge $\epsilon\mu\partial_t\Phi + \vec{\nabla}\cdot\vec{A} = 0$. The inhomogeneous Maxwell's equations are then

$$(-\nabla^2 + \epsilon\mu\partial_t^2)\Phi = \frac{1}{\epsilon}\rho_a,$$
$$(-\nabla^2 + \epsilon\mu\partial_t^2)\vec{A} = \mu\vec{j}_a. \quad (26)$$

Provided that the first equation is satisfied at an initial time, it is satisfied at all times as a consequence of the second equation. The second equation is solved by $\vec{A}(\vec{x},t) = \text{Re}[\vec{A}(\vec{x})e^{-i\omega t}]$ provided that

$$(-\nabla^2 - \epsilon\mu\omega^2)\vec{A}(\vec{x}) = \mu\vec{j}_a(\vec{x}), \quad (27)$$

where

$$\vec{j}_a(\vec{x}) = ig\omega A\vec{B}_0(\vec{x})e^{i\vec{k}_a\cdot\vec{x}}. \quad (28)$$

The solution of interest, involving the retarded Green's function, is

$$\vec{A}(\vec{x}) = \frac{\mu}{4\pi}\int_V d^3x' \frac{e^{ik|\vec{x}-\vec{x}'|}}{|\vec{x}-\vec{x}'|}\vec{j}_a(\vec{x}'), \quad (29)$$

with $k = \sqrt{\epsilon\mu}\omega$. V is the volume of the region over which the magnetic field extends. Let $\vec{x} = r\hat{n}$, and let $r \to \infty$. In that limit

$$\vec{A}(\vec{x}) = \mu\frac{e^{ikr}}{4\pi r}\vec{j}_a(\vec{k}) + O\left(\frac{1}{r^2}\right), \quad (30)$$

where $\vec{k} = k\hat{n}$ and

$$\vec{j}_a(\vec{k}) = \int_V d^3x e^{-i\vec{k}\cdot\vec{x}}\vec{j}_a(\vec{x}) = i\omega gA\int_V d^3x e^{i(\vec{k}_a-\vec{k})\cdot\vec{x}}\vec{B}_0(\vec{x}). \quad (31)$$

The electromagnetic power radiated per unit solid angle in direction $\hat{n}$ is

$$\frac{dP}{d\Omega} = \lim_{r\to\infty}\langle\hat{n}\cdot(\vec{E}\times\vec{H})\rangle r^2 = \frac{\mu k\omega}{32\pi^2}|\hat{n}\times\vec{j}_a(\vec{k})|^2. \quad (32)$$

The $\langle\ldots\rangle$ brackets indicate that a time average is being taken.

We derived Eq. (32) using a classical field theory calculation but the actual world is quantum mechanical. Whereas the conversion of axion field energy to electromagnetic field energy happens continuously in the classical description, in

reality it happens one quantum at a time. Because the magnetic field is static, the energy of each photon produced is exactly the energy of the axion that disappeared. Equation (32) gives the time-averaged power for the quantum process of axion to photon conversion.

B. Conversion cross section

Dividing by the magnitude of the incident axion energy flux

$$\vec{\mathcal{P}}_a = \langle -\dot{a}\,\vec{\nabla}\,a \rangle = \tfrac{1}{2}|A|^2\omega\vec{k}_a, \tag{33}$$

we obtain the differential cross section (Sikivie, 1983):

$$\frac{d\sigma}{d\Omega}(a \to \gamma) = \frac{1}{|\vec{\mathcal{P}}_a|}\frac{dP}{d\Omega}$$
$$= g^2\frac{\mu k\omega}{16\pi^2\beta_a}\left|\int_V d^3x\, e^{i(\vec{k}_a-\vec{k})\cdot\vec{x}}\hat{n}\times\vec{B}_0(\vec{x})\right|^2, \tag{34}$$

where $\beta_a = |\vec{k}_a|/\omega$ is the speed of the incident axions. We may rewrite the rhs of Eq. (34) as a sum over final state photon polarizations $\hat{e}_1(\hat{n})$ and $\hat{e}_2(\hat{n})$, using the completeness relation

$$\delta_{ij} = n_i n_j + e_{1i}e_{1j} + e_{2i}e_{2j}. \tag{35}$$

In that form

$$\frac{d\sigma}{d\Omega}(a\to\gamma) = g^2\frac{\mu k\omega}{16\pi^2\beta_a}\sum_{\lambda=1,2}\left|\int_V d^3x\, e^{i(\vec{k}_a-\vec{k})\cdot\vec{x}}\hat{e}_\lambda(\hat{n})\cdot\vec{B}_0(\vec{x})\right|^2. \tag{36}$$

Because the axion and photon have equal energy but satisfy different dispersion relations, their momenta differ in general. The momentum transfer $\vec{q} \equiv \vec{k} - \vec{k}_a$ is provided by the inhomogeneity of the magnetic field. The conversion cross section is proportional to the power in the Fourier component of $\vec{B}_0(\vec{x})$ with wave vector $\vec{q}$. An analogous calculation, starting with Eq. (22), yields the following differential cross section for the inverse process, the conversion in a static magnetic field of a photon with 4-momentum $(p^\mu_\gamma) = (\omega, \vec{k})$ to an axion with 4-momentum $(p^\mu_a) = (E_a, \vec{k}_a)$:

$$\frac{d\sigma}{d\Omega}(\gamma\to a) = g^2\frac{\omega k_a}{16\pi^2}\sqrt{\frac{\mu}{\epsilon}}\left|\int_V d^3x\, e^{i(\vec{k}-\vec{k}_a)\cdot\vec{x}}\hat{\imath}\cdot\vec{B}_0(\vec{x})\right|^2, \tag{37}$$

where $\hat{\imath}$ is the polarization vector of the initial photon.

C. Colinear conversion

Consider the particular case where the magnetic field is smooth on a length scale λ_B, much larger than k_a^{-1} and k^{-1}. The conversion process is colinear then since $|\vec{q}| = |\vec{k} - \vec{k}_a| \sim \lambda_B^{-1} \ll k_a, k$. Let z be the position coordinate along the path of the axion and photon. The conversion probability depends only on the magnetic field along the path. To calculate it, we may take $\vec{B}_0$ to be independent of the coordinates orthogonal to z over a cross-sectional area S. Since $\hat{n} = \hat{z}$ in this case

$$\left|\int_V d^3x\, e^{-i\vec{q}\cdot\vec{x}}\hat{n}\times\vec{B}_0(\vec{x})\right|^2$$
$$= (2\pi)^2\delta^2(\vec{q}_\perp)S\left|\int_0^L dz\, e^{-iqz}\vec{B}_{0\perp}(z)\right|^2, \tag{38}$$

where L is the depth over which the magnetic field extends, the subscript $\perp$ indicates the component perpendicular to the direction of propagation, and

$$q = k - k_a = \sqrt{\epsilon\mu}\omega - \sqrt{\omega^2 - m_a^2}. \tag{39}$$

The conversion probability is

$$p(a\to\gamma) = \frac{1}{S}\int d\Omega_{\vec{k}}\frac{d\sigma}{d\Omega_{\vec{k}}} = \frac{g^2}{4\beta_a}\sqrt{\frac{\mu}{\epsilon}}\left|\int_0^L dz\, e^{-iqz}\vec{B}_{0\perp}(z)\right|^2. \tag{40}$$

The produced photon is linearly polarized in the direction of $\vec{B}_{0\perp}(z)$ in case $\vec{B}_{0\perp}(z)$ has the same direction everywhere. Similarly, from Eq. (37) we find the conversion probability of a photon to an axion

$$p(\gamma\to a) = \frac{g^2}{4\beta_a}\sqrt{\frac{\mu}{\epsilon}}\left|\int_0^L dz\, e^{+iqz}\hat{\imath}\cdot\vec{B}_0(z)\right|^2. \tag{41}$$

For a given polarization state of the photon, $p(a\to\gamma)$ and $p(\gamma\to a)$ are equal, as required by the principle of detailed balance.

For $\vec{B}_0 = \hat{\imath}B_0\cos[(2\pi/d)z]$ with $\hat{\imath}\cdot\hat{z} = 0$, we have

$$p = \frac{g^2B_0^2}{4\beta_a}\sqrt{\frac{\mu}{\epsilon}}\left|\frac{\sin[(q+2\pi/d)L/2]}{q+2\pi/d}\right.$$
$$\left.+ e^{2i\pi(L/2)}\frac{\sin[(q-2\pi/d)L/2]}{q-2\pi/d}\right|^2. \tag{42}$$

The conversion is resonant when $q = \pm 2\pi/d$, with probability

$$p = \frac{g^2B_0^2L^2}{16\beta_a}\sqrt{\frac{\mu}{\epsilon}}, \tag{43}$$

assuming that $d \ll L$.

If the magnetic field is homogeneous

$$p = \frac{g^2B_0^2}{\beta_a}\sqrt{\frac{\mu}{\epsilon}}\sin^2\left(\frac{qL}{2}\right)\frac{1}{q^2}. \tag{44}$$

The axion and photon oscillate into each other, with oscillation length $\ell_{\rm osc} = \pi/q$. After a distance $\ell_{\rm osc}$, a fraction $(g^2B_0^2/\beta_a q^2)\sqrt{\mu/\epsilon}$ of the axions have converted to photons; after a distance $2\ell_{\rm osc}$, those photons have converted back to axions, etc. This is similar to neutrino flavor oscillations. In fact, the conversion probability can be derived (Maiani, Petronzio, and Zavattini, 1986; Raffelt and Stodolsky, 1988) using this analogy; see Sec. IX.

In a homogeneous magnetic field, the conversion is resonant when $q \ll 1/L$. In that case

$$p = \frac{g^2}{4\beta_a} \sqrt{\frac{\mu}{\epsilon}} B_0^2 L^2. \qquad (45)$$

The L^2 behavior of the conversion probability in Eqs. (43) and (45), characteristic of resonant conversion, persists only as long as coherence between the axion and photon excitations is maintained. Various effects may limit this coherence, such as the absorption or scattering of the photon out of the path of the axion. If coherence persists up to a distance $\ell < L$, L^2 should be replaced by $L\ell$.

To convert Eq. (45) into practical units, we note that the energy stored in a volume V permeated by a magnetic field B_0 is

$$E = \tfrac{1}{2} V B_0^2 \qquad (46)$$

in the Heaviside-Lorentz units used here, whereas in Gaussian units

$$E = \frac{1}{8\pi} \text{erg} \left(\frac{V}{\text{cm}^3} \right) \left(\frac{B_0}{\text{G}} \right)^2. \qquad (47)$$

The implied conversion factor is

$$\text{gauss} = \sqrt{\frac{\text{erg}}{4\pi \ \text{cm}^3}} = 1.9535 \times 10^{-2} \ \text{eV}^2. \qquad (48)$$

Equation (45) then becomes

$$p = 1.71 \times 10^{-17} \left(\frac{g_\gamma}{0.36} \right)^2 \left(\frac{10^7 \ \text{GeV}}{f_a} \right)^2$$
$$\times \left(\frac{B_0}{10 \ \text{T}} \right)^2 \left(\frac{L}{10 \ \text{m}} \right)^2 \frac{1}{\beta_a} \sqrt{\frac{\mu}{\epsilon}}. \qquad (49)$$

When $\omega \gg m_a$,

$$q \simeq (\sqrt{\epsilon\mu} - 1)\omega + \frac{m_a^2}{2\omega}. \qquad (50)$$

The resonance condition $qL < 1$ can be satisfied even for large L by using a dielectric medium with a plasmalike dispersion law (van Bibber et al., 1989)

$$\epsilon(\omega) = 1 - \frac{\omega_{\text{pl}}^2}{\omega^2}. \qquad (51)$$

For $\mu = 1$, resonance is obtained when $\omega_{\text{pl}} = m_a$.

Flambaum et al. (2018) proposed to replace axion-photon conversion in a magnetic field with axion-photon conversion through resonant forward scattering on atoms or molecules.

D. Applications

Axion to photon conversion in a magnetic field was originally proposed as a method to detect dark matter axions and axions emitted by the Sun (Sikivie, 1983). These applications are discussed in Secs. V.A and VI.A, respectively. Other applications are "shining light through walls" and the conversion of axions to photons in astrophysical magnetic fields.

In a shining light through walls experiment, photons are converted to axions in a magnetic field on one side of a wall and the axions are converted back to photons in a magnetic field on the other side of that wall (Van Bibber et al., 1987). The sensitivity of the experiment can be improved by introducing matched Fabry-Perot cavities in the two conversion regions, producing a resonance (Hoogeveen and Ziegenhagen, 1991; Fukuda et al., 1996; Sikivie, Tanner, and van Bibber, 2007). Shining light through walls with resonant axion-photon reconversion is discussed in Sec. VIII.

Axion-photon conversion can occur in astrophysical magnetic fields and may have implications for observation. Axions can readily convert to photons, and vice versa, in the magnetospheres of neutron stars (Morris, 1986; Hook et al., 2018; Huang et al., 2018). With $B_0 = 10^{13}$ G and $L = 10$ km, the conversion probability is of the order of 1 for f_a up to 10^{10} GeV provided that $q \simeq 0$. The latter condition is satisfied if the axions are sufficiently energetic. For example, if the axion energy is 1 keV and the axion mass is 10^{-4} eV, the oscillation length is $2\pi\omega/m_a^2 = 126$ km. The neutron star may therefore convert axions produced in its core or axions emitted by a companion star. It may also convert dark matter axions in regions of its magnetosphere where the resonance condition is satisfied because the plasma frequency is near the axion mass.

The magnetic fields in galaxies and galaxy clusters are weak, of the order of 10^{-6} G, but extend over enormous distances. With $B_0 = 10^{-6}$ G and $L = 1$ Mpc the conversion probablity is of the order of 1 for g larger than 10^{-12} GeV^{-1} provided that $qL < 1$. The latter condition cannot easily be satisfied by QCD axions since they are massive but may be satisfied by light ALPs. Conceivable phenomena involving the conversion of Nambu-Goldstone bosons or ALPs into photons, or vice versa, in large scale astrophysical magnetic fields include the production of high-energy gamma rays (Sikivie, 1988), distortions of the cosmic microwave background spectrum (Harari and Sikivie, 1992), and alterations in the apparent luminosity of faraway sources (Csaki, Kaloper, and Terning, 2002).

Brockway, Carlson, and Raffelt (1996), Grifols, Masso, and Toldra (1996), and Payez et al. (2015) placed a limit on light ALPs from the nonobservation of gamma ray photons from the direction of SN1987a coincident with that supernova's neutrino signal. ALPs are emitted by the Primakoff process in the supernova core and convert to photons in the magnetic field of the Milky Way. A recent published limit was $g < 5.3 \times 10^{-12}$ GeV^{-1} for $m < 4.4 \times 10^{-10}$ eV (Payez et al., 2015).

It has been proposed that the apparently excessive transparency of the Universe to high-energy gamma rays is due to the existence of ALPs (De Angelis, Roncadelli, and Mansutti, 2007; De Angelis, Mansutti, and Roncadelli, 2008; Sanchez-Conde et al., 2009; Horns et al., 2012). High-energy gamma rays above approximately 100 GeV are absorbed over cosmological distances because they produce e^+e^- pairs by colliding with extragalactic background photons. Observations show the Universe to be more transparent than expected. The proposed

explanation is that the high-energy photons convert to ALPs in astrophysical magnetic fields and that the ALPs, after traveling unimpeded over great distances, convert back to high-energy photons by the inverse process.

Conlon *et al.* (2017) provided a guide to the literature of axion-photon conversion in astrophysical magnetic fields and placed an upper limit $g \lesssim 2 \times 10^{-12}$ GeV^{-1} on ALPs of mass $m \lesssim 10^{-12}$ eV from the nonobservation of spectral modulations of x rays from chosen active galactic nuclei, caused by the conversion of the x rays to ALPs in the magnetic fields of foreground galaxy clusters.

IV. THE CAVITY HALOSCOPE

The dark halo of our Milky Way Galaxy has density of the order of 10^{-24} g/cm^3 in the solar neighborhood. The halo particles have velocities v of the order of $10^{-3}c$. If the dark matter is axions, we are surrounded by a pseudoscalar field oscillating with angular frequency

$$\omega_a = E_a = m_a + \tfrac{1}{2}m_a v^2 = m_a[1 + \mathcal{O}(10^{-6})]. \quad (52)$$

In an externally applied magnetic field $\vec{B}_0$, the axion electromagnetic interaction (4) becomes

$$\mathcal{L}_{a\gamma\gamma} = -g_\gamma \frac{\alpha}{\pi} \frac{1}{f_a} a\vec{E} \cdot \vec{B}_0. \quad (53)$$

Equation (53) allows the conversion of axions to photons, and vice versa, as discussed in Sec. III. In the case of dark matter axions, assuming their mass is in the $10^{-6} - 10^{-4}$ eV range, it is useful to have the conversion process occur inside an electromagnetic cavity (Sikivie, 1983, 1985). The cavity captures the photons produced and enhances the conversion process through resonance when one of the cavity modes equals the angular frequency of the axion signal.

Cavity searches for galactic halo axions have been carried out at Brookhaven National Laboratory (De Panfilis *et al.*, 1987; Wuensch *et al.*, 1989), the University of Florida (Hagmann, Sikivie, Sullivan, and Tanner, 1990; Hagmann, 1990), Kyoto University (Matsuki and Yamamoto, 1991; Tada *et al.*, 1999), Lawrence Livermore National Laboratory (Hagmann *et al.*, 1998; Asztalos *et al.*, 2001, 2002, 2004, 2010; Duffy *et al.*, 2005, 2006), the University of Washington (Asztalos *et al.*, 2011; Hoskins *et al.*, 2011, 2016; Boutan *et al.*, 2018; Du *et al.*, 2018; Braine *et al.*, 2020), Yale University (Brubaker, Zhong *et al.*, 2017; Brubaker *et al.*, 2017; Zhong *et al.*, 2018), the University of Western Australia (McAllister, Flower *et al.*, 2017), the INFN National Laboratory in Legnaro, Italy (Alesini *et al.*, 2019a), and the Center for Axion and Precision Physics (CAPP) in Daejeon, Korea (Lee *et al.*, 2020). New cavity detectors are under construction at CAPP (Petrakou, 2017; Semertzidis *et al.*, 2019) and at CERN (Álvarez Melcón *et al.*, 2020). A large cavity detector has been proposed for the INFN National Laboratory in Frascati, Italy (Alesini *et al.*, 2019b). A summary of limits from axion dark matter searches using the cavity technique is shown in Fig. 1.
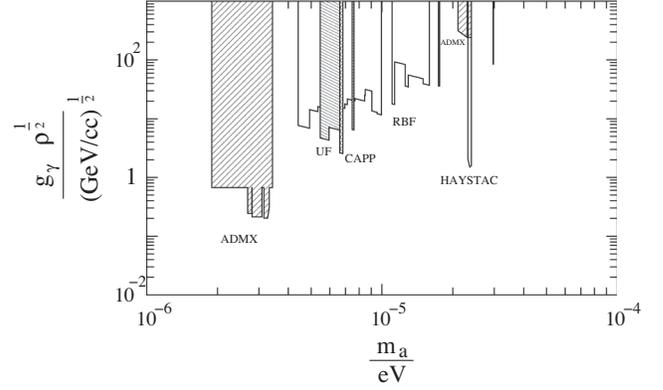
FIG. 1. Limits on $g_\gamma \sqrt{\rho_a}$, where g_γ is the dimensionless axion electromagnetic coupling defined in Eq. (4), and ρ_a is the local axion dark matter density, as a function of axion mass m_a, obtained by the RBF (Wuensch *et al.*, 1989), UF (Hagmann, 1990), ADMX (Boutan *et al.*, 2018; Du *et al.*, 2018; Braine *et al.*, 2020), HAYSTYAC (Zhong *et al.*, 2018), and CAPP-8TB (Lee *et al.*, 2020) cavity searches. Additional limits were obtained by the ORGAN (McAllister, Flower *et al.*, 2017) and QUAX$_{a\gamma}$ (Alesini *et al.*, 2019a) experiments. The limits shown are in rough outline only.

A. The signal

Axion to photon conversion occurs in large externally imposed electric $\vec{E}_0$ and/or magnetic $\vec{B}_0$ fields because the axion induced electric charge and current densities [Eqs. (24)] are sources of electromagnetic waves. For nonrelativistic axions, the

$$\vec{j}_a = -g\vec{B}_0 \partial_t a \quad (54)$$

term in the current density is most relevant since $|\partial_t a| \gg |\vec{\nabla} a|$.

Consider an electromagnetic cavity of volume V, inside of which exists a large static magnetic field $\vec{B}_0(\vec{x})$, dielectric constant $\epsilon(\vec{x})$, and magnetic permeability $\mu(\vec{x})$. We choose $\Phi = 0$ gauge and expand the vector potential into cavity eigenmodes

$$\vec{A}(\vec{x}, t) = \sum_\alpha \vec{e}_\alpha(\vec{x}) \psi_\alpha(t). \quad (55)$$

In the limit of vanishing skin depth, the normalized mode functions $\vec{e}_\alpha(\vec{x})$ satisfy

$$\vec{\nabla} \cdot (\epsilon \vec{e}_\alpha) = 0,$$

$$\vec{\nabla} \times \left(\frac{1}{\mu} \vec{\nabla} \times \vec{e}_\alpha\right) - \epsilon \omega_\alpha^2 \vec{e}_\alpha = 0,$$

$$\hat{n} \times \vec{e}_\alpha|_S = 0,$$

$$\int_V d^3x \epsilon(\vec{x}) \vec{e}_\alpha(\vec{x}) \cdot \vec{e}_\beta(\vec{x}) = \delta_{\alpha\beta}, \quad (56)$$

where S is the surface of the cavity volume and $\hat{n}$ is the unit normal to the surface. The ω_α are the eigenfrequencies. In the absence of axions, the amplitudes $\psi_\alpha(t)$ satisfy

$$\left(\frac{d^2}{dt^2} + \gamma_\alpha \frac{d}{dt} + \omega_\alpha^2\right)\psi_\alpha(t) = 0, \tag{57}$$

where the term proportional to γ_α describes energy dissipation. $Q_\alpha = \omega_\alpha/\gamma_\alpha$ is the quality factor of the cavity in its α eigenmode.

We write the axion field as

$$a(\vec{x}, t) = \mathrm{Re}(Ae^{-i\omega_a t}). \tag{58}$$

Its $\vec{x}$ dependence is ignored because the cavity size is generally of the order of $1/m_a$, whereas the de Broglie wavelength of halo axions is of the order of $10^3/m_a$. Equation (58) implies the following local axion energy density:

$$\rho_a = \tfrac{1}{2}[(\partial_t a)^2 + (\vec{\nabla}a)^2 + m_a^2 a^2] = \tfrac{1}{2}m_a^2|A|^2. \tag{59}$$

In the presence of axions, $\psi_\alpha(t)$ satisfy the equation of motion

$$\left(\frac{d^2}{dt^2} + \gamma_\alpha \frac{d}{dt} + \omega_\alpha^2\right)\psi_\alpha(t)$$
$$= -g\int_V d^3x \vec{B}_0(\vec{x}) \cdot \vec{e}_\alpha(\vec{x})\mathrm{Re}(-i\omega_a Ae^{-i\omega_a t}), \tag{60}$$

obtained by substituting Eqs. (55) and (58) into Eqs. (23), setting $\rho_{\rm el} = \vec{j}_{\rm el} = 0$, and using Eqs. (56). The term describing energy dissipation was added by hand. Up to transients, the solution of Eq. (60) is

$$\psi_\alpha(t) = g\omega_a\left(\int_V d^3x \vec{B}_0 \cdot \vec{e}_\alpha\right)\mathrm{Re}\left(\frac{iAe^{-i\omega_a t}}{\omega_\alpha^2 - \omega_a^2 - i\gamma_\alpha\omega_a}\right). \tag{61}$$

The time-averaged power from axion conversion into the α mode of the cavity is therefore

$$P_\alpha = \gamma_\alpha \int_V d^3x\left(\frac{1}{2}\epsilon\vec{E}_\alpha \cdot \vec{E}_\alpha + \frac{1}{2\mu}\vec{B}_\alpha \cdot \vec{B}_\alpha\right)$$
$$= \frac{\gamma_\alpha}{2}\left[\left(\frac{d\psi_\alpha}{dt}\right)^2 + \omega_\alpha^2\psi_\alpha^2\right]$$
$$= \frac{\gamma_\alpha}{4}\frac{g^2\omega_a^2(\omega_\alpha^2 + \omega_a^2)}{(\omega_\alpha^2 - \omega_a^2)^2 + \gamma_\alpha^2\omega_a^2}|A|^2\left(\int_V d^3x \vec{B}_0(\vec{x}) \cdot \vec{e}_\alpha(\vec{x})\right)^2. \tag{62}$$

The ratio of the energy of galactic halo axions to their energy spread is usually called the "quality factor" Q_a of the axion signal. Equation (52) indicates that Q_a is of the order of 10^6. If $Q_a \gg Q_\alpha$ and the axion signal falls at the center of the cavity bandwidth ($\omega_\alpha = \omega_a$), Eq. (62) implies that (Sikivie, 1983, 1985; Krauss *et al.*, 1985)

$$P_\alpha = g^2\rho_a B_0^2 V C_\alpha \frac{1}{m_a}Q_\alpha, \tag{63}$$

where B_0 is a nominal magnetic field inside the cavity and

$$C_\alpha \equiv \frac{1}{B_0^2 V}\left(\int_V d^3x \vec{B}_0(\vec{x}) \cdot \vec{e}_\alpha(\vec{x})\right)^2$$
$$= \frac{[\int_V d^3x \vec{B}_0(\vec{x}) \cdot \vec{E}_\alpha(\vec{x})]^2}{B_0^2 V \int_V d^3x\epsilon(\vec{x})\vec{E}_\alpha(\vec{x}) \cdot \vec{E}_\alpha(\vec{x})}. \tag{64}$$

C_α expresses the coupling strength of mode α to galactic halo axions and is called its "form factor."

The conversion factor between mass and frequency is ($\hbar = c = 1$)

$$10^{-5} \text{ eV} = 2\pi(2.418 \text{ GHz}). \tag{65}$$

The gigahertz region is a good hunting ground since 10^{-5} eV is a likely mass for axion dark matter. It is also convenient since an electromagnetic cavity whose fundamental mode has gigagertz frequency has size of the order of GHz^{-1} = 30 cm. Expressed in practical units, Eq. (63) is

$$P_\alpha = 1.34 \times 10^{-26} \text{ W}\left(\frac{g_\gamma}{0.36}\right)^2\left(\frac{\rho_a}{1/2 \times 10^{-24} \text{ g/cm}^3}\right)$$
$$\times \left(\frac{B_0}{8 \text{ T}}\right)^2\left(\frac{V}{\text{m}^3}\right)C_\alpha\left(\frac{m_a}{2\pi \text{ GHz}}\right)Q_\alpha\left(\frac{6 \times 10^{15} \text{ eV}^2}{f_a m_a}\right)^2. \tag{66}$$

The last factor in Eq. (66) is approximately 1 in view of Eq. (3). We include it here so that the numerical prefactor in Eq. (66) may be written with precision unmarred by the uncertainty in the relationship between m_a and f_a.

Because the axion mass is unknown, the cavity should be tunable. In all experiments thus far, tunability is achieved by inserting movable metal and/or dielectric posts inside the cavity. For definiteness, consider a cylindrical cavity in which there is a longitudinal homogeneous magnetic field $\vec{B}_0 = B_0\hat{z}$ and a z-independent dielectric constant $\epsilon(x, y)$. By cylindrical cavity we mean one that is invariant under translations in the $\hat{z}$ direction, except for the end caps (Jackson, 1998). The cross-sectional shape is arbitrary. Only the transverse magnetic (TM) modes of a cylindrical cavity couple to the axion field. Indeed the transverse electric and transverse electromagnetic modes have vanishing form factors since their electric fields are perpendicular to $\vec{B}_0$. TM modes are labeled by three integers $\alpha = (l, n, p)$ with $\hat{z} \cdot \vec{e}_{lnp} \propto \cos(p\pi z/L)$ and $p = 0, 1, 2, \ldots$, where L is the length of the cavity. Only the TM$_{ln0}$ have nonzero form factor. For TM$_{ln0}$,

$$\vec{E}_{ln0}(\vec{x}) = \hat{z}\phi_{ln}(x, y), \tag{67}$$

$$\left(\frac{\partial^2}{\partial x^2} + \frac{\partial^2}{\partial y^2} + \epsilon(x, y)\omega_{ln0}^2\right)\phi_{ln} = 0, \tag{68}$$

$$\phi_{ln}|_S = 0. \tag{69}$$

Here we assume that the magnetic permeability $\mu = 1$.

For a circular cross section of radius R and $\epsilon = \mu = 1$,

$$\phi_{ln} \propto J_l\left(x_{ln}\frac{\rho}{R}\right)e^{il\theta}, \quad \omega_{ln0} = \frac{x_{ln}}{R}, \quad C_{ln0} = \frac{4}{(x_{on})^2}\delta_{l0}, \quad (70)$$

where (ρ, θ) are axial coordinates and x_{ln} is the nth zero of the Bessel function $J_l(x)$. In particular, $C_{010} = 0.69$.

For a rectangular cross section

$$\phi_{ln} \propto \sin\left(\frac{l\pi x}{L_x}\right)\sin\left(\frac{n\pi y}{L_y}\right)$$

$$C_{ln0} = \begin{cases} \frac{64}{\pi^4 l^2 n^2} & \text{for } l \text{ and } n \text{ odd,} \\ 0 & \text{otherwise,} \end{cases} \quad (71)$$

where L_x and L_y are the transverse sizes.

Equations (70) and (71) show that, when $\vec{B}_0$ is homogeneous, the lowest TM mode has the strongest coupling. Indeed the electric field profiles $\phi_{ln}(x, y)$ of the higher TM modes have nodes, so the contributions to the form factor from different regions of the cavity tend to cancel each other out.

B. Signal to noise and search rate

The microwave power from axion conversion is coupled out through a small hole in the cavity walls and brought to the front end of a microwave receiver. The quality factor Q of the cavity may be written

$$\frac{1}{Q} = \frac{1}{Q_h} + \frac{1}{Q_w}. \quad (72)$$

In Eq. (72) and henceforth we are suppressing the label α that indicates the mode dependence. $\gamma_h = \omega/Q_h$ is the contribution to γ from emission through the hole and $\gamma_w = \omega/Q_w$ is the contribution from absorption by the cavity walls. The maximum power that can be brought to the microwave receiver is $P_d = (Q/Q_h)P$, where P is given by Eq. (66).

Because the cavity volume is permeated by a strong magnetic field, the cavity walls are ordinarily made of normal metal, although superconducting material can be used for the sidewalls (van Bibber and Carosi, 2013; Ahn et al., 2019; Alesini et al., 2019a). At low temperatures ($T \lesssim$ a few K) and frequencies f in the gigahertz range, a cavity made of high purity copper has $Q_w \sim 2 \times 10^5$. In that case, the cavity bandwidth $B_c \equiv f/Q$ is larger by a factor of 10 or so than the bandwidth $B_a \equiv f/Q_a$ of the axion signal.

The axion signal is searched for by tuning the cavity to successive frequencies, separated by a cavity bandwidth B_c or less, and by integrating for an amount of time t at each tune. To proceed at a reasonably fast rate, e.g., to cover a factor of 2 in frequency in 1 yr, the amount of time t spent at each tune is of the order of $(1/3)(\text{year}/Q) \sim 100$ s. $1/3$ is an assumed duty factor. During each time interval t, the power leaving the cavity is amplified by a receiver, shifted down in frequency by mixing with one or more local oscillators, digitized, and spectrum analyzed. The signal can be analyzed with different resolutions. For example, the Axion Dark Matter Experiment (ADMX) (Asztalos et al., 2001) has a 125 Hz medium resolution channel (MedRes), obtained by coadding many

($\sim 10^4$) short spectra taken during the measurement integration time t, and a high resolution channel (HiRes), with 0.01 Hz resolution, the highest possible when $t = 100$ s. Any resolution less than $\delta f = 1/t$ can be obtained by averaging the highest resolution spectrum.

After an axion signal is found, the energy spectrum of halo axions will immediately become known in great detail. Therefore, it is interesting to try to anticipate what that spectrum will look like.

As do all other cold effectively collisionless dark matter candidates, axions lie on a thin continuous three-dimensional hypersurface in phase space. This hypersurface wraps and folds but does not break. This fact implies that, at any location and any time, dark matter axions form a discrete set of flows, each with a well-defined density and velocity vector (Sikivie and Ipser, 1992; Natarajan and Sikivie, 2005). Predictions for the velocity vectors and densities of the dark matter flows at our location in the Milky Way halo have been made (Sikivie, Tkachev, and Wang, 1995, 1997; Duffy and Sikivie, 2008). Discrete flows are also produced when satellites, such as the Sagittarius dwarf galaxy (Newberg et al., 2002; Majewski et al., 2003), are tidally disrupted by the gravitational field of the Milky Way. Discrete flows are called "streams" in this context. Each flow or stream at our location produces a narrow peak in the cavity detector, since the axions in the flow or stream have well-defined kinetic energy in the laboratory frame. The peaks have a daily frequency modulation due to Earth's rotation and an annual frequency modulation due to Earth's orbital motion (Ling, Sikivie, and Wick, 2004). Over 100 s of data taking, the frequency of a peak at 1 GHz shifts at most by 10^{-2} Hz due to Earth's rotation, and therefore stays within the 10^{-2} Hz highest possible resolution bandwidth. Because of each peak's diurnal and annual modulations it is possible to measure the velocity vector of the associated flow or stream. Searching for narrow peaks increases the sensitivity of the cavity experiment provided that a sufficiently large fraction of the local halo density is in one or more cold flows (Duffy et al., 2005, 2006).

The output of the receiver chain is mostly noise, thermal noise from the cavity plus electronic noise from the receiver. If the axion signal frequency ω_a falls within the cavity bandwidth B_c, the output spectrum has extra power within the axion signal bandwidth B_a. The ratio s/n of the signal to a 1σ fluctuation in the noise within a B_a bandwidth is given by Dicke's radiometer equation

$$\frac{s}{n} = \frac{P_d}{T_n}\sqrt{\frac{t}{B_a}}, \quad (73)$$

where T_n is the total noise temperature. Each candidate peak is checked by taking more data. If the peak is a statistical fluctuation in the noise, it averages away. If a peak does not average away, it is a signal of something but most likely not an axion signal. The nonstatistical peaks found thus far have all been the result of leakage of microwave power into the cavity from the environment of the experiment. Such spurious signals are referred to as "environmental peaks." It is straightforward to distinguish an axion signal from an environmental peak by exploiting the following properties: (1) an

axion signal does not depend on the degree of microwave isolation of the cavity, (2) it cannot be picked up by a simple antenna outside the apparatus, (3) its dependence on the central frequency ω_α of the cavity mode is a Lorentzian [see Eq. (62)], and (4) it is proportional to B_0^2.

In a search, every $p\sigma$ candidate peak is checked to see whether or not it is due to galactic halo axions. p should be chosen to be neither too high nor too low. If too high, the search loses sensitivity. If too low, an excessive amount of time is wasted investigating fluctuations in the noise. In the ADMX MedRes channel, the noise is Gaussian distributed because each spectrum is the sum of many independent spectra. There is therefore a 2.3% chance that the background fluctuates downward by 2σ or more in each B_a-wide bin.

Hence, to put a 97.7% confidence level limit on the product $g_\gamma^2 \rho_a$, the s/n ratio must be $p + 2$ and every candidate peak larger than $p\sigma$ must be ruled out as an axion signal. Through Eq. (73), this determines the minimum measurement integration time t per cavity bandwidth B_c and hence the maximum rate at which the search may proceed in frequency space

$$\frac{df}{dt} \simeq \frac{B_c}{t} = \frac{Q_a}{Q} \frac{1}{(s/n)^2} \left(\frac{P_d}{T_n}\right)^2 = \frac{1}{(s/n)^2} \left(\frac{P_0}{T_n}\right)^2 Q_a \frac{Q^3}{Q_h^2}, \quad (74)$$

where we used $P_d = (Q/Q_h)P$ and defined $P_0 \equiv P/Q$. We may choose Q_h/Q_w to maximize the search rate. One readily finds that the optimum occurs at $Q = (1/3)Q_w$, in which case

$$\frac{d\ln f}{dt} \simeq \frac{1}{f}\frac{1}{(s/n)^2}\left(\frac{P_0}{T_n}\right)^2 Q_a \left(\frac{2}{3}\right)^2 Q$$

$$\simeq \frac{27}{\text{yr}}\left(\frac{4}{s/n}\right)^2 \left(\frac{V}{\text{m}^3}\right)^2 \left(\frac{B_0}{8\ \text{T}}\right)^4 C^2 \left(\frac{g_\gamma}{0.36}\right)^4 \left(\frac{\rho_a}{1/2\times 10^{-24}\ \text{g/cm}^3}\right)^2 \left(\frac{1\ \text{K}}{T_n}\right)^2 \left(\frac{f}{\text{GHz}}\right)\left(\frac{Q}{1/3\times 10^5}\right)\left(\frac{Q_a}{10^6}\right). \quad (75)$$

At gigahertz frequencies, electronic noise temperatures of the order of 2 K are achieved by using cooled heterostructure field-effect transistors as microwave amplifiers (Bradley, 1999). The cavity is then cooled to liquid He temperatures so that the thermal noise qualitatively matches the electronic noise. This was the approach of the earliest experiments (De Panfilis et al., 1987; Wuensch et al., 1989; Hagmann, Sikivie, Sullivan, and Tanner, 1990). An experiment at Kyoto University (Matsuki and Yamamoto, 1991; Ogawa, Matsuki, and Yamamoto, 1996) explored the use of a beam of Rydberg atoms to detect the microwave photons from axion conversion. The more recent experiments (Asztalos et al., 2010; Brubaker et al., 2017) use superconducting quantum interference devices (SQUIDs) (Muck et al., 1998; Muck, Welzel, and Clarke, 2003) or Josephson parametric amplifiers (Al Kenany et al., 2017). These devices approach the so-called quantum limit defined by a noise temperature equal to the angular frequency in units where $k_B = \hbar = 1$:

$$T_n = \omega = 48\ \text{mK}\left(\frac{f}{\text{GHz}}\right). \quad (76)$$

To reduce thermal noise accordingly, the cavity is cooled to temperatures in the 100 mK range using a dilution refrigerator. The sensitivity of microwave photon detection for axion haloscopes may be boosted further by "vacuum squeezing" (Malnou et al., 2019) or single photon counting (Lamoreaux et al., 2013; Kuzmin et al., 2018) techniques.

We may use Eq. (75) to estimate the search rate in the ADMX HiRes channel as well. When searching for peaks with widths less than 0.01 Hz, the HiRes channel is sensitive to cold axion flows with quality factor $Q_a \gtrsim 10^{11}$ at gigahertz frequencies. A large increase in Q_a is the main motivation for the HiRes channel. However, it is partially offset by decreases in other parameters. The relevant ρ_a is the density of the

largest flow that produces a peak with a width less than 0.01 Hz. If δv is the velocity dispersion of a flow of cold axions, its energy dispersion is $\delta E \sim m_a v\delta v$, where $v \sim 10^{-3}$ is the flow velocity. Hence, $Q_a > 10^{11}$ requires $\delta v < 3$ m/s. An additional consideration is that the noise is exponentially distributed in the HiRes channel (Duffy et al., 2005, 2006), whereas it is Gaussian distributed in the MidRes channel. Because each HiRes spectrum has of the order of $Q_c/Q_a \sim 10^6$ bins, the threshold for a peak to be admitted as a candidate signal has to be set high. The signal to noise ratio for a practical HiRes search was found to be of the order of 20 (Duffy et al., 2005, 2006).

Chaudhuri et al. (2019) studied the sensitivity of a cavity haloscope that searches for a signal both inside and outside the cavity's resonant bandwidth and optimized the frequency-integrated sensitivity of such a search.

C. Cavity design

After many years of improvement, the cavity technique has reached sufficient sensitivity to detect dark matter axions even with the weaker DFSZ value of the electromagnetic coupling (Boutan et al., 2018; Du et al., 2018). The next challenge is to extend the technique to the widest possible axion mass range.

A large superconducting solenoid is the type of magnet that has most commonly been used for the experiment, although dipole, wiggler, and toroidal magnets have specific advantages and are being considered as well (Baker et al., 2012; Miceli, 2015; Melcón et al., 2018). At first, the bore of a solenoidal magnet is filled with a single cylindrical cavity. Its resonant frequency may be tuned upward approximately 50% by moving a metal post transversely from the side of the cavity to its center, and 30% downward by similarly moving a dielectric rod (Hagmann, Sikivie, Sullivan, Tanner, and Cho, 1990). Provided that longitudinal symmetry is maintained (the rods must extend from end cap to end cap and remain parallel to the cavity walls), the form factor C stays of the order of 1

over the tuning range. If longitudinal symmetry is broken, the mode may become localized in a small part of the cavity. The form factor is then severely degraded.

To reach higher frequencies, one may fill up the volume available inside a magnet bore with many identical cavities and power combine their outputs (Hagmann, Sikivie, Sullivan, Tanner, and Cho, 1990; Hagmann, 1990). A two-port Wilkinson power combiner produces the output voltage $(1/\sqrt{2})(a + be^{-i\varphi})e^{-i\omega t}$ when the input voltages are $ae^{-i\omega t}$ and $be^{-i\varphi - i\omega t}$. The power combiner adds the axion signals from the cavities provided that they are equal in magnitude and phase. Thus, one may power combine the outputs of identical cavities provided that the largest distance between the cavities is less than the de Broglie wavelength ($\sim 10^{+3}/m_a$) of galactic halo axions, that the cavities are in tune, and that the phase shifts between the individual cavities and the power combiner are identical. Since the noise in the different cavities is uncorrelated in phase, the noise temperature at the output of the power combiner is the average of the noise temperatures at its input ports. Properly built multicavity arrays have effective form factors of the order of 1 and allow, at the cost of engineering complexity, the upward extension of the frequency range over which a galactic halo axion search can be carried out with a given magnet.

Alternatively, one may reach higher frequencies by dividing a cavity into cells separated by metal vanes (Stern *et al.*, 2015; Jeong, Youn, Ahn, Kang, and Semertzidis, 2018; Jeong, Youn, Ahn, Kim, and Semertzidis, 2018). Such multicell cavities must be carefully designed to avoid mode crowding and mode localization. Kim *et al.* (2020) presented a design achieving a large form factor for the TM$_{030}$ mode of a cylindrical cavity by inserting dielectric vanes. Another proposal is to introduce materials that produce a plasma frequency for the electromagnetic field inside the cavity (Lawson *et al.*, 2019).

The frequency range of cavity haloscopes can also be extended upward by controlling the spatial variation of the magnetic field inside the cavity or by introducing dielectric plates to control the mode structure. These two approaches are discussed in Sec. V.A.

Berlin *et al.* (2020), Sikivie (2010), and Lasenby (2020) proposed searching for axion dark matter in an electromagnetic cavity that is driven with input power instead of being permeated by a magnetic field. The relevant process is $a + \gamma \rightarrow \gamma'$, where γ is a microwave photon in the mode that is driven by input power and γ' is a microwave photon, in another mode of the cavity, to be detected as the signal. This approach can be pursued using an optical cavity as well (Melissinos, 2009).

Goryachev, McAllister, and Tobar (2019) proposed searching for dark matter axions by detecting the phase noise induced by the oscillating axion field in driven cavity modes separated in frequency by the axion mass. An experiment of this type was reported on by Thomson *et al.* (2019).

V. OTHER APPROACHES TO AXION DARK MATTER DETECTION

The cavity technique works well for axion masses between perhaps 10^{-7} and a few times 10^{-5} eV, but not, at any rate, for

all masses that dark matter axions may plausibly have. Therefore, there is good motivation to look for alternatives. Over the years, different approaches have been proposed that collectively address the entire QCD axion mass range, from 10^{-2} to 10^{-12} eV. They are the topic of this section. Several methods were anticipated by Vorobev, Kakhidze, and Kolokolov (1995) and rediscovered later.

A. Wire arrays and dielectric plates

The conversion of axions to photons in a magnetic field can be enhanced by controlling the spatial variation of the magnetic field or by introducing dielectric plates to modify the mode structure of the electromagnetic field. In such schemes, it is likely useful to introduce a cavity as well.

1. Wire arrays

The differential cross section for axion to photon conversion in a static magnetic field is given in Eq. (36). Multiplying by the axion flux $\beta_a n_a$ and integrating over solid angles yields the conversion rate

$$R = \frac{g^2 n_a}{16\pi^2\epsilon} \int d^3k\, \delta\left(\frac{k}{\sqrt{\epsilon\mu}} - \omega\right) \sum_{\lambda=1,2}$$
$$\times \left| \int_V d^3x\, e^{i(\vec{k}_a - \vec{k})\cdot\vec{x}} \hat{e}_\lambda(\hat{n}) \cdot \vec{B}_0(\vec{x}) \right|^2. \tag{77}$$

To maximize R for a given field strength and volume, the magnetic field should be made inhomogeneous on the length scale set by the momentum transfer $\vec{q} = \vec{k} - \vec{k}_a$. Since dark matter axions are nonrelativistic, $k_a \ll k$ and hence $q \simeq k = \sqrt{\epsilon\mu}\omega \simeq \sqrt{\epsilon\mu}m_a$. Thus, the inhomogeneity length scale should be of the order of $1/\sqrt{\epsilon\mu}m_a$.

In view of this, it was proposed to build an array of superconducting wires embedded in a dielectric medium transparent to microwave radiation (Sikivie, Tanner, and Wang, 1994). Magnetic fields are produced by passing electric currents through the wires. The dielectric medium keeps the wires in place. We set $\mu = 1$ here for simplicity.

A possible realization consists of wires parallel to the y axis whose intersections with the x-z plane form a regular lattice with lattice constant d. The wires intersect the x-z plane at $(n_x d, n_z d)$, where n_x and n_z are integers that range from $-L_x/2d$ to $+L_x/2d$ and $-L_z/2d$ and $+L_z/2d$, respectively. L_x and L_z are the dimensions of the detector in the $\hat{x}$ and $\hat{z}$ directions. The currents $I(n_x, n_z)$ in the wires are chosen to produce a particular magnetic field profile. For example,

$$I(n_x, n_z) = I(n_z) = I_0 \sin(\kappa n_z d) \tag{78}$$

produces the magnetic field

$$\vec{B} = -\hat{x}\frac{I_0}{\kappa d^2}\cos(\kappa z) \tag{79}$$

in the limit $L \rightarrow \infty$ and $d \rightarrow 0$. In practice the magnetic field deviates from Eq. (79) because of finite size L and finite lattice constant d effects. Such deviations, which can be calculated without much difficulty, are ignored here for simplicity.

For definiteness we assume Eq. (79) within a rectangular volume $V = L_x L_y L_z$. Because the photons produced are polarized in the direction $\hat{x}$ perpendicular to the wires, the effect of the wires on their propagation is minimized. In using Eq. (77) we are assuming that the photons propagate as if the wires were absent. For the magnitude squared of the space integral in Eq. (77) we have

$$\left| \int_V d^3x e^{-i\vec{q}\cdot\vec{x}} B_0 \cos(\kappa z) \right|^2$$
$$= (2\pi)^2 \delta_{L_x}(q_x)\delta_{L_y}(q_y) L_x L_y B_0^2$$
$$\times \left(\frac{\sin\left[(q_z + \kappa)L_z/2\right]}{q_z + \kappa} + \frac{\sin\left[(q_z - \kappa)L_z/2\right]}{q_z - \kappa} \right)^2, \quad (80)$$

where $\delta_L(q)$ is a Dirac delta function spread over a width of the order of $1/L$. Resonant conversion is obtained for $q_z = \pm\kappa$. Since $\vec{k} \simeq \vec{q}$, the photons are emitted in the $\pm\hat{z}$ direction and can therefore be focused by mirrors onto one or two microwave receivers.

The wave vector κ of the current configuration can be changed to tune the detector over a range of possible axion masses. The detector bandwidth is $\Delta k_z \simeq \pi/L_z$, whereas the bandwidth of the axion signal is $\Delta k_{az} \simeq 2 \times 10^{-3} m_a$. The conversion rate is obtained by inserting Eq. (80) into Eq. (77) and carrying out the integral over $\vec{k}$. Provided that the axion signal falls entirely within the bandwidth of the detector, the signal power is

$$P = m_a R = \frac{g^2}{8\sqrt{\epsilon}} V L_z B_0^2 \rho_a$$
$$= 2 \times 10^{-25} \text{ W} \left(\frac{VL_z}{\text{m}^4}\right)\left(\frac{B_0}{8 \text{ T}}\right)^2 \left(\frac{g_\gamma}{0.36}\right)^2 \left(\frac{m_a}{10^{-5} \text{ eV}}\right)^2 \frac{1}{\sqrt{\epsilon}} \left(\frac{\rho_a}{\frac{1}{2} \times 10^{-24} \text{ g/cm}^3}\right). \quad (81)$$

The discussion of the signal to noise and search rate is similar to that for the cavity detector addressed in Sec. IV.B and need not be repeated here.

The previously mentioned design is convenient for signal calculation but not so convenient for construction and operation. In practice one wishes to minimize the number of connections between wires. A possible way to do this is to deform the previously mentioned rectangular array into a cylinder so that all the wires at a given n_z combine to form a spiral. The spiral could be a NbTi strip etched by photolithographic techniques onto a low loss insulating sheet. The sheets would then be stacked to form the body of the detector.

Comparing Eqs. (63) and (81), the expression for the conversion power of a wire array is seen to be similar to that of a cavity haloscope but with the product CQ of the cavity form and quality factors replaced by $L_z m_a/8\sqrt{\epsilon}$. If the

axions have velocity dispersion $\delta v \sim 10^{-3}$, the requirement $\Delta k_z \gtrsim \Delta k_a$ implies that $L_z m_a \lesssim 1600$. When searching for low velocity dispersion flows, such as the big flow of Eq. (19), $L_z m_a$ can be made much larger. However, the detector must in that case be kept aligned with respect to a particular flow.

It is generally advantageous to place the wire array inside an electromagnetic cavity (Rybka et al., 2015). A small wire array was built at the University of Washington and placed in an open Fabry-Perot resonator in an experiment called ORPHEUS (Rybka et al., 2015). A schematic drawing of such a setup is shown in Fig. 2. The detector is now in effect a cavity haloscope and the considerations of Sec. IV apply to it. If the electric field for the Fabry-Perot mode is

$$\vec{E}_\omega = \hat{x} E_\omega \cos(\kappa z) \quad (82)$$
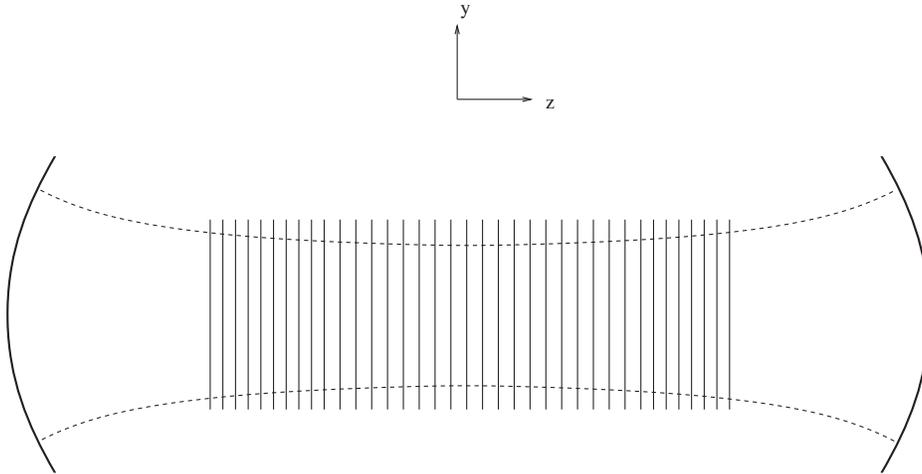
FIG. 2. Wire array detector of dark matter axions discussed in Sec. V.A.1. The $\hat{y}$ and $\hat{z}$ directions are defined in the text. The dashed lines represent the envelope of an electromagnetic mode in a confocal resonator. The mode is driven by axion to photon conversion in the magnetic field produced by currents in an array of wires. The wires are represented by vertical lines.
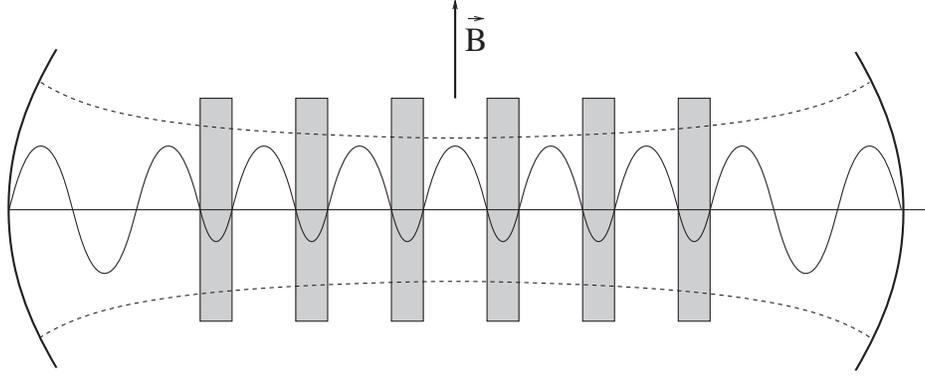
FIG. 3. Dielectric plate detector of dark matter axions discussed in Sec. V.A.2. The dashed lines represent the envelope of an electromagnetic mode in a confocal resonator. The mode is driven by axion to photon conversion in a uniform static externally applied magnetic field $\vec{B}$. The vertical shaded rectangles represent dielectric plates arranged in such a way as to make the overlap integral of the applied static magnetic field $\vec{B}$ with the oscillating electric field of the mode as large as possible. The electric field profile of the mode is shown.

within the volume of the wire array and the magnetic field is as in Eq. (79), the conversion power is given by Eq. (63), with V the volume of the wire array and $C = 0.5F$, where F is the fraction of the distance between the mirrors that is occupied by the wire array. The detector is tuned by changing the distance between the mirrors. In the ORPHEUS detector, the distances between the wire planes were changed proportionately.

2. Dielectric plates

Instead of making the magnetic field inhomogeneous on the $q^{-1} \sim m_a^{-1}$ length scale, one may instead have the dielectric constant vary on that length scale (Morris, 1984; Caldwell et al., 2017; Ioannisian et al., 2017; Millar, Redondo, and Steffen, 2017; Baryakhtar, Huang, and Lasenby, 2018; McAllister et al., 2018). MADMAX (Brun et al., 2019) is a proposed experiment using dielectric plates, although in a different manner from the setup described below. MADMAX evolved from an earlier broadband axion dark matter detection scheme, called the dish antenna (Horns et al., 2013).

Here we consider a stack of parallel plates of thickness d and dielectric constant ϵ placed in a Fabry-Perot resonator, as shown schematically in Fig. 3. The distance D between the plates is chosen to be the half wavelength π/m_a in vacuum of the photons produced by axion conversion, whereas the plate thickness d is chosen to be of the order of the half wavelength $\pi/\sqrt{\epsilon}m_a$ of those photons in the dielectric material. The intended electric field profile of the electromagnetic mode in the region occupied by the dielectric plates is

$$\vec{E}_\omega = \begin{cases} \hat{x} E_\omega \sin\left[\omega(z - z_j)\right] & \text{for } 0 \leq z - z_j \leq D, \\ \hat{x} \frac{E_\omega}{\sqrt{\epsilon}} \sin\left[\sqrt{\epsilon}\omega(z - z_j)\right] & \text{for } -d \leq z - z_j \leq 0, \end{cases} \tag{83}$$

where z_j are the positions of the right faces of the plates; see Fig. 3. With this electric field profile and a uniform magnetic field $\vec{B}_0 = B_0 \hat{x}$, the conversion power is given by Eq. (63), with V the volume of the stack of plates (including the spaces between plates) and

$$C = \frac{8}{\pi^2} \frac{(\epsilon - 1)^2}{\epsilon(\sqrt{\epsilon} + 1)^2} F, \tag{84}$$

where F is the fraction of the distance between the mirrors that is occupied by the stack of plates. Some materials (such as Al_2O_3) have a high dielectric constant ($\epsilon \sim 10$) but low dielectric losses ($\tan \delta_e \sim 10^{-4}$). The mirrors, if placed outside the magnetic field region, can be made of superconducting material so that their contribution to dissipative losses is small.

B. Magnetic resonance

Ignoring the small CP violating term shown explicitly in Eq. (9), the interaction energy of the axion with a non-relativistic electron is

$$H_{a\bar{e}e} = \frac{g_e}{2f_a}\left(\vec{\nabla}a \cdot \vec{\sigma} + \partial_t a \frac{\vec{p} \cdot \vec{\sigma}}{m_e}\right), \tag{85}$$

where $\vec{p}$ is the electron momentum, m_e is its mass, and $\vec{S} = (1/2)\vec{\sigma}$ is its spin. The first term in Eq. (85) is similar to the coupling of a magnetic field to electron spin. The effective magnetic field associated with a gradient in the axion field is

$$\vec{B}_{\text{eff}} = -\frac{g_e}{\gamma_e f_a}\vec{\nabla}a, \tag{86}$$

where γ_e is the electron gyromagnetic ratio. The axion has analogous interactions (9) with quarks. We therefore expect the following interaction energy of the axion field with nuclear spin $\vec{I}$:

$$H_{a\bar{N}N} = \frac{g_N}{f_a}\vec{\nabla}a \cdot \vec{I}, \tag{87}$$

where the g_N are dimensionless couplings of the order of 1 that are determined by nuclear physics in terms of g_p and g_n (Stadnik and Flambaum, 2015). Equations (85) and (87) suggest that one may search for dark matter axions using magnetic resonance techniques. Barbieri et al. (1989, 2017)

proposed detecting the power from axion to magnon conversion in a medium containing a high density of aligned electron spins. Graham and Rajendran (2013) and Budker *et al.* (2014) proposed to detect the transverse magnetization induced by the axion field onto a sample of aligned nuclear spins.

We briefly recall basic aspects of magnetic resonance (Kittel, 1968). A macroscopic sample of particles with spin $\vec{I}$ and magnetic moment

$$\vec{\mu} = \gamma \vec{I} \tag{88}$$

is polarized in a static magnetic field $\vec{B}_0 = B_0 \hat{z}$, or by some other means, resulting in a magnetization $M_0 \hat{z}$. We use $\vec{I}$ to represent electron spin $(1/2)\vec{\sigma}$ or nuclear spin, whichever applies. In addition to $\vec{B}_0$, a weak transverse time-dependent magnetic field $\vec{B}_\perp = \hat{x} B_x(t) + \hat{y} B_y(t)$ is applied. The transverse components of the magnetization satisfy the Bloch equations

$$\frac{dM_x}{dt} = \gamma(\vec{M} \times \vec{B})_x - \frac{1}{t_2} M_x = -\gamma M_0 B_y + \gamma B_0 M_y - \frac{1}{t_2} M_x$$

$$\frac{dM_y}{dt} = \gamma(\vec{M} \times \vec{B})_y - \frac{1}{t_2} M_y = +\gamma M_0 B_x - \gamma B_0 M_x - \frac{1}{t_2} M_y, \tag{89}$$

where t_2 is the transverse relaxation time. When $\vec{B}_\perp = 0$, an initial transverse magnetization precesses about the z axis with angular frequency $\omega_0 = -\gamma B_0$ and decays in a time t_2. For definiteness, we assume that the $\hat{z}$ axis is chosen so that $\omega_0 > 0$. If the transverse field has the form

$$\vec{B}_\perp(t) = B_\perp(\hat{x} \cos \omega t + \hat{y} \sin \omega t), \tag{90}$$

the sample acquires in steady state the transverse magnetization

$$\vec{M}_\perp = M_\perp[\hat{x} \cos(\omega t - \phi) + \hat{y} \sin(\omega t - \phi)], \tag{91}$$

with

$$\tan \phi = \frac{1}{(\omega_0 - \omega) t_2} \tag{92}$$

and

$$M_\perp = \frac{\gamma M_0 t_2 B_\perp}{\sqrt{1 + (\omega_0 - \omega)^2 t_2^2}}. \tag{93}$$

On resonance ($\omega = \omega_0$) the transverse magnetization has its maximum magnitude $\gamma M_0 t_2 B_\perp$ and its phase is $\pi/2$ behind that of $\vec{B}_\perp$.

We now consider a magnetized sample bathed in a flow of axions described by the field

$$a(\vec{x}, t) = A \sin(\vec{k} \cdot \vec{x} - \omega t), \tag{94}$$

with $\omega = \sqrt{m_a^2 + \vec{k} \cdot \vec{k}} \simeq m_a + k^2/2m_a$. The energy density of such a flow is

$$\rho_a = \tfrac{1}{2} \omega^2 A^2. \tag{95}$$

Comparing Eq. (87) with the interaction $H_B = -\gamma \vec{I} \cdot \vec{B}$ of a magnetic field with spin, the axion field (94) is seen to produce an effective tranverse magnetic field

$$\vec{B}_{\perp,\text{eff}} = -\frac{1}{\gamma} \frac{g_N}{f_a} A \vec{k}_\perp \cos(\omega t), \tag{96}$$

where $\vec{k}_\perp = \vec{k} - \hat{z}(\hat{z} \cdot \vec{k})$. In contrast to Eq. (90), it drives the transverse magnetization in only one spatial direction. In addition, the field due to dark matter axions in the Milky Way halo does not have the infinite coherence time implied by Eq. (90) or (94). The direction and time dependence of $\vec{B}_{\perp,\text{eff}}$ depends on the model of the galactic halo. Two contrasting proposals were mentioned in Sec. II. In the isothermal model, the energy dispersion $\delta\omega \simeq 10^{-6} m_a$, and hence the coherence time $t_c = 1/\delta\omega \simeq 0.16$ s (MHz/ν_a), where ν_a is the frequency associated with the axion mass $m_a = 2\pi\nu_a$. In the caustic ring model, the local dark matter density is dominated by a single flow, the big flow, with velocity dispersion $\delta v \lesssim 70$ m/s. Its energy dispersion $\delta\omega = m_a v \delta v \lesssim 2 \times 10^{-10} m_a$, and hence its coherence time $t_c \gtrsim 700$ s (MHz/ν_a).

1. Nuclear magnetic resonance (NMR)

When the transverse magnetic field is in only one spatial direction, say, $\vec{B}_\perp(t) = B_\perp \cos(\omega t) \hat{x}$, the Bloch equations are solved by

$$\vec{M}_a(t) = M_{\perp a}[\hat{x} \cos(\omega t - \phi) + \hat{y} \sin(\omega t - \phi)] + \mathcal{O}\left(\frac{1}{\omega + \omega_0}\right), \tag{97}$$

with ϕ given in Eq. (92) and

$$M_{\perp a} = \frac{1}{2} \frac{\gamma M_0 t_2 B_\perp}{\sqrt{1 + (\omega_0 - \omega)^2 t_2^2}}. \tag{98}$$

The terms of the order of $(\omega + \omega_0)^{-1}$ in Eq. (97) are nonresonant and can be ignored. The effect of frequency dispersion in the axion field is included by replacing t_2 with $\min(t_2, t_c)$. We have then on resonance ($\omega_0 = m_a$)

$$M_{\perp a} = \frac{g_N}{f_a} v_\perp \sqrt{\frac{\rho_a}{2}} M_0 \min(t_2, t_c)$$

$$= 0.5 \times 10^{-14} \, M_0 g_N \left(\frac{m_a}{10^{-8} \text{ eV}}\right)\left(\frac{v_\perp}{10^{-3}}\right)$$

$$\times \left(\frac{\rho_a}{\text{GeV/cm}^3}\right)^{1/2} \frac{\min(t_2, t_c)}{\text{s}}. \tag{99}$$

The transverse magnetization may be detected by a SQUID magnetometer. The present sensitivity of such devices is of the

order of 10^{-16} T/$\sqrt{\text{Hz}}$. The CASPEr-Wind experiment (Budker *et al.*, 2014; Garcon *et al.*, 2018) searches for axion dark matter using this technique.

Graham and Rajendran (2013), Budker *et al.* (2014), and Garcon *et al.* (2018) proposed a second approach to axion dark matter detection using NMR techniques called CASPEr-Electric. In it a static electric field $\vec{E}_0$ is applied in a direction transverse to $\vec{M}_0$. The electric field interacts with the oscillating electric dipole moment induced onto the nucleus by the local axion field

$$\vec{d}_e(t) = D_N \bar{\theta}(t)\vec{I} = D_N \frac{a(t)}{f_a}\vec{I}, \qquad (100)$$

where $D_N \sim 3 \times 10^{-16}$ e cm; see Eq. (2). The relevant interaction is thus

$$H'_{a\bar{N}N} = -\vec{d}_e \cdot \vec{E}_N = -D_N \frac{a(t)}{f_a}\vec{I} \cdot \vec{E}_N, \qquad (101)$$

where $\vec{E}_N$ is the electric field at the location of the nucleus. In an atom, a static externally applied electric field $\vec{E}_0$ is screened at the location of the nucleus by the electron cloud, implying that $\vec{E}_N = 0$. Indeed, if $\vec{E}_N \neq 0$, the nucleus moves until $\vec{E}_N = 0$. However, because of finite nuclear size effects, $\vec{E}_N$ does not vanish entirely but is suppressed by a factor of ϵ_S, called the Schiff factor, of the order of 10^{-2} for a large nucleus (Graham and Rajendran, 2013; Budker *et al.*, 2014). Relative to $H_{a\bar{N}N}$ the strength of the interaction $H'_{a\bar{N}N}$ is then

$$\frac{\epsilon_S D_N E_0}{g_N v_\perp m_a} \sim 10^4 \left(\frac{\epsilon_s}{10^{-2}}\right)\left(\frac{E_0}{3 \times 10^8 \text{ V/cm}}\right)\left(\frac{10^{-10} \text{ eV}}{m_a}\right), \quad (102)$$

suggesting that this approach is attractive for small axion masses.

2. Axion to magnon conversion

When the axion field excites transverse magnetization, axions are converted to magnons (Barbieri *et al.*, 1989, 2017; Chigusa, Moroi, and Nakayama, 2020). Whereas an amplitude measurement such as CASPEr is more sensitive at low frequencies, a power measurement is more sensitive at high frequencies. The power from axion to magnon conversion on resonance ($\omega_0 = m_a$) is

$$\begin{aligned} P_m &= -\vec{M}_{\perp a} \cdot \frac{d\vec{B}_{\perp,\text{eff}}}{dt} V = m_a M_{\perp a} B_{\perp,\text{eff}} V \\ &= \left(\frac{g_e}{f_a}\right)^2 m_a \rho_a (v_\perp)^2 \frac{M_0 V}{\gamma} \min(t_2, t_c) \\ &= 7.9 \times 10^{-20} \text{ W} g_e^2 \left(\frac{m_a}{10^{-4} \text{ eV}}\right)^3 \left(\frac{n_s V}{10^{24}}\right)\left(\frac{v_\perp}{10^{-3}}\right)^2 \\ &\quad \times \left(\frac{\rho_a}{\text{GeV/cm}^3}\right)\frac{\min(t_2, t_c)}{\text{s}} \end{aligned} \qquad (103)$$

in a volume V of aligned electron spins with density n_s. The QUAX experiment at the INFN Laboratory in Legnaro, Italy,
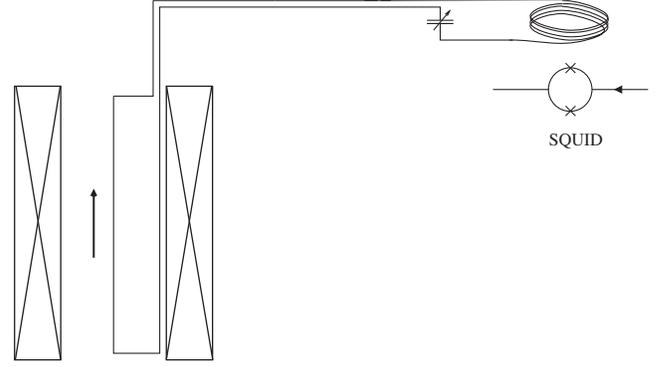
FIG. 4. Schematic drawing of the *LC* circuit axion dark matter detector in case the magnet is a solenoid. The two crossed rectangles indicate cross sections of the solenoid's windings. The arrow shows the direction of the magnetic field that the solenoid produces. From Sikivie, Sullivan, and Tanner, 2014.

searches for axion dark matter using a magnetized sample placed in an electromagnetic cavity (Barbieri *et al.*, 2017; Crescini *et al.*, 2018, 2020). The electron spins are coupled to a cavity resonant mode, tuned to the frequency ω_0, so that the magnons convert to microwave photons. The electromagnetic power is coupled out and detected using a microwave receiver. The cavity is cooled to temperatures of the order of 100 mK to suppress thermal noise. The approach was also discussed by Flower *et al.* (2019) with results from an initial experiment.

C. *LC* circuit

For axion masses below 10^{-7} eV, the size of the cavity detector is of the order of 10 m or larger. For such small masses it may be advantageous to replace the cavity by a *LC* circuit (Sikivie, Sullivan, and Tanner, 2014; Kahn, Safdi, and Thaler, 2016; McAllister, Parker, and Tobar, 2016; Silva-Feaver *et al.*, 2017; Chaudhuri *et al.*, 2018; Chu *et al.*, 2018; Crisosto *et al.*, 2018, 2020; Ouellet *et al.*, 2019a).[3]

Equations (23) tell us that in an externally applied magnetic field $\vec{B}_0$ dark matter axions produce an electric current density $\vec{j}_a = -g\vec{B}_0\partial_t a$. Assuming that the magnetic field is static, $\vec{j}_a$ oscillates with frequency $\omega = m_a[1 + (1/2)\vec{v} \cdot \vec{v}]$, where $\vec{v}$ is the axion velocity. If the spatial extent of the externally applied magnetic field is much less than ω^{-1}, the Maxwell displacement current $\partial_t(\epsilon\vec{E})$ can be neglected in the second of Eqs. (23). The magnetic field $\vec{B}_a$ produced by $\vec{j}_a$ then satisfies $\vec{\nabla} \times \vec{B}_a = \vec{j}_a$. We set $\mu = 1$ for simplicity. One may amplify $\vec{B}_a$ using a *LC* circuit and detect the amplified field with a SQUID magnetometer.

Figure 4 shows a schematic drawing in case the magnet producing $\vec{B}_0$ is a solenoid. The field $\vec{B}_a$ has flux Φ_a through a

---

[3]Unpublished work on the *LC* circuit axion dark matter detector was done in the early 2000s by Sikivie, Sullivan, and Tanner, and independently by Cabrera and Thomas. The work of Cabrera and Thomas was presented in a talk given at the Axions 2010 Conference in Gainesville, Florida, on January 15–17, 2010 (http://www.physics.rutgers.edu/~scthomas/talks/Axion-LC-Florida.pdf).

loop of superconducting wire. Because the wire is superconducting, the total magnetic flux through the loop circuit is constant. In the limit where the capacitance C of the circuit is infinite (the capacitance is removed) the current in the wire is $I = -\Phi_a/L$, where L is the inductance of the circuit. The magnetic field seen by the magnetometer is

$$B_d \simeq \frac{N_d}{2r_d} I = -\frac{N_d}{2r_d L} \Phi_a, \tag{104}$$

where N_d is the number of turns and r_d is the radius of the small coil facing the magnetometer. Ignoring for the moment the mutual inductances of the LC circuit with neighboring circuits in its environment, L is a sum

$$L \simeq L_m + L_c + L_d \tag{105}$$

of contributions L_m from the large pickup loop inside the externally applied magnetic field L_d from the small coil facing the magnetometer, and L_c from the coaxial cable in between. We have

$$L_d = r_d N_d^2 c_d \tag{106}$$

with

$$c_d \simeq \ln\left(\frac{8r_d}{a_d}\right) - 2, \tag{107}$$

where a_d is the radius of the wire in the small coil. The mutual inductances of the LC circuit with neighboring circuits can be measured in any actual setup and taken into account when optimizing the circuit and estimating the detector's sensitivity.

For finite C, the LC circuit resonates at frequency $\omega = 1/\sqrt{LC}$. When ω equals the axion rest mass, the magnitude of the current in the wire is multiplied by the quality factor Q of the circuit, and hence

$$B_d \simeq \frac{Q N_d \Phi_a}{2 L r_d}. \tag{108}$$

Let us consider the case where the externally applied magnetic field is homogeneous $\vec{B}_0 = B_0 \hat{z}$, as is approximately true inside a long solenoid. In such a region

$$\vec{B}_a = -\tfrac{1}{2} g(\partial_t a) B_0 \rho \hat{\phi}, \tag{109}$$

where z, ρ, and ϕ are cylindrical coordinates. For the pickup loop depicted in Fig. 4, a rectangle whose sides l_m and r_m are approximately the length and radius of the magnet bore, the flux of $\vec{B}_a$ through the pickup loop is

$$\Phi_a = -V_m g B_0 \partial_t a, \tag{110}$$

with $V_m = (1/4) l_m r_m^2$. Assuming that $l_m \gg r_m$, the self-inductance of the pickup loop is $L_m \simeq (1/\pi) l_m \ln(r_m/a_m)$, where a_m is the radius of the wire.

The time derivative of the axion field is given in terms of the axion density by $\partial_t a = \sqrt{2\rho_a} \cos(\omega t)$. Hence, combining Eqs. (108) and (110), we obtain the magnitude of the magnetic field seen by the magnetometer

$$B_d \simeq \frac{N_d Q}{2r_d L} V_m g \sqrt{2\rho_a} B_0$$

$$= 1.25 \times 10^{-15} \text{ T} \left(\frac{\rho_a}{\text{GeV/cm}^3}\right)^{1/2} \left(\frac{Q}{10^4}\right)$$

$$\times \left(\frac{g}{10^{-17} \text{ GeV}^{-1}}\right) N_d \left(\frac{\text{cm}}{r_d}\right) \left(\frac{V_m}{\text{m}^3}\right) \left(\frac{\mu\text{H}}{L}\right) \left(\frac{B_0}{10 \text{ T}}\right). \tag{111}$$

In comparison, the sensitivity of today's best magnetometers is $\delta B = B_n \sqrt{\Delta\nu/\text{Hz}}$, with B_n of the order of 10^{-16} T. The detector bandwidth is ν/Q. If a factor of 2 in frequency is to be covered per year and the duty factor is 30%, the amount of time t spent at each tune of the LC circuit is of the order of $10^7 \text{ s}/Q$. The signal to noise ratio depends on the signal coherence time t_c, and hence on the axion velocity distribution. The coherence times of two contrasting galactic halo models were given in Sec. V.B. The magnetometer is sensitive to magnetic fields of magnitude $\delta B = B_n(t \text{ Hz})^{-1/2}$ when $t < t_c$, and $\delta B = B_n(\text{Hz})^{-1/2}(t_c t)^{-1/4}$ when $t > t_c$.

An important source of noise, in addition to the flux noise in the magnetometer, is the thermal (Johnson-Nyquist) noise in the LC circuit. It causes voltage fluctuations $\delta V_T = \sqrt{4k_B T R \Delta\nu}$ (Nyquist, 1928), and hence current fluctuations

$$\delta I_T = \frac{\delta V_T}{R} = \sqrt{\frac{4k_B T Q \Delta\nu}{L\omega}}$$

$$= 2.96 \times 10^{-13} \text{ A} \sqrt{\left(\frac{\text{MHz}}{\nu}\right)\left(\frac{\mu\text{H}}{L}\right)\left(\frac{Q}{10^4}\right)\left(\frac{T}{\text{mK}}\right)\left(\frac{\Delta\nu}{\text{mHz}}\right)}, \tag{112}$$

where we use the relation $R = L\omega/Q$ between the resistance and quality factor of a LC circuit. Equation (112) should be compared with the current due to the signal

$$I = \frac{Q}{L} V_m g B_0 \partial_t a$$

$$= 1.99 \times 10^{-11} \text{ A} \left(\frac{Q}{10^4}\right)\left(\frac{V_m}{\text{m}^3}\right)\left(\frac{\mu\text{H}}{L}\right)$$

$$\times \left(\frac{g}{10^{-17} \text{ GeV}^{-1}}\right) \sqrt{\frac{\rho_a}{\text{GeV/cm}^3}} \left(\frac{B_0}{10 \text{ T}}\right) \tag{113}$$

and with the fluctuations in the measured current due to the noise in the magnetometer

$$\delta I_B \simeq \frac{2r_d}{N_d} \delta B = 5.03 \times 10^{-14} \text{ A} \frac{1}{N_d}\left(\frac{r_d}{\text{cm}}\right)\left(\frac{B_n}{10^{-16} \text{ T}}\right) \sqrt{\frac{\Delta\nu}{\text{mHz}}}. \tag{114}$$

Another possible source of noise is jumps in the $\vec{B}_0$ field, caused by small sudden displacements in the positions of the wires in the magnet windings.

The LC circuit detector appears to be well suited to axion dark matter detection in the $10^{-7} - 10^{-9}$ eV range. The ABRACADABRA experiment at MIT (Kahn, Safdi, and Thaler, 2016; Ouellet et al., 2019a, 2019b) and the ADMX SLIC experiment at the University of Florida (Crisosto et al.,

2018, 2020) have published results. An experiment is also under construction at Stanford (DM Radio) (Silva-Feaver *et al.*, 2017; Chaudhuri *et al.*, 2018).

A reentrant cavity is an electromagnetic cavity with properties similar to those of a *LC* circuit. McAllister, Shen *et al.* (2017) described such a cavity and computed its form factor as a function of frequency.

D. Atomic transitions

The interaction of an axion with a nonrelativistic electron [Eq. (85)] and the interaction of an axion with nuclear spin [Eq. (87)] allow atomic transitions in which an axion is emitted or absorbed. The transitions are resonant between atomic states that differ in energy by an amount equal to the axion mass. Such energy differences can be conveniently tuned using the Zeeman and Stark effects. One approach to axion dark matter detection is to cool a kilogram-sized sample to millikelvin temperatures and count axion induced atomic or molecular transitions using laser techniques (Sikivie, 2014; Santamaria *et al.*, 2015; Braggio *et al.*, 2017; Avignone, Creswick, and Vergados, 2018).

Equation (87) and the first term on the rhs of Eq. (85) are similar to the coupling of the magnetic field to spin. Those interactions may cause magnetic dipole ($M1$) transitions in atoms and molecules. The second term in Eq. (85) allows $\Delta j = 0$, $\Delta l = 1$ parity changing transitions. As usual, l is the quantum number giving the magnitude of orbital angular momentum, and j that of total angular momentum. We do not consider that last interaction further because, starting from the ground state ($l = 0$), it causes atomic transitions only if the energy absorbed is of the order of eV, which is much larger than the axion mass. Molecular transitions in the eV range were discussed as a technique for dark matter detection by Arvanitaki, Dimopoulos, and Van Tilburg (2018).

The ground state of most atoms is accompanied by several other states related to it by hyperfine splitting, i.e., by flipping the spin of one or more valence electrons or by changing the z component I_z of the nuclear spin. The transition rate by axion absorption from an atomic ground state $|0\rangle$ to an excited state $|i\rangle$ is

$$R_i = \frac{1}{2m_a f_a^2} \min(t, t_1, t_c) \int d^3 p \frac{d^3 n}{dp^3}(\vec{p}) |\langle i|(g_e \vec{S} + g_N \vec{I}) \cdot \vec{p}|0\rangle|^2 \tag{115}$$

on resonance. Here $\vec{S}$ is electron spin, t is the measurement integration time, t_1 is the lifetime of the excited state, and t_c is the coherence time of the signal. The latter is related to the energy dispersion of dark matter axions, $t_c \sim 1/\delta E$, as already discussed. The resonance condition is $m_a = E_i - E_0$, where E_i and E_0 are the energies of the two states. The detector bandwidth is $B = 1/\min(t, t_1)$. $(d^3 n/dp^3)(\vec{p})$ is the local axion momentum distribution. The local axion energy density is

$$\rho_a \simeq m_a \int d^3 p \frac{d^3 n}{dp^3}(\vec{p}). \tag{116}$$

We define g_i by

$$g_i^2 \overline{v^2} m_a \rho_a \equiv \int d^3 p \frac{d^3 n}{dp^3}(\vec{p}) |\langle i|(g_e \vec{S} + g_N \vec{I}) \cdot \vec{p}|0\rangle|^2, \tag{117}$$

where $\overline{v^2} \sim 10^{-6}$ is the average velocity squared of dark matter axions. g_i is a number of the order of 1 giving the coupling strength of the target atom. g_i depends on the atomic transition used, the direction of polarization of the atom, and the momentum distribution of the axions. It varies with time of day and of year since the momentum distribution changes on those timescales due to the motion of Earth.

For a mole of target atoms, the transition rate on resonance is

$$\begin{aligned} N_A R_i &= g_i^2 N_A \overline{v^2} \frac{\rho_a}{2f_a^2} \min(t, t_1, t_c) \\ &= \frac{535}{\text{s}} \left(\frac{\rho_a}{\text{GeV/cm}^3}\right) \left(\frac{10^{11} \text{ GeV}}{f_a}\right)^2 g_i^2 \left(\frac{\overline{v^2}}{10^{-6}}\right) \\ &\quad \times \frac{\min(t, t_1, t_c)}{\text{s}}, \end{aligned} \tag{118}$$

where N_A is Avogadro's number. There is an almost equal transition rate for the inverse process $|i\rangle \rightarrow |0\rangle$ with emission of an axion. It is proposed to allow axion absorptions only by cooling the target to a temperature T such that there are no atoms in the excited state. The requirement $N_A e^{-m_a/T} < 0.1$ implies that

$$T = 12 \text{ mK} \left(\frac{10^{11} \text{ GeV}}{f_a}\right). \tag{119}$$

The transitions are detected by shining a tunable laser on the target. The laser's frequency is set so that it causes transitions from state $|i\rangle$ to a highly excited state (with energy of the order of eV above the ground state) but does not cause such transitions from the ground state or any other low-lying state. When the atom deexcites, the associated photon is counted. The efficiency of this technique for counting atomic transitions is between 50% and 100%.

Consider a sweep in which the frequency is shifted by the bandwidth B after each measurement integration time t. The expected number of events per tune and per mole on resonance is $t N_A R_i$. If $B_a < B$, events occur during only one tune, whereas events occur during B_a/B successive tunes if $B_a > B$. Thus, the total number of events per mole during a sweep through the axion frequency $\nu_a = m_a/2\pi$ is

$$\frac{\text{events}}{\text{mole}} = t N_A R_i \frac{\min(t, t_1)}{\min(t, t_1, t_c)}. \tag{120}$$

To proceed at a reasonably fast pace, the search should cover a frequency range of the order of ν_a per year. Assuming a 30% duty cycle, one needs a search rate

$$\frac{B}{t} = \frac{1}{t \min(t, t_1)} = \frac{\nu_a}{0.3 \text{ yr}} = \frac{1.5 \text{ kHz}}{\text{s}} \left(\frac{10^{11} \text{ GeV}}{f_a}\right). \tag{121}$$

The expected number of events per sweep through the axion frequency is then

$$\frac{\text{events}}{\text{mole}} = 0.35 g_i^2 \left(\frac{\overline{v^2}}{10^{-6}}\right) \left(\frac{\rho_a}{\text{GeV/cm}^3}\right) \left(\frac{10^{11} \text{ GeV}}{f_a}\right). \quad (122)$$

Note that when the search rate is fixed, as in Eq. (121), the number of events per sweep through the axion frequency is independent of t, t_1, and t_c.

A suitable target material may be found among the numerous salts of transition group ions that have been studied extensively using electron paramagnetic resonance techniques (Abragam and Bleany, 1970). Braggio *et al.* (2017) carried out a pilot experiment on a a small crystal of YLiF$_4$ doped with Er^{3+} target ions at concentrations of 0.01% and 1%. They studied the heating of the sample by the laser and found that it did not produce an unmanageable background in the case studied.

E. Axion echo

Electromagnetic radiation of angular frequency equal to half the axion mass ($\omega = m_a/2$) stimulates the decay of axions to two photons and produces an echo, i.e., faint electromagnetic radiation traveling in the opposite direction. Hence, one may search for axion dark matter by sending to space a powerful beam of microwave radiation and listening for its echo (Arza and Sikivie, 2019). Stimulated axion decay is described next, first in the rest frame of a perfectly cold axion fluid, then in the case where the observer is moving with respect to a perfectly cold axion fluid, and finally in the case where the axion fluid has velocity dispersion.

1. Perfectly cold axion fluid at rest

In the rest frame of a perfectly cold axion fluid of density ρ the axion field is

$$a(t) = A \sin(m_a t), \quad (123)$$

with $\rho = (1/2) m_a^2 A^2$. In radiation gauge ($\vec{\nabla} \cdot \vec{A} = 0$), the second of Eqs. (23) becomes

$$(\partial_t^2 - \nabla^2)\vec{A} = -g(\vec{\nabla} \times \vec{A})\partial_t a. \quad (124)$$

We set $\epsilon = \mu = 0$ for simplicity. Let the vector potential of the outgoing radiation be

$$\vec{A}_0(\vec{x}, t) = \text{Re} \int d^3k \vec{A}_0(\vec{k}) e^{i(\vec{k}\cdot\vec{x} - \omega t)}, \quad (125)$$

where $\omega = |\vec{k}|$. In the presence of the axion fluid, $\vec{A}_0$ is itself a source of electromagnetic radiation $\vec{A}_1(\vec{x}, t)$:

$$(\partial_t^2 - \nabla^2)\vec{A}_1 = -g(\vec{\nabla} \times \vec{A}_0)\partial_t a + \mathcal{O}(g^2). \quad (126)$$

We therefore have

$$\vec{A}_1(\vec{x}, t) = \text{Re} \int d^3k \vec{A}_1(\vec{k}, t) e^{i\vec{k}\cdot\vec{x}}, \quad (127)$$

with

$$(\partial_t^2 + \omega^2)\vec{A}_1(\vec{k}, t) = -gAm_a \cos(m_a t) i\vec{k} \times \vec{A}_0(\vec{k}) e^{-i\omega t}. \quad (128)$$

The frequencies appearing on the rhs of Eq. (128) are $\omega \pm m_a$. Resonance occurs when $\omega - m_a = -\omega$, i.e., when $\omega = m_a/2$.

We now write

$$\vec{A}_1(\vec{k}, t) = \vec{\mathcal{A}}_1(\vec{k}, t) e^{i\omega t}. \quad (129)$$

In terms of $\vec{\mathcal{A}}_1$, Eq. (128) is

$$\partial_t \vec{\mathcal{A}}_1(\vec{k}, t) = -\frac{1}{4\omega} gAm_a \vec{k} \times \vec{A}_0(\vec{k}) e^{i(m_a - 2\omega)t} \quad (130)$$

when $\partial_t^2 \vec{\mathcal{A}}_1$ is neglected versus $\omega \partial_t \vec{\mathcal{A}}_1$ and only the resonance producing term is kept on the rhs. Solving Eq. (130) with $\vec{\mathcal{A}}_1(\vec{k}, 0) = 0$ yields

$$\vec{\mathcal{A}}_1(\vec{k}, t) = -\tfrac{1}{4} gAm_a \hat{k} \times \vec{A}_0(\vec{k}) e^{i\epsilon t} \frac{\sin(\epsilon t)}{\epsilon}, \quad (131)$$

where $\hat{k} = \vec{k}/\omega$ and $\epsilon = m_a/2 - \omega$. For large t,

$$\left(\frac{\sin(\epsilon t)}{\epsilon}\right)^2 \to \pi t \delta(\epsilon). \quad (132)$$

Hence, if we write the power in the outgoing $\vec{A}_0$ wave as

$$P_0 = \int d\omega \frac{dP_0}{d\omega}(\omega), \quad (133)$$

the power in the $\vec{A}_1$ wave is (Arza and Sikivie, 2019)

$$P_1 = \frac{1}{16} g^2 A^2 m_a^2 t \int d\omega \frac{dP_0}{d\omega}(\omega) \pi \delta(m_a/2 - \omega) = \frac{1}{16} g^2 \rho \frac{dP_0}{d\nu} t, \quad (134)$$

where $dP_0/d\nu$ is the spectral density of the outgoing power at frequency $\nu = \omega/2\pi = m_a/4\pi$.

Only outgoing power of frequency $\nu = m_a/4\pi$ stimulates axion decay and produces an echo. If the outgoing wave is stationary, with angular frequency $\omega = m_a/2$ and linear polarization $\vec{e}$,

$$\vec{A}_0(\vec{x}, t) = \text{Re}\left[e^{-i(m_a/2)t}\vec{e} \int_{|\vec{k}|=m_a/2} d^2k A_0(\vec{k}) e^{i\vec{k}\cdot\vec{x}}\right], \quad (135)$$

the echo wave is

$$\vec{A}_1(\vec{x}, t) = +\tfrac{1}{4} gAm_a t \text{Re}\left[e^{i(m_a/2)t}\vec{e} \times \int_{|\vec{k}|=m_a/2} d^2k \hat{k} A_0(\vec{k}) e^{i\vec{k}\cdot\vec{x}}\right]. \quad (136)$$

The echo wave is linearly polarized at 90° relative to the outgoing wave and traces it exactly backward in time since it has the same spatial Fourier transform but the opposite frequency. If the outgoing beam is emitted as a parallel beam of finite cross section, it will spread as a result of its transverse

wave vector components. The echo wave retraces the outgoing wave backward in time, returning to the location of emission of the outgoing wave with the latter's original transverse size. If the outgoing power P_0 is turned on for a time t and then turned off, the echo power P_1 given by Eq. (134) will last forever in the future under the assumption that the perfectly cold axion fluid has infinite spatial extent. In the rest frame of a perfectly cold axion fluid it does not matter in which direction P_0 is emitted. A finite amount of energy emitted at angular frequency $\omega = m_a/2$ in any direction produces an everlasting faint echo.

2. Perfectly cold axion fluid in motion

We next consider the case where the perfectly cold axion fluid is moving with velocity $\vec{v}$ with respect to the source of outgoing power. Nothing changes from the previous discussion except that each increment of outgoing energy $dE_0 = P_0 dt$ is emitted from a different location in the cold axion fluid rest frame. The incremental echo power, given by the rhs of Eq. (134) with t replaced by dt,

$$dP_1 = \frac{1}{16} g^2 \rho \frac{dP_0}{d\nu} dt, \qquad (137)$$

returns forever to the location in the axion fluid rest frame from which the increment dE_0 of outgoing energy was emitted. In the rest frame of the outgoing power source, the echo from outgoing power emitted a time t_e ago arrives displaced from the point of emission of the outgoing power by $\vec{d} = \vec{v}_\perp t_e$, where $\vec{v}_\perp$ is the component of $\vec{v}$ perpendicular to the direction $\hat{k}$ of emission. Figure 5 illustrates the relative
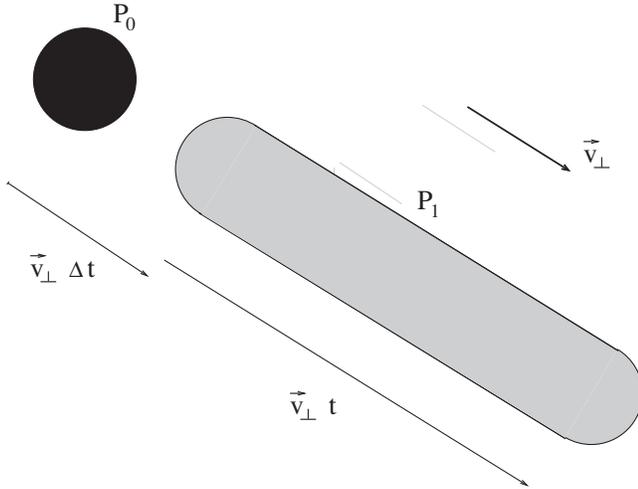
FIG. 5. Relative positions of the outgoing power and echo power in the scheme described in Sec. V.E. The figure is drawn in a reference frame where the outgoing power source is at rest and where a perfectly cold axion fluid moves with velocity $\vec{v}$. If the outgoing power P_0 is emitted in the direction perpendicular to the plane of the figure from the area of the black circle for a time t and is then turned off, the echo power P_1 arrives in the gray area at a time Δt after the outgoing power was turned off. The echo power lasts forever but moves away from the source of outgoing power with velocity $\vec{v}_\perp$, where $\vec{v}_\perp$ is the component of $\vec{v}$ transverse to the direction of emission of the outgoing power.

locations of the outgoing power and echo power in case the outgoing power is turned on for a while and then turned off. The echo moves away from the place of emission of the outgoing power with velocity $\vec{v}_\perp$. To detect as much echo power as possible at or near the place of emission of the outgoing power, the observer wants $\vec{v}_\perp$ to be as small as possible, i.e., $\hat{k}$ in the same direction as $\vec{v}$ or the opposite direction. In the frame of its source, the angular frequency at which the outgoing power stimulates axion decay is

$$\omega_0 = \frac{m_a}{2} (1 + \vec{v} \cdot \hat{k}) + \mathcal{O}(v^2), \qquad (138)$$

whereas

$$\omega_1 = \frac{m_a}{2} (1 - \vec{v} \cdot \hat{k}) + \mathcal{O}(v^2) \qquad (139)$$

is the angular frequency of the echo.

An attractive target for the echo method is the big flow, the locally prominent cold dark matter flow in the caustic ring model of the Milky Way halo. Its velocity vector $\vec{v}_{\mathrm{BF}}$ in a nonrotating galactic reference frame is given in Eq. (19). In a reference frame attached to the surface of Earth its velocity is

$$\vec{v}(t) = \vec{v}_{\mathrm{BF}} - \vec{v}_{\mathrm{LSR}} - \vec{v}_\odot - \vec{v}_\otimes(t), \qquad (140)$$

where $\vec{v}_{\mathrm{LSR}}$ is the velocity of the local standard of rest (LSR) in that same reference frame, $\vec{v}_\odot$ is the velocity of the Sun with respect to the LSR, and $\vec{v}_\otimes$ is the velocity of the observer with respect to the Sun as a result of the orbital and rotational motions of Earth. We are particularly interested in the extent to which the uncertainties in the several terms on the rhs of Eq. (140) affect our ability to minimize $\vec{v}_\perp$. $\vec{v}_\otimes(t)$ is known with great precision. The components of $\vec{v}_\odot$ are known with a precision of the order of 2 or 3 km/s. $\vec{v}_{\mathrm{LSR}}$ is in the direction of galactic rotation by definition. Its magnitude (often quoted to be 220 km/s) is known within an uncertainty of the order of 20 km/s. The magnitude of $\vec{v}_{\mathrm{BF}}$ scales with the magnitude of $\vec{v}_{\mathrm{LSR}}$ and has been estimated at approximately 520 km/s (Duffy and Sikivie, 2008). The direction of $\vec{v}_{\mathrm{BF}}$ is mostly in the direction of galactic rotation [see Eq. (19)] and is known with a precision of the order of 1° (Chakrabarty *et al.*, 2020). Therefore, we expect that it is possible to reduce $|\vec{v}_\perp|$ to approximately 5 km/s, the nominal value that we use later.

Consider a dish (such as a radio telescope) of radius R collecting echo power near the location of the outgoing power source. Because the echo from outgoing power emitted a time t_e ago is displaced by $\vec{d} = \vec{v}_\perp t_e$, the amount of echo power collected by the dish is

$$P_c = \frac{1}{16} g^2 \rho \frac{dP_0}{d\nu} C \frac{R}{|\vec{v}_\perp|}, \qquad (141)$$

where C is a number of the order of 1 that depends on the configuration of the source relative to the receiver dish

$$C = \frac{|\vec{v}_\perp|}{2RP_0} \int dt \int_{S_0} d^2 x I_0(\vec{x}) \Theta_c(\vec{x} + \vec{v}_\perp t). \qquad (142)$$

Here S_0 is the surface from which the outgoing power is emitted, $I_0(\vec{x})$ is the outgoing power per unit surface, and $\Theta_c(\vec{x})$ is a function that equals 1 if $\vec{x}$ belongs to the receiver dish area and 0 otherwise. For example, $C = 0.5$ if the outgoing power is emitted from the center of the receiver dish, whereas $C = 0.424$ if the outgoing power is emitted uniformly from the area of the receiver dish. However, neither of these configurations is likely to be optimal. It is probably better to place several source dishes around the receiver dish. C can be straightforwardly calculated for each configuration.

We assume that a pulse of outgoing power P_0, with frequency ν_0 and uniform spectral density $dP_0/d\nu = P_0/\Delta\nu_0$ over bandwidth $\Delta\nu_0$, is emitted during a time t_m. Provided that

$$t_m \gtrsim \frac{R}{2|\vec{v}_\perp|} = 0.5 \times 10^{-2} \text{ s} \frac{R}{50 \text{ m}} \frac{5 \text{ km/s}}{|\vec{v}_\perp|}, \quad (143)$$

echo power

$$P_c = 2.33 \times 10^{-31} P_0 \left(\frac{10 \text{ kHz}}{\Delta\nu_0}\right) \left(\frac{g_\gamma}{0.36}\right)^2 \left(\frac{10^{12} \text{ GeV}}{f_a}\right)^2$$
$$\times \left(\frac{\rho}{\text{GeV/cm}^3}\right) \left(\frac{C}{0.30}\right) \left(\frac{R}{50 \text{ m}}\right) \left(\frac{5 \text{ km/s}}{|\vec{v}_\perp|}\right), \quad (144)$$

is received over the same time interval t_m. Since the magnitude of the velocity of the big flow relative to us $v \simeq 520 - 220 \text{ km/s} = 300 \text{ km/s}$, the frequency of the echo power is redshifted or blueshifted from ν_0 by $\Delta\nu \simeq 2 \times 10^{-3} \nu_0$. The echo power has bandwidth $B = 2\delta v \nu < 5 \times 10^{-7} \nu$ since the velocity dispersion of the big flow is less than 70 m/s (Banik and Sikivie, 2016). The frequency range of interest is approximately 30 MHz to 30 GHz because Earth's atmosphere is mostly transparent at those frequencies. It corresponds to the mass range $2.5 \times 10^{-7} < m_a < 2.5 \times 10^{-4}$ eV, which happens to be prime hunting ground for QCD axions.

The cosmic microwave background and radio emission by astrophysical sources are irreducible sources of noise. In addition, there is instrumental noise. The total noise temperature depends on frequency, on the location of the telescope, and on the direction of observation. As an example we may consider the system noise temperature of the Green Bank Telescope[4]: approximately 20 K from 1 to 8 GHz, rising approximately linearly from 20 K at 8 GHz to 40 K at 30 GHz, and rising exponentially toward low frequencies from 20 K at 1 GHz to 100 K at 300 MHz. The rise at low frequencies is due to galactic emission and is strongly direction dependent. 100 K at 300 MHz is a typical value. The rise at high frequencies is due to atomic and molecular transitions in the atmosphere. It can be mitigated by placing the telescope at a high elevation. We use here a nominal system noise temperature of 20 K at all frequencies for the purpose of stating the results of our sensitivity calculations.

The signal to noise ratio with which the echo power is detected when ω_0 falls within the angular frequency range of the emitted power is given by Dicke's radiometer

---

[4]See https://science.nrao.edu/facilities/gbt/proposing/GBTpg.pdf.

equation (73). Combining Eqs. (144) and (73) and setting $B = 5 \times 10^{-7}\nu$, the total outgoing energy per logarithmic frequency interval necessary to detect the axion echo with a given signal to noise ratio is found to be

$$\left.\frac{dE_0}{d\ln\nu}\right|_{\text{BF}} = 7.2 \text{ MW yr} \left(\frac{s/n}{5}\right) \left(\frac{10 \text{ GHz}}{\nu}\right)^{1/2}$$
$$\times \left(\frac{0.36}{g_\gamma}\right)^2 \left(\frac{T_n}{20 \text{ K}}\right) \left(\frac{\text{GeV/cm}^3}{\rho}\right)$$
$$\times \left(\frac{0.30}{C}\right) \left(\frac{t_m}{10^{-2} \text{ s}}\right)^{1/2} \left(\frac{50 \text{ m}}{R}\right) \left(\frac{|v_\perp|}{5 \text{ km/s}}\right). \quad (145)$$

We used Eq. (3) and $m_a = 4\pi\nu$.

3. General axion fluid

In the most general case, the axion fluid is moving with respect to the observer and has velocity dispersion. Its density can be expressed as an integral over cold flows

$$\rho = \int d^3v \frac{d^3\rho}{dv^3}(\vec{v}). \quad (146)$$

Everything stated in Sec. V.E.2 holds true for each infinitesimal cold flow increment. The echo frequency has a spread $\delta\omega_- = (m/2)\delta v_\parallel$, where $\delta v_\parallel$ is the spread of axion velocities in the $\hat{k}$ direction. The echo of power emitted a time t_e ago is spread over a transverse size $\delta\vec{d} = \delta\vec{v}_\perp t_e$, where $\delta\vec{v}_\perp$ is the spread of axion velocities perpendicular to $\hat{k}$.

We now consider the isothermal model of the Milky Way, in particular. According to it, the dark matter has density 300 MeV/cm³ on Earth. Its velocity distribution is Gaussian and isotropic in a nonrotating galactic reference frame with dispersion $\sqrt{\vec{v}\cdot\vec{v}} = 270 \text{ km/s} \equiv \sqrt{3}\sigma$. In the LSR, the axion fluid moves with speed 220 km/s in the direction opposite that of galactic rotation. Assuming the direction $\hat{k}$ of the outgoing power is parallel (antiparallel) to the direction of galactic rotation the echo power is blueshifted (redshifted) in frequency by a fractional amount whose average is $\langle\Delta\nu/\nu\rangle \simeq 440 \text{ km/s} = 1.47 \times 10^{-3}$ and whose rms deviation is $\delta\nu/\nu = 2\sigma \simeq 1.04 \times 10^{-3}$. The echo from the outgoing energy that was emitted a time t_e ago is spread in space over a fuzzy circular region whose radius is Gaussian distributed with an average value σt_e. Equation (141) holds with $1/|\vec{v}_\perp|$ replaced by

$$\left\langle\frac{1}{|\vec{v}_\perp|}\right\rangle = \sqrt{\frac{\pi}{2}}\frac{1}{\sigma} = \frac{1}{124 \text{ km/s}}. \quad (147)$$

In view of Eq. (143) we now require $t_m > 2 \times 10^{-4}$ s $(R/50 \text{ m})$. Using Eq. (73) with $B = 4\sigma\nu = 2.1 \times 10^{-3}\nu$ and setting $\rho = 0.3$ GeV/cm³, we find that

$$\left.\frac{dE_0}{d\ln\nu}\right|_{\text{iso}} = 5.3 \text{ GW yr} \left(\frac{s/n}{5}\right) \left(\frac{10 \text{ GHz}}{\nu}\right)^{1/2} \left(\frac{0.36}{g_\gamma}\right)^2$$
$$\times \left(\frac{T_n}{20 \text{ K}}\right) \left(\frac{0.30}{C}\right) \left(\frac{t_m}{2 \times 10^{-4} \text{ s}}\right)^{1/2} \left(\frac{50 \text{ m}}{R}\right). \quad (148)$$

In the case of a known cold flow, the echo method appears to be an attractive approach because it uses relatively old technology and is applicable over a wide range of axion masses.

VI. SOLAR AXION DETECTION

The solar axion flux presents an attractive search opportunity. It has been pursued using a number of methods. Equations (15) and (16) provide an estimate of the flux on Earth of axions produced in the Sun by the Primakoff process.

A. The axion helioscope

Solar axions can be searched for by converting them to photons in a magnetic field (Sikivie, 1983, 1985; Van Bibber et al., 1987); see Sec. III. Multiplying the axion flux by the conversion probability Eq. (49) yields the photon flux

$$\Phi_\gamma = \frac{0.79}{\text{cm}^2\,\text{d}} \left(\frac{g_{a\gamma\gamma}}{10^{-10}\,\text{GeV}^{-1}}\right)^4 \left(\frac{L}{10\,\text{m}}\right)^2 \left(\frac{B_0}{10\,\text{T}}\right)^2 \quad (149)$$

for the case $qL \ll 1$, $\epsilon = \mu = 1$. The photons produced are x rays with approximately 4 keV average energy. They point back to the solar core. If a signal is found, it becomes possible to see directly into the solar interior. The inverse of the momentum transfer in the axion-photon conversion process is

$$\frac{1}{q} \simeq \frac{2E}{m_a^2} = 15.8\,\text{m}\left(\frac{10^{-2}\,\text{eV}}{m_a}\right)^2 \left(\frac{E}{4\,\text{keV}}\right). \quad (150)$$

The resonance condition $qL < 1$ is satisfied in vacuum for axion masses up to approximately 1.5×10^{-2} eV if $L = 10$ m. One may extend this range by introducing gas under pressure in the conversion region (Van Bibber et al., 1987), giving the photon an effective mass equal to the plasma frequency ω_{pl}. Alternatively one may make the magnetic field periodic with wavelength $d = 2\pi/q$.

Axion helioscope experiments have been carried out at Brookhaven National Laboratory (Lazarus et al., 1992), at the University of Tokyo (Moriyama et al., 1998; Inoue et al., 2002, 2008), and by the CAST Collaboration at CERN (Zioutas et al., 2005; Andriamonje et al., 2007; Arik et al., 2009; Anastassopoulos et al., 2017a). New experiments have been proposed by the IAXO (Armengaud et al., 2019; Dafni et al., 2019) and TASTE (Anastassopoulos et al., 2017b) collaborations. The Tokyo helioscope magnet (2.3 m long, 4 T field) was mounted on a platform that allowed the Sun to be tracked at all times. The CAST magnet tracks the Sun for only part of the day, approximately 1.5 h at sunrise and 1.5 h at sunset, but is longer (9.3 m) and more powerful (9 T). Both experiments have introduced He gas in the conversion region to extend the search range upward in axion mass (Inoue et al., 2008; Arik et al., 2014, 2015). The limits obtained by the CAST and Tokyo experiments are shown in Fig. 6 in rough outline. For details, see the original publications. Additional limits on axion couplings were obtained by the CAST Collaboration (Andriamonje et al., 2009, 2010) from a search for monoenergetic axions emitted in nuclear $M1$ transitions in
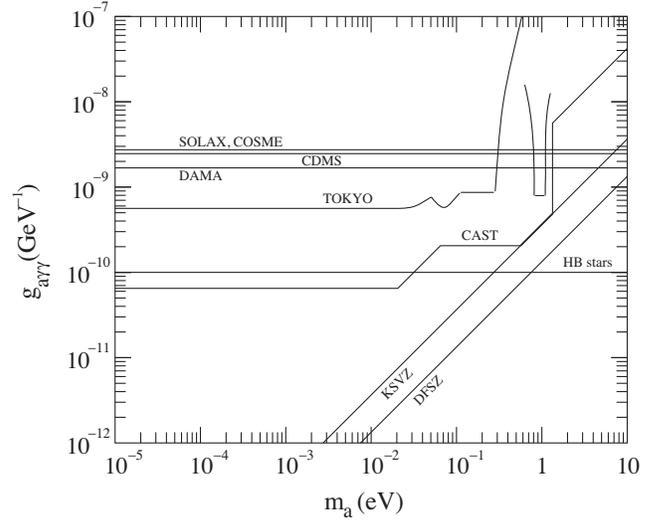
FIG. 6. Limits on the electromagnetic coupling $g_{a\gamma\gamma}$ obtained by the solar axion searches discussed in Sec. VI as a function of axion mass m_a. The relationship between mass and coupling in the KSVZ and DFSZ axion models and the limit from stellar evolution [horizontal branch (HB) stars] are shown as well. The Tokyo and CAST limits are indicated only in rough outline; for details see Inoue et al. (2008) and Anastassopoulos et al. (2017a).

the Sun. Axion emission rates in the $M1$ transitions of ^{57}Fe, ^{55}Mn, and ^{23}Na were calculated by Haxton and Lee (1991).

It has been proposed to search for solar axions converting to x rays in the magnetic field of Earth (Davoudiasl and Huber, 2006) or that of the Sun (Hong et al., 2019) using an x-ray detector placed in orbit around Earth or the Sun.

B. Axioelectric and Mössbauer effects

Solar axions may be searched for using the axioelectric effect, which is the same as the photoelectric effect but with an axion instead of a photon. It uses the coupling of the axion to the electron. Through this coupling, axions are produced in the Sun by axion bremsstrahlung, Compton-like scattering, and axion recombination. Theoretical discussions of the axioelectric effect were given by Zhitnitsky and Skovpen (1979), Dimopoulos, Starkman, and Lynn (1986), and Derevianko et al. (2010). Results from experimental searches were reported by Avignone et al. (1987), Ljubicic et al. (2004), Avignone (2009), Bellini et al. (2012), Abe et al. (2013), Alessandria et al. (2013), Armengaud et al. (2013), Derbin et al. (2013), Aprile et al. (2014), Akerib et al. (2017), Fu et al. (2017), Liu et al. (2017), and Wang et al. (2020). The bounds on the electron coupling obtained by these searches are of the order of

$$g_{a\bar{e}e} = g_e \frac{m_e}{f_a} \lesssim 10^{-11}. \quad (151)$$

The most severe limit reported is 3.5×10^{-12} (90% C.L.) (Akerib et al., 2017).

Solar axions may also be searched for by using the Mössbauer effect (De Rujula, and Zioutas, 1989; Moriyama, 1995). Nearly monochromatic axions are emitted

in nuclear transitions in the Sun, e.g., 14.4 keV axions in transitions between the first excited and ground states of ^{57}Fe. Such axions may be searched for by resonant absorption on the same nucleus on Earth. The nucleus emits an x ray when it deexcites. The process uses the coupling of axions to nucleons. An experimental search of this type was reported by Krcmar *et al.* (2001).

C. Primakoff effect

Solar axions may be searched for by converting them to photons in the Coulomb field of nuclei, i.e., the Primakoff effect. The cross section for Primakoff conversion of an axion to a photon in the Coulomb field of a nucleus can be obtained by repeating the steps of Sec. III.B but keeping the first term in $\vec{j}_a = g(\vec{E}_0 \times \vec{\nabla}a - \vec{B}_0 \partial_t a)$ instead of the second term, and setting $E_0(\vec{x}) = Ze\vec{x}/4\pi|\vec{x}|^3$. For $\epsilon = \mu = 1$, this yields

$$\frac{d\sigma}{d\Omega} = \frac{g^2 Z^2 \alpha}{4\pi \beta_a} \frac{\omega^2}{q^4}[q^2 - (\hat{n} \cdot \vec{q})^2], \qquad (152)$$

where $\vec{q} = \vec{k} - \vec{k}_a$, $\vec{k}_a = \omega \vec{\beta}_a$ is the initial axion momentum and $\vec{k} = \omega \hat{n}$ is the final photon momentum. The conversion rate on nuclei forming a crystal lattice is resonantly enhanced when the Bragg scattering condition is satisfied (Paschos and Zioutas, 1994). As Earth spins, the varying orientation of the detector with respect to the direction of the Sun produces a distinctive temporal pattern of the counting rate, which helps one to distinguish signal from background. Searches of this type have been carried out by the SOLAX Collaboration (Avignone *et al.*, 1998) in Sierra Grande, Argentina, the DAMA Collaboration (Bernabei *et al.*, 2001) in the Gran Sasso Laboratory, Italy, the COSME Collaboration (Morales *et al.*, 2002) in the Canfranc Laboratory, Spanish Pyrenees, and the CDMS Collaboration (Ahmed *et al.*, 2009) in the Soudan Underground Laboratory in Minnesota. The limits obtained are shown in Fig. 6.

VII. DICHROISM AND BIREFRINGENCE IN A MAGNETIC FIELD

The existence of an axion field causes the vacuum to be birefringent and dichroic in the presence of a magnetic field (Maiani, Petronzio, and Zavattini, 1986; Raffelt and Stodolsky, 1988). The purpose of this section is to derive these properties. A medium is called "birefringent" if it has different indices of refraction for the two states of linear polarization of light. It is "dichroic" if it has different absorption coefficients for those two states. In general, light traveling in the z direction has amplitude

$$\vec{A} = \text{Re}[(\mathcal{A}_x \hat{x} + \mathcal{A}_y \hat{y})e^{-i\omega t}], \qquad (153)$$

where $\mathcal{A}_x$ and $\mathcal{A}_y$ are complex numbers. Equation (153) implies that, as a function of time t, the vector $\vec{A}$ describes an ellipse in the x-y plane. By definition, the ellipticity of the light is the ratio of the minor to major axes of that ellipse. If the light is linearly polarized, $\mathcal{A}_x$ and $\mathcal{A}_y$ have the same phase and we may write $\mathcal{A}_x = \mathcal{A}\cos\alpha$, $\mathcal{A}_y = \mathcal{A}\sin\alpha$, where α is the

angle of the plane of polarization with the x axis. The ellipticity of such light is zero. When light that is initially linearly polarized travels through a birefringent material, the relative phase between $\mathcal{A}_x$ and $\mathcal{A}_y$ changes and the light acquires ellipticity. When light that is initially linearly polarized travels through a dichroic material, the plane of polarization rotates toward the direction with least absorption.

We recall that, even if there is no axion, the vacuum is birefringent in the presence of a magnetic field as a consequence of the box diagram of quantum electrodynamics. Euler and Heisenberg showed that it implies the effective interaction (Heisenberg and Euler, 1936; Itzykson and Zuber, 1980)

$$\mathcal{L}_{\text{EH}} = \frac{2\alpha^2}{45m_e^4}[(E^2 - B^2)^2 + 7(\vec{E} \cdot \vec{B})^2], \qquad (154)$$

as a consequence of which light traveling through a magnetic field $\vec{B}_0$ has different indices of refraction depending on whether it is polarized parallel or perpendicular to $\vec{B}_0$.

We assume that an axion exists and consider light traveling in the $\hat{z}$ direction in a constant magnetic field $\vec{B} = B_0\hat{x}$, and initially linearly polarized ($\vec{A}_{\text{in}}$) at an angle α relative to the direction of the magnetic field; see Fig. 7. In view of Sec. III, we expect the x component of light to become depleted by $\gamma \to a$ conversion, whereas the y component propagates as usual. Specifically, after a distance L, the magnitude of the x component of light is reduced as $|\mathcal{A}_x| \to [1 - (1/2)p(L)]|\mathcal{A}_x|$, where $p(L)$ is the conversion probability given in Eq. (44), whereas $|\mathcal{A}_y|$ is unchanged. The plane of polarization rotates therefore by the angle

$$\delta\alpha(L) = \tfrac{1}{4}p(L)\sin(2\alpha). \qquad (155)$$

In addition, the light acquires ellipticity because the relative phase between $\mathcal{A}_x$ and $\mathcal{A}_y$ changes (Maiani, Petronzio, and Zavattini, 1986; Raffelt and Stodolsky, 1988), i.e.,

$$\mathcal{A}_y \to \mathcal{A}_y, \qquad \mathcal{A}_x \to [1 - \tfrac{1}{2}p(L) + i\phi(L)]\mathcal{A}_x. \qquad (156)$$

In terms of $\phi(L)$, the acquired ellipticity is

$$e(L) = \tfrac{1}{2}|\phi(L)|\sin(2\alpha). \qquad (157)$$

Thus, if an axion exists, there is dichroism and a new source of birefringence in the presence of a magnetic field. We now derive the expression for the phase shift $\phi(L)$ (Maiani, Petronzio, and Zavattini, 1986). As a by-product, we rederive Eq. (44) for the conversion probability $p(L)$ later as well (Maiani, Petronzio, and Zavattini, 1986; Raffelt and Stodolsky, 1988).

Consider a region of homogeneous dielectric constant ϵ and homogeneous static external magnetic field $\vec{B}_0$. Axion-photon dynamics in such a region is described by the modified Maxwell's equations

$$\epsilon\vec{\nabla} \cdot \vec{E} = g\vec{B}_0 \cdot \vec{\nabla}a,$$
$$\vec{\nabla} \times \vec{B} - \epsilon\partial_t\vec{E} = -g\vec{B}_0\partial_t a, \qquad (158)$$

and the equation of motion for the axion field

(a)

(b)
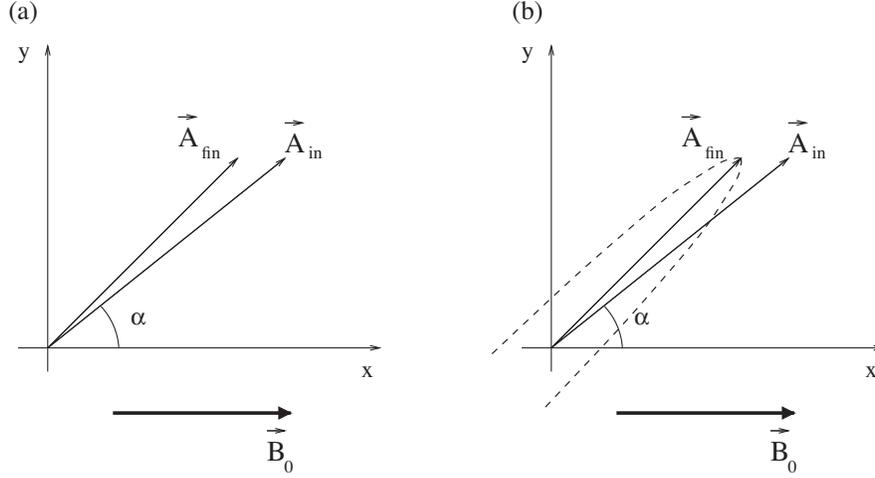
FIG. 7. Axion effects on the propagation of light in a magnetic field $\vec{B}_0$. Initially the light is linearly polarized in the direction $\vec{A}_{\rm in}$. Its direction of propagation is perpendicular to the plane. (a) The component of light polarized parallel to the magnetic field converts partially to axions, whereas the perpendicular component is unaffected. This causes a rotation of the plane of polarization away from the direction of the magnetic field. (b) In addition, a phase difference is induced between the parallel and perpendicular components, causing light that is initially linearly polarized to acquire ellipticity.

$$(\partial_t^2 - \vec{\nabla}^2 + m_a^2)a = -g\vec{B}_0 \cdot \vec{E}. \qquad (159)$$

We choose the gauge $\Phi = 0$. Any solution of Eqs. (158) and (159) is a linear superposition of plane waves

$$\vec{A}(\vec{x}, t) = \vec{\mathcal{A}}e^{i(\vec{k}\cdot\vec{x}-wt)}, \qquad \mathbf{a}(\vec{x}, t) = \mathbf{a}\, e^{i(\vec{k}\cdot\vec{x}-wt)}, \qquad (160)$$

where the relation between ω and $\vec{k}$ depends on the direction of polarization. Let $\vec{k} = k\hat{z}$, and let

$$\vec{B}_0 = B_{0z}\hat{z} + B_{0x}\hat{x}, \qquad \vec{\mathcal{A}} = \mathcal{A}_z\hat{z} + \mathcal{A}_x\hat{x} + \mathcal{A}_y\hat{y}. \qquad (161)$$

Equations (158) and (159) are equivalent to

$$i\omega\epsilon\mathcal{A}_z = +gB_{0z}\mathbf{a},$$
$$(k^2 - \epsilon\omega^2)\mathcal{A}_y = 0, \qquad (162)$$

and

$$k^2\begin{pmatrix} \mathcal{A}_x \\ \mathbf{a} \end{pmatrix} = \begin{pmatrix} \epsilon\omega^2 & +igB_{0x}\omega \\ -igB_{0x}\omega & \omega^2 - m_a^2 - \epsilon^{-1}g^2B_{0z}^2 \end{pmatrix}\begin{pmatrix} \mathcal{A}_x \\ \mathbf{a} \end{pmatrix}. \qquad (163)$$

Thus, the A_y mode propagates in the usual fashion, whereas the A_x mode oscillates into the axion field and vice versa. From Eq. (163), one finds the following k^2 eigenvalues for given ω:

$$k_{\pm}^2 = \frac{1}{2}\left[(\epsilon + 1)\omega^2 - m_a^2 - \frac{(gB_{0z})^2}{\epsilon} \pm \sqrt{\left((\epsilon - 1)\omega^2 + m_a^2 + \frac{(gB_{0z})^2}{\epsilon}\right)^2 + 4g^2B_{0x}^2\omega^2}\right]. \qquad (164)$$

The corresponding eigenmodes are proportional to

$$\begin{pmatrix} \mathcal{A}_x \\ \mathbf{a} \end{pmatrix}_{\pm} \equiv \begin{pmatrix} -igB_{0x}\omega \\ \epsilon\omega^2 - k_{\pm}^2 \end{pmatrix}. \qquad (165)$$

The general solution is therefore

$$\mathcal{A}_y = (\mathcal{A}_{y+}e^{ikz} + \mathcal{A}_{y-}e^{-ikz})e^{-i\omega t},$$
$$\begin{pmatrix} \mathcal{A}_x \\ \mathbf{a} \end{pmatrix} = \left[(\mathcal{A}_{++}e^{ik_+z} + \mathcal{A}_{+-}e^{-ik_+z})\begin{pmatrix} \mathcal{A}_x \\ \mathbf{a} \end{pmatrix}_{+} + (\mathcal{A}_{-+}e^{ik_-z} + \mathcal{A}_{--}e^{-ik_-z})\begin{pmatrix} \mathcal{A}_x \\ \mathbf{a} \end{pmatrix}_{-}\right]e^{-i\omega t}, \qquad (166)$$

where $\mathcal{A}_{y\pm}, \mathcal{A}_{+\pm}$ and $\mathcal{A}_{-\pm}$ are constants, and $k = \sqrt{\epsilon}\omega$.

We are interested in the solution describing a wave traveling in the $+\hat{z}$ direction, which is initially, at $z = 0$, a purely electromagnetic wave linearly polarized at an angle α relative to $\hat{x}$. For that case

$$\mathcal{A}_{y-} = \mathcal{A}_{+-} = \mathcal{A}_{--} = 0,$$
$$\mathcal{A}_y|_{z=0} = \mathcal{A}\sin\alpha\, e^{-i\omega t}, \qquad \mathcal{A}_x|_{z=0} = \mathcal{A}\cos\alpha\, e^{-i\omega t}, \qquad \mathbf{a}|_{z=0} = 0, \tag{167}$$

and therefore

$$A_y(z,t) = \mathrm{Re}[\mathcal{A}\sin\alpha\, e^{i(kz-\omega t)}],$$
$$A_x(z,t) = \mathrm{Re}\left[\frac{\mathcal{A}\cos\alpha}{k_+^2 - k_-^2}[(\epsilon\omega^2 - k_-^2)e^{i(k_+z-\omega t)} - (\epsilon\omega^2 - k_+^2)e^{i(k_-z-\omega t)}]\right],$$
$$a(z,t) = \mathrm{Re}\left[-i\mathcal{A}\cos\alpha\,\frac{gB_{0x}\omega}{k_+^2 - k_-^2}\left(e^{i(k_+z-\omega t)} - e^{i(k_-z-\omega t)}\right)\right]. \tag{168}$$

We used the identity $(\epsilon\omega^2 - k_-^2)(\epsilon\omega^2 - k_+^2) = -g^2 B_{0x}^2\omega^2$. From Eq. (168) one may obtain the energy fluxes in the axion field $\mathcal{P}_a(z) = \langle -\partial_t a\partial_z a\rangle$ and in each polarization state of the photon field: $\mathcal{P}_x(z) = \langle -\partial_t A_x\partial_z A_x\rangle$ and $\mathcal{P}_y(z) = \langle -\partial_t A_y\partial_z A_y\rangle$. The brackets indicate time averages. The $a \to \gamma$ conversion probability is found to be

$$p(z) = \frac{\mathcal{P}_a(z)}{\mathcal{P}_x(0)} = \frac{4g^2 B_{0x}^2\omega^2\sin^2[(k_+ - k_-)z/2]}{(k_+^2 - k_-^2)^2}\left[1 + \mathcal{O}\left(\frac{k_+ - k_-}{k}\right)\right]. \tag{169}$$

Since

$$gB_0 = \frac{\alpha}{\pi}\frac{g_\gamma}{f_a}B_0 = 1.63\times 10^{-16}\text{ eV}\left(\frac{10^7\text{ GeV}}{f_a}\right)\left(\frac{B_0}{10\text{ T}}\right)\left(\frac{g_\gamma}{0.36}\right), \tag{170}$$

$(gB_0)^2$ is much smaller than $\epsilon\omega^2$ and $\omega^2 - m_a^2$ in most cases of practical interest. If so, Eq. (164) becomes

$$k_+^2 = \epsilon\omega^2 + \frac{g^2 B_{0x}^2\omega^2}{(\epsilon-1)\omega^2 + m_a^2} + \mathcal{O}(g^4 B_0^4),$$
$$k_-^2 = \omega^2 - m_a^2 - \frac{g^2 B_{0z}^2}{\epsilon} - \frac{g^2 B_{0x}^2\omega^2}{(\epsilon-1)\omega^2 + m_a^2} + \mathcal{O}(g^4 B_0^4). \tag{171}$$

We then have

$$p(z) = \frac{g^2 B_{0x}^2}{\epsilon q^2}\sin^2\left(\frac{qz}{2}\right)\left[1 + \mathcal{O}\left(g^2 B_0^2, \frac{q}{k}\right)\right], \tag{172}$$

where

$$q = \sqrt{\epsilon}\omega - \sqrt{\omega^2 - m_a^2}. \tag{173}$$

Equation (172) agrees with Eq. (44) on resonace, i.e., when $q \to 0$ and hence $\beta_a \to \sqrt{\epsilon}$. Rewriting the second part of Eq. (168) in the form

$$A_x = \mathrm{Re}\{\mathcal{A}\cos\alpha[1 + \delta(z) + i\phi(z)]e^{i(kz-\omega t)}\}, \tag{174}$$

we find that $\delta(z) = -(1/2)p(z)$, as anticipated, and (Maiani, Petronzio, and Zavattini, 1986; Raffelt and Stodolsky, 1988)

$$\phi(z) = \frac{g^2 B_{0x}^2}{4\epsilon q^2}[qz - \sin(qz)]\left[1 + \mathcal{O}\left(g^2 B_0^2, \frac{q}{k}\right)\right] \tag{175}$$

for the phase shift.

Dichroism and birefringence of the vacuum in the presence of a magnetic field was searched for by the RBFT Collaboration at Brookaven National Laboratory (Cameron et al., 1993) and by the PVLAS Collaboration at the INFN National Laboratory in Legnaro, Italy (Zavattini et al., 2006, 2008). The sensitivity to optical rotation achieved in these experiments is of the order of 10^{-8} rad. The Cotton-Mouton and Voigt effects are important backgrounds. The Cotton-Mouton effect is the birefringence of liquids in the presence of a magnetic field transverse to the direction of propagation. The Voigt effect is the analogous effect in gases. The signal is enhanced by the use of an optical cavity that allows the laser beam to be passed through the magnetic field many times. Equation (155) is replaced in that case by

$$\delta\alpha(L) = \tfrac{1}{4}p(L)\sin(2\alpha)N, \tag{176}$$

where N is the number of passes through the magnet. With $N \sim 10^5$, $B\sim$ few Tesla, and $L \sim 10$ m, the sensitivity in g is of the order of $(10^7\text{ GeV})^{-1}$ when the resonance condition $qL < 1$ is satisfied. For laser light ($\omega \sim$ eV) in vacuum ($\epsilon = 1$) and $L \sim 10$ m, the resonance condition is satisfied when $m_a \lesssim 0.3$ meV. For $m_a > $ meV, the sensitivity to g decreases as m_a^{-2}. The PVLAS Collaboration claimed a signal (Zavattini et al. (2006)) but retracted it after additional measurements were made (Zavattini et al., 2008).

Zarei et al. (2019) and Shakeri, Marsh, and Xue (2020) proposed schemes to measure the birefringence of light due to

virtual axion exchange in a magnetic field or in a high intensity laser beam.

VIII. SHINING LIGHT THROUGH WALLS

Another approach to axion detection is $\gamma \to a$ conversion in a magnetic field followed by $a \to \gamma$ back-conversion, also in a magnetic field (Van Bibber et al., 1987). This type of experiment is commonly referred to as shining light through walls. If P_0 is the power of the laser and p and p' are the conversion probabilities in the magnets on the left-hand and right-hand sides of the wall, the power in regenerated photons is $P = p'pP_0$. Formulas for the conversion probabilities can be found in Sec. III. Shining light through walls experiments have been carried out by multiple groups (Ruoso et al., 1992; Robilliard et al., 2007; Afanasev et al., 2008; Chou et al., 2008; Pugnat et al., 2008; Ehret et al., 2010; Ballou et al., 2015). For $m_a < 3 \times 10^{-4}$ eV, the following limit on the axion coupling to two photons has been obtained (Ballou et al., 2015):

$$g_{a\gamma\gamma} < 3.5 \times 10^{-8} \text{ GeV}^{-1}. \qquad (177)$$

It is less severe than the limit from the CAST solar axion search (Andriamonje et al., 2007). This is due largely to the high intensity of the solar axion flux compared to the flux produced by photon conversion in a laboratory magnetic field, and the fact that solar axions have keV energies, whereas axions produced by lasers have eV energies. On the other hand, shining light through walls is a purely laboratory experiment and the previously described simple version can be improved upon.

A first improvement is to introduce an optical cavity in which the photons, on the axion production side of the wall, are bounced back and forth multiple times (Ruoso et al., 1992). Each photon in the cavity converts to axions with probability p for each pass through the cavity. If the reflectivity of the mirrors is $R = 1 - \eta$ and P_0 is the laser power, the power of the right-moving wave in the cavity is $(1/2\eta)P_0$. The axion power through the wall is then increased by the factor $1/2\eta$. Presently available mirrors may have η as small as 10^{-5}.

A further improvement (Hoogeveen and Ziegenhagen, 1991; Fukuda et al., 1996; Sikivie, Tanner, and van Bibber, 2007; Mueller et al., 2009) is to have tuned Fabry-Perot cavities on both sides of the wall. It is shown below that the probability of axion to photon conversion in the reconversion cavity is $(2/\pi)\mathcal{F}'p'$, where $\mathcal{F}'$ is the finesse of the reconversion cavity and p' is the reconversion probability in the absence of a cavity. The finesse of a cavity is $\mathcal{F} = \pi/\eta$ if the reflectivity of its mirrors is $R = 1 - \eta$. Including both improvements, the regenerated photon power is

$$P = \frac{1}{\eta'\eta} p'pP_0. \qquad (178)$$

Half of the power P is right moving and half is left moving. To detect all the regenerated photons, detectors should be installed on both sides of the regeneration cavity. We implicitly assume in Eq. (178) that the loss of power from the regeneration cavity is enirely due to transmission through its mirrors. In general there are other contributions, $\eta' = \eta'_{\text{trans}} + \eta'_{\text{abs}} + \eta'_{\text{scatt}}$, where the last two terms represent absorption and scattering (including diffraction) losses. If transmission is not entirely dominant, the rhs of Eq. (178) is multiplied by the factor $f = \eta'_{\text{trans}}/\eta'$. An experiment of this type, named ALPS II, is presently under construction at DESY (Bähre et al., 2013). A derivation (Mueller et al., 2009) of Eq. (178) follows.

The modes of a Fabry-Perot cavity are described in $\Phi = 0$ gauge by standing waves

$$\vec{A} = A\hat{x}\sin(kz)\cos(\omega t), \qquad (179)$$

with $k = \sqrt{\epsilon}\omega$. ϵ is the dielectric constant in the cavity. We set the magnetic permeability $\mu = 1$ for simplicity. The cavity has mirrors that enforce $E_x = 0$ at $z = 0$ and $z = L$. Thus, the wave vector has quantized values $k = \pi n/L$, with $n = 1, 2, 3, \ldots$. The energy stored in the cavity is

$$E = \tfrac{1}{4}SLA^2\epsilon\omega^2, \qquad (180)$$

where S is the transverse area of the standing wave. Equation (179) assumes that $kS \gg L$.

When a cavity mode $\vec{A} = \hat{x}A(t)\sin(kz)$ is not driven, its amplitude satisfies

$$\left(\frac{d^2}{dt^2} + \gamma\frac{d}{dt} + \omega^2\right)A(t) = 0. \qquad (181)$$

The quality factor is $Q = \omega/\gamma$. The power in the right-moving component is

$$P_+ = \tfrac{1}{8}SA^2\sqrt{\epsilon}\omega^2. \qquad (182)$$

If the mirrors have reflectivity $R = 1 - \eta$ and there are no other losses, the power emitted through the two mirrors is $2\eta P_+ = \gamma E$. Hence,

$$Q = L\frac{\sqrt{\epsilon}\omega}{\eta} = n\mathcal{F}, \qquad (183)$$

where $\mathcal{F}$ is the finesse.

In the presence of a large static magnetic field $\vec{B}_0$, the inhomogeneous Maxwell's equations (158) apply. The axion beam traveling through the regeneration cavity is described by

$$a(z, t) = a\sin(k_a z - \omega t). \qquad (184)$$

It is assumed to have the same transverse area S as the regeneration cavity mode. In practice, S varies along the beam path. The following calculation assumes that the axion wave and the photon wave in the regeneration cavity follow the profile of the hypothetically unimpeded photon wave in the production cavity. The power in the axion beam is

$$P_a = S\langle -\partial_t a\partial_z a\rangle = \tfrac{1}{2}Sa^2\omega k_a. \qquad (185)$$

Let $\vec{B}_0 = B_0\hat{x}$, and let $\vec{A}(z, t) = A(z, t)\hat{x}$. The first of Eqs. (158) is trivially satisfied, whereas the second becomes

$$\left(\epsilon\frac{\partial^2}{\partial t^2} - \frac{\partial^2}{\partial z^2}\right)A(z,t) = \omega g B_0 a \cos(k_a z - \omega t). \quad (186)$$

Since $A(0,t) = A(L,t) = 0$, we may expand

$$A(z,t) = \sum_{n=1}^{\infty} A_n(t) \sin\left(\frac{n\pi}{L}z\right). \quad (187)$$

Substituting back in Eq. (186) one finds that

$$\left(\frac{d^2}{dt^2} + \omega_n^2\right)A_n(t) = D \sin\left(\omega t + \frac{qL}{2}\right), \quad (188)$$

where $\omega_n = n\pi/\sqrt{\epsilon}L$ and

$$D = \frac{1}{\epsilon}g\omega B_0 a \frac{2}{Lq}\sin\left(\frac{qL}{2}\right). \quad (189)$$

$q = k_n - k_a = n\pi/L - \sqrt{\omega^2 - m_a^2}$ is the momentum transfer, as before. Nonresonant terms are neglected. When dissipation is included, Eq. (188) becomes

$$\left(\frac{d^2}{dt^2} + \gamma\frac{d}{dt} + \omega_n^2\right)A_n(t) = D \sin\left(\omega t + \frac{qL}{2}\right). \quad (190)$$

Up to transients, the solution is

$$A_n(t) = \frac{D \sin(\omega t - \phi)}{\sqrt{(\omega_n^2 - \omega^2)^2 + \omega^2\gamma^2}}, \quad (191)$$

with

$$\phi = -\frac{qL}{2} + \tan^{-1}\left(\frac{\omega\gamma}{\omega_n^2 - \omega^2}\right). \quad (192)$$

When the laser cavity and the regeneration cavity are tuned to the same frequency ($\omega_n = \omega$)

$$\vec{A} = \hat{x}A \sin\left(\frac{n\pi}{L}z\right)\sin\left(\omega t + \frac{qL}{2} - \frac{\pi}{2}\right), \quad (193)$$

with

$$A = \frac{D}{\omega\gamma} = \frac{gB_0 a}{\epsilon\gamma}\frac{2}{Lq}\sin\left(\frac{qL}{2}\right). \quad (194)$$

The energy E stored in the mode is given by Eq. (180). Dividing the power γE that the cavity emits by the axion power P_a, one obtains the axion to photon conversion probability

$$p_{FP} = \frac{2g^2 B_0^2}{\epsilon\beta_a\omega L}Q\frac{1}{q^2}\sin^2\left(\frac{qL}{2}\right). \quad (195)$$

In terms of the conversion probability p in the same region without cavity [Eq. (44) with $\mu = 1$] we have

$$p_{FP} = \frac{2Q}{\sqrt{\epsilon}L\omega}p = \frac{2\mathcal{F}}{\pi}p, \quad (196)$$

as announced.

Hoogeveen (1992), Caspers, Jaeckel, and Ringwald (2009), Bogorad et al. (2019), and Janish et al. (2019) proposed shining light through walls using microwaves instead of visible light. Axions are produced in one electromagnetic cavity permeated by a magnetic field and detected in an other.

IX. LONG-RANGE FORCES MEDIATED BY AXIONS

The exchange of virtual axions produces forces between macroscopic bodies that may manifest themselves as deviations from the $1/r^2$ gravitational law (Moody and Wilczek, 1984). It also produces effective interactions in atoms that slightly modify atomic spectroscopy (Weinberg, 1978).

The general form of the interaction of the axion with a Dirac fermion f is given in Eq. (8). It implies the interaction energy given in Eq. (9) in case the fermion is nonrelativistic. It also implies that the fermion is a source for the axion field

$$(\partial_t^2 - \nabla^2 + m_a^2)a(\vec{x},t) = +\frac{g_f}{2f_a}\vec{\nabla}\cdot[\chi^\dagger(\vec{x},t)\vec{\sigma}\chi(\vec{x},t)]$$
$$+ \frac{m_f\theta_f}{f_a}\chi^\dagger(\vec{x},t)\chi(\vec{x},t), \quad (197)$$

where $\chi(\vec{x},t)$ is the nonrelativistic fermion's two-component spinor field. We assume that a spin $1/2$ fermion is localized at $\vec{x}_1$ and that its spin state is slowly varying on the timescale set by m_a^{-1}. Equation (197) then implies

$$a(\vec{x}) = \frac{1}{f_a}\left(m_f\theta_f + \frac{g_f}{2}\vec{\sigma}\cdot\vec{\nabla}\right)\frac{e^{-m_a r}}{4\pi r}$$
$$= \frac{1}{f_a}\left[m_f\theta_f - \frac{g_f}{2}(\vec{\sigma}\cdot\hat{r})\left(m_a + \frac{1}{r}\right)\right]\frac{e^{-m_a r}}{4\pi r}, \quad (198)$$

where $\vec{r} = r\hat{r} = \vec{x} - \vec{x}_1$ and $\vec{\sigma}$ acts on the fermion spin state. We assume further that a second fermion f' is localized at $\vec{x}_2$. Equation (9) implies an interaction energy between the two fermions

$$V(\vec{x}_2 - \vec{x}_1; \vec{\sigma}, \vec{\sigma}') = \frac{1}{f_a}\left(-m_f'\theta_f' + \frac{g_f'}{2}\vec{\sigma}'\cdot\vec{\nabla}_2\right)a(\vec{x}_2 - \vec{x}_1), \quad (199)$$

where the primed quantities refer to the second fermion. Substituting Eq. (198) the interaction energy is seen to be the following sum of three terms:

$$V(\vec{x}_2 - \vec{x}_1; \vec{\sigma}, \vec{\sigma}') = V_{mon\text{-}mon} + V_{mon\text{-}dip} + V_{dip\text{-}dip}, \quad (200)$$

called "monopole-monopole," "monopole-dipole," and "dipole-dipole" interactions:

$$V_{\text{mon-mon}} = -\frac{m_f \theta_f m'_f \theta'_f}{f_a^2} \frac{e^{-m_a r}}{4\pi r},$$

$$V_{\text{mon-dip}} = -\frac{1}{f_a^2}[m_f \theta_f g'_f \vec{r} \cdot \vec{\sigma}' - m'_f \theta'_f g_f \vec{r} \cdot \vec{\sigma}]\frac{e^{-m_a r}}{8\pi r^2}\left(m_a + \frac{1}{r}\right),$$

$$V_{\text{dip-dip}} = -\frac{g_f g'_f}{4 f_a^2}\sigma_j \sigma'_k \left\{\delta_{jk}\left[\frac{e^{-m_a r}}{4\pi r^2}\left(m_a + \frac{1}{r}\right) + \frac{1}{3}\delta^3(\vec{r})\right]\right.$$
$$\left. - r_j r_k \frac{e^{-m_a r}}{4\pi r^3}\left(m_a^2 + 3\frac{m_a}{r} + 3\frac{1}{r^2}\right)\right\}, \qquad (201)$$

where $\vec{r} = \vec{x}_2 - \vec{x}_1$.

Relative to the gravitational potential $-G_N m_f m'_f / r$, the potential due to axion exchange is enhanced by the factor $(M_{\text{Planck}}/f_a)^2$ but has a finite range m_a^{-1}. When the coupling f_a^{-1} is large, the range m_a^{-1} is small, and vice versa. The monopole-monopole force is small at any rate compared to the gravitational force because it is suppressed by 2 powers of θ_f. Recall that θ_f are expected to be of the order of θ_{QCD}, and θ_{QCD} is less than 10^{-10} in view of the upper limit on the neutron electric dipole moment. If there is Peccei-Quinn symmetry and no other physics beyond the standard model, $\theta_{\text{QCD}} \sim 10^{-17}$ due to CP violation in the weak interactions. The dipole-dipole force is not suppressed by any powers of θ_f and is therefore relatively large. It has a background from ordinary magnetic forces but this background can be suppressed to some extent by using superconducting shields. The monopole-dipole force may be the most attractive target as it has only 1 factor of θ_f and does not have such a large background from ordinary magnetic forces.

The monopole-dipole force has been searched for using a variety of approaches, including torsion balance techniques (Ritter, Winkler, and Gillies, 1993; Hammond et al., 2007; Hoedl et al., 2011; Terrano et al., 2015), the effect of a large unpolarized mass on a nearby comagnetometer (Youdin et al., 1996; Lee, Almasi, and Romalis, 2018), its effect on a paramagnetic salt sample (Ni et al., 1999; Crescini et al., 2017), the spin relaxation of cold neutrons (Ignatovich and Pokotilovski, 2009; Serebrov et al., 2010) and ^{3}He nuclei (Guigue et al., 2015) due to their collisions with trap walls, the shift in the nuclear spin precession frequency due to the presence of a nearby unpolarized mass (Tullney et al., 2013), and the shifts in atomic energy levels due to P and T violating interactions (Stadnik, Dzuba, and Flambaum, 2018). These searches place lower bounds on $f_a/\sqrt{\theta_f}$ that reach of the order of 10^{15} GeV for ALPs that are massless or sufficiently light (Youdin et al., 1996; Tullney et al., 2013; Crescini et al., 2017; Lee, Almasi, and Romalis, 2018). The bounds do not reach QCD axions because the range of QCD axion mediated forces is too short in all cases.

The dipole-dipole force has been searched for using a variety of approaches as well, including the shifts in nuclear Zeeman frequency (Glenday et al., 2008) and nuclear precession frequency (Vasilakis et al., 2009) due to proximity with a polarized source, atomic spectroscopy (Ledbetter, Romalis, and Jackson-Kimball, 2013; Ficek et al., 2017), torsion balance techniques (Terrano et al., 2015), scanning tunneling microscopy (Luo et al., 2017), and the effect of a polarized source on a nearby comagnetometer (Lee et al.,

2018). The resulting lower bounds on f_a reach of the order of 10^5 GeV for ALPs that are massless or sufficiently light (Terrano et al., 2015; Lee et al., 2018). They do not reach QCD axions for the previously stated reason.

The ARIADNE experiment (Arvanitaki and Geraci, 2014) proposed to produce an oscillating axion field by rotating an unpolarized nonaxially symmetric macroscopic body at a frequency ω. The axion field produces an effective transverse magnetic field at the location of a nearby sample that is nuclear spin polarized by a laboratory magnetic field adjusted so that its Larmor frequency equals ω. The oscillating axion field then resonantly excites transverse magnetization in the polarized body. The transverse magnetization is detected by a SQUID magnetometer.

X. PHOTON FLUX FROM RELIC AXION DECAY

Through its electromagnetic coupling, the axion decays to two photons at the rate

$$\Gamma_{a\to 2\gamma} = g_\gamma^2 \frac{\alpha^2}{64\pi^3}\frac{m_a^3}{f_a^2} \simeq \frac{1.5 \times 10^{-50}}{s}\left(\frac{m_a}{10^{-5}\text{ eV}}\right)^5\left(\frac{g_\gamma}{0.36}\right)^2.$$
$$(202)$$

One may search for the photon flux from the decay of relic axions (Bershady, Ressell, and Turner, 1991; Ressell, 1991; Blout et al., 2001). The signal is largest when the decay rate is of the order of the Hubble rate today. If the decay rate is much larger, the axions have already decayed. If it is much less, too few axions are decaying at present. Equation (202) indicates that the largest signal is for an axion mass of the order of 10 eV. Such large axion masses are inconsistent with the constraints from laboratory searches and stellar evolution. We may, however, consider a broader class of ALPs. We assume that the ALP is a light pseudoscalar similar to the axion except that its coupling to two photons $g_{A\gamma\gamma}$ and its mass m_A are unrelated. We use A to indicate the ALP field.

The two photon coupling $g_{A\gamma\gamma}$, defined by

$$\mathcal{L}_{A\gamma\gamma} = -g_{A\gamma\gamma}A\vec{E}\cdot\vec{B}, \qquad (203)$$

is bounded from above by

$$g_{A\gamma\gamma} < 10^{-10}\text{ GeV}^{-1} \qquad (204)$$

by requiring that ALP emission does not excessively shorten the lifetimes of horizontal branch stars in globular clusters (Raffelt, 2008). In terms of this bound and the present age of the Universe $t_0 = 1.38 \times 10^{10}$ yr, the ALP decay rate is

$$\Gamma_{A\to 2\gamma} \simeq \frac{1}{t_0}\left(\frac{g_{A\gamma\gamma}}{10^{-10}\text{ GeV}^{-1}}\right)^2\left(\frac{m_A}{310\text{ eV}}\right)^3 \qquad (205)$$

assuming no other decay modes. ALPs are produced in the early Universe through processes analogous to those that produce axions. Both thermal and cold relic ALP populations may occur.

We now consider an aggregate of relic ALPs of total mass M, such as all ALPs that are part of a galaxy cluster.

The aggregate emits photons with frequency $\omega = (1/2)m_A$. Its luminosity is $L = M\Gamma_{A\to 2\gamma}$. In a flat static universe, the energy flux observed at a large distance r from the aggregate is $I = L/4\pi r^2$. Let S be the cross-sectional area of the aggregate as seen from the direction of the observer, and therefore let $\Delta\Omega = S/r^2$ be the subtended solid angle. We may write

$$M = \int_S d^2x \int dr\, \rho_A(\vec{r}) = \int_{\Delta\Omega} r^2 d\Omega \Sigma(\hat{n}), \quad (206)$$

where

$$\Sigma(\hat{n}) = \int dr\, \rho_A(\vec{r} = r\hat{n}) \quad (207)$$

is the column density in the direction $\hat{n}$. The energy flux per unit solid angle is therefore

$$\frac{dI}{d\Omega}(\hat{n}) = \Gamma_{A\to 2\gamma}\frac{dM}{4\pi r^2 d\Omega} = \frac{1}{4\pi}\Gamma_{A\to 2\gamma}\Sigma(\hat{n}). \quad (208)$$

Equation (208) is valid in a flat static space-time, or on sufficiently small scales in a curved space-time.

We next discuss how these equations are modified in an expanding homogeneous spatially flat universe. The metric is

$$ds^2 = -dt^2 + R(t)^2 d\vec{x} \cdot d\vec{x}, \quad (209)$$

where $R(t)$ is the cosmological scale factor. We assume that both the observer and aggregate occupy fixed positions in comoving coordinates. The light emitted at time t_E and observed at time t_0 travels a distance

$$r = xR(t_0) = \int_{t_E}^{t_0} dt \frac{R(t_0)}{R(t)}, \quad (210)$$

where x is the comoving coordinate distance between the observer and the source. Consider N photons emitted over a small time interval Δt_E and arriving at the observer over time interval Δt_0. Since

$$x = \int_{t_E + \Delta t_E}^{t_0 + \Delta t_0} dt \frac{1}{R(t)} \quad (211)$$

is unchanged, we have

$$\Delta t_0 = \Delta t_E \frac{R(t_0)}{R(t_E)}. \quad (212)$$

Therefore, the observed photons are redshifted to the angular frequency

$$\omega = \frac{m_A}{2} \frac{1}{1 + z_E}, \quad (213)$$

where

$$1 + z_E = \frac{R(t_0)}{R(t_E)}. \quad (214)$$

Equation (212) also implies that the N photons arrive at the observer at a rate that is $1/(1 + z_E)$ times the rate at which they are emitted. The observed energy flux is therefore

$$I = \frac{\Gamma_{A\to 2\gamma}M}{4\pi r^2} \frac{1}{(1 + z_E)^2}. \quad (215)$$

To obtain the energy flux per unit solid angle, we imagine that the source is spread over the sphere formed by all points that are at comoving coordinate distance x from the observer. At the time of emission the surface of that sphere is $4\pi x^2 R(t_E)^2$. Since the actual surface of the source is S, its solid angle as viewed from the observer is

$$\Delta\Omega = 4\pi \frac{S}{4\pi x^2 R(t_E)^2} = \frac{S}{r^2}(1 + z_E)^2. \quad (216)$$

Hence,

$$\frac{dI}{d\Omega}(\hat{n}) = \frac{\Gamma_{A\to 2\gamma}dMr^2}{4\pi r^2(1 + z_E)^2 dS(1 + z_E)^2} = \frac{\Gamma_{A\to 2\gamma}}{4\pi}\frac{\Sigma(\hat{n})}{(1 + z_E)^4}. \quad (217)$$

The wavelength of the observed light is

$$\lambda = \frac{4\pi}{m_A}(1 + z_E) = 2.4797\ \mu m\left(\frac{eV}{m_A}\right)(1 + z_E). \quad (218)$$

In general the light is not monochromatic because the ALPs are not at rest in their aggregate. If their velocity dispersion along the line of sight is $\delta v(\vec{n})$, we have

$$\frac{dI}{d\Omega d\lambda}(\hat{n}) = \frac{\Gamma_{A\to 2\gamma}m_A\Sigma(\hat{n})}{(4\pi)^2\delta v(\hat{n})(1 + z_E)^5} \quad (219)$$

since the linewidth is $\delta\lambda = \delta v\lambda$.

We assume that ALPs are the dark matter and consider the ALP aggregate associated with a galaxy cluster of mass $M = 10^{15}M_\odot$ and radius 1.3 Mpc. Its column density is of the order of $\Sigma \sim 0.04$ g/cm^2. Its line of sight velocity dispersion is of the order of $\delta v \sim 3 \times 10^{-3}$. If, for example, $m_A = 5$ eV and the two photon coupling saturates the bound from horizontal branch stars, we have $\Gamma_{A\to 2\gamma}^{-1} = 3.3 \times 10^{15}$ yr. In this case, the signal strength is

$$\frac{dI}{d\Omega d\lambda} \sim 4 \times 10^{-17} \frac{erg}{cm^2\ sec\ \text{Å}\ (arcsec)^2\ (1 + z_E)^5}. \quad (220)$$

This is of the same order of magnitude as the background due to air glow of the night sky (Bershady, Ressell, and Turner, 1991). The signal to noise ratio can be improved by looking at several clusters since the line from ALP decay appears at different wavelengths for the different clusters, at ratios determined by the known cluster redshifts, whereas the background due to air glow is approximately constant and can be approximately subtracted out. Results from searches for photons from relic ALP decay were reported by Bershady,

Ressell, and Turner (1991), Ressell (1991), and Blout *et al.* (2001).

XI. OPTICAL ACTIVITY OF A BACKGROUND AXION FIELD

The plane of polarization of light traveling through a space-time varying axion field rotates according to the rule

$$\Delta\Phi = \tfrac{1}{2}g\Delta a, \qquad (221)$$

where Δa is the variation of the axion field along the path traveled by the light and $\Delta\Phi$ is the angle by which the plane of polarization rotates in the clockwise direction when looking in the direction of propagation. Equation (221) assumes that the wavelength of light is short relative to the distance scale over which the axion field varies. A material is said to be "optically active" if it causes the plane of polarization to rotate as light travels through it. Optical activity occurs when right and left circularly polarized light satisfy slightly different dispersion laws. Faraday rotation is a well-known example. Unlike Faraday rotation, the optical activity of a background axion field is achromatic. Equation (221) is derived below.

The optical activity of a background axion field was first noted in studies of the propagation of light through an axion domain wall (Sikivie, 1984; Huang and Sikivie, 1985) and in the neighborhood of an axion string (Naculich, 1988; Harvey and Naculich, 1989). Carroll, Field, and Jackiw (1990) found that the vacuum is optically active in electrodynamics modified by the addition of a Chern-Simons term

$$\mathcal{L}_{\mathrm{CS}} = -\tfrac{1}{2}p_\alpha A_\beta(x)\tilde{F}^{\alpha\beta}(x) \qquad (222)$$

to the action density. p_α was introduced as an external Lorentz symmetry breaking parameter. Upon integration by parts, the axion-photon-photon interaction [Eq. (4)] is the Chern-Simons term with $p_\alpha = g\partial_\alpha a$. Therefore, the effect found by Carroll, Field, and Jackiw (1990) is the optical activity of a background axion field, arrived at from a somewhat different point of view.

To derive the effect, we consider Eqs. (21) in the limit where the axion field is slowly varying on the distance and timescale set by the wavelength of light. We take $\partial_t a$ and $\vec{\nabla}a$ to be constants, set $\rho_{\mathrm{el}} = \vec{j}_{\mathrm{el}} = 0$, and assume ϵ and μ to be constants as well. We may then look for solutions in which $\vec{E}$ and $\vec{B}$ are proportional to $e^{i\vec{k}\cdot\vec{x}-i\omega t}$. Equations (21) are satisfied provided that the complex amplitudes of the magnetic and electric fields satisfy

$$\vec{k}\times\vec{E} - \omega\vec{B} = 0,$$

$$\frac{1}{\mu}\vec{k}\times\vec{B} + \epsilon\omega\vec{E} = -ig(\vec{E}\times\vec{\nabla}a - \vec{B}\partial_t a). \qquad (223)$$

These two equations may be combined to yield

$$\left(\epsilon\omega^2 - \frac{1}{\mu}k^2\right)\vec{B} = ig\left(\partial_t a + \frac{\omega}{k^2}\vec{k}\cdot\vec{\nabla}a\right)\vec{k}\times\vec{B} + \mathcal{O}(g^2). \qquad (224)$$

Setting $\vec{k} = k\hat{z}$ and $\vec{B} = B_1\hat{x} + B_2\hat{y}$, we have

$$\begin{pmatrix} \epsilon\omega^2 - \frac{1}{\mu}k^2 & i\eta k \\ -i\eta k & \epsilon\omega^2 - \frac{1}{\mu}k^2 \end{pmatrix}\begin{pmatrix} B_1 \\ B_2 \end{pmatrix} = 0, \qquad (225)$$

where $\eta \equiv g[\partial_t a + (\omega/k^2)\vec{k}\cdot\vec{\nabla}a]$. The eigenmodes are therefore the right and left circular polarization amplitudes $B_\pm = B_1 \mp iB_2$, and

$$\omega_\pm = \frac{k}{\sqrt{\epsilon\mu}} \pm \frac{1}{2}\sqrt{\frac{\mu}{\epsilon}}\eta + \mathcal{O}(g^2) \qquad (226)$$

are the corresponding eigenfrequencies. This implies that the plane of polarization rotates at a rate (angle per unit time) equal to $(1/2)(\sqrt{\mu/\epsilon})\eta$ clockwise when looking in the direction of propagation. Since $\partial_t a + (\omega/k^2)\vec{k}\cdot\vec{\nabla}a$ is the rate of change of the axion field following the motion of the photon, the plane of polarization rotates by an angle

$$\Delta\Phi = \frac{1}{2}g\sqrt{\frac{\mu}{\epsilon}}\Delta a \qquad (227)$$

when the axion field changes by Δa. Equation (221) is for the particular case $\epsilon = \mu = 1$.

The direction of polarization of light from distant galaxies and quasars is observed to be correlated with the direction of their elongation on the sky (Haves and Conway, 1975; Clarke, Kronberg, and Simard-Normandin, 1980). That correlation disappears if there is excessive optical activity in the intervening space. The resulting upper limit on a constant $g\partial_0 a$ or $g\vec{\nabla}a$ is of the order of 6×10^{-26} GeV (Carroll, Field, and Jackiw, 1990). The axion is massive, and hence $a = 0$ on large scales. Outside of domain walls the axion field has no optical activity on average. However, a useful constraint can be placed on a massless Nambu-Goldstone boson ϕ associated with an exact global symmetry that is spontaneously broken by a vacuum expectation value v (Harari and Sikivie, 1992). Such a particle couples to two photons as in Eq. (203) with $g_{\phi\gamma\gamma} = c(\alpha/\pi v)$, where c is the electromagnetic anomaly of the symmetry of which ϕ is the Nambu-Goldstone boson. Provided that the ϕ field was not homogenized during an inflationary epoch, its values are uncorrelated from one horizon to the next, implying that $\Delta\phi \sim v\pi/2$, and therefore $\Delta\Phi \sim (c/2)(\alpha/4)$ on cosmological distances. Demanding that $\Delta\Phi < 10°$ to avoid destroying the observed correlation between the polarization and elongation of distant sources implies that $c \lesssim 100$.

DeRocco and Hook (2018) proposed searching for low mass ($m_A \sim 10^{-12}$ eV) ALP dark matter by detecting the optical activity that the slowly oscillating ALP field produces in large baseline optical interferometers. Obata, Fujita, and Michimura (2018) discussed the use of a ring cavity for this purpose.

ACKNOWLEDGMENTS

APPENDIX: UNITS AND CONVENTIONS

As in most particle physics treatises, we adopt units in which $\hbar = c = 1$. All dimensionful quantities are expressed in terms of a single unit, taken to be the electron volt, written as eV. The conversion factors to the standard macroscopic units of energy, mass, length, and time are

$$\text{eV} = 1.602 \times 10^{-12} \text{ erg,}$$
$$\text{eV}/c^2 = 1.783 \times 10^{-33} \text{ g,}$$
$$\hbar c/\text{eV} = 1.973 \times 10^{-5} \text{ cm,}$$
$$\hbar/\text{eV} = 6.582 \times 10^{-16} \text{ s.} \tag{A1}$$

For describing fields we use the Heaviside-Lorentz system of units, also of common use in particle physics. In Heaviside-Lorentz units, the permitivity and permeability of the vacuum $\epsilon_0 = \mu_0 = 1$. The fine structure constant α is related to the charge e of the electron by $\alpha = e^2/4\pi\hbar c$. All electric charges and currents have values $\sqrt{4\pi}$ times their values in Gaussian units; i.e., the Heaviside-Lorentz unit of electric charge is $1/\sqrt{4\pi}$ times the Gaussian unit. Electric fields and magnetic fields have values $1/\sqrt{4\pi}$ times their values in Gaussian units; i.e., the Heaviside-Lorentz units of electric and magnetic fields are $\sqrt{4\pi}$ times their Gaussian units. The electric and magnetic field units are the same when $c = 1$.

REFERENCES

Abbott, L., and P. Sikivie, 1983, Phys. Lett. **120B**, 133.

Abe, K., et al., 2013, Phys. Lett. B **724**, 46.

Abragam, A., and B. Bleany, 1970, Electronic Paramagnetic Resonance of Transition Ions (Oxford University Press, New York).

Adler, S. L., J. Colglazier, E. W., J. Healy, I. Karliner, J. Lieberman, Y. J. Ng, and H.-S. Tsao, 1975, Phys. Rev. D **11**, 3309.

Afanasev, A., O. Baker, K. Beard, G. Biallas, J. Boyce, M. Minarni, R. Ramdon, M. Shinn, and P. Slocum, 2008, Phys. Rev. Lett. **101**, 120401.

Ahmed, Z., et al. (CDMS Collaboration), 2009, Phys. Rev. Lett. **103**, 141802.

Ahn, D., O. Kwon, W. Chung, W. Jang, D. Lee, J. Lee, S. W. Youn, D. Youm, and Y. K. Semertzidis, 2019, arXiv:1904.05111.

Akerib, D., et al. (LUX Collaboration), 2017, Phys. Rev. Lett. **118**, 261301.

Alesini, D., et al., 2019a, Phys. Rev. D **99**, 101101.

Alesini, D., et al., 2019b, arXiv:1911.02427.

Alessandria, F., et al. (CUORE Collaboration), 2013, J. Cosmol. Astropart. Phys. 05, 007.

Al Kenany, S., et al., 2017, Nucl. Instrum. Methods Phys. Res., Sect. A **854**, 11.

Álvarez Melcón, A., et al., 2020, J. High Energy Phys. 07, 084.

Anastassopoulos, V., et al. (CAST Collaboration), 2017a, Nat. Phys. **13**, 584.

Anastassopoulos, V., et al. (TASTE Collaboration), 2017b, J. Instrum. **12**, P11019.

Andriamonje, S., et al. (CAST Collaboration), 2007, J. Cosmol. Astropart. Phys. 04, 010.

Andriamonje, S., et al. (CAST Collaboration), 2009, J. Cosmol. Astropart. Phys. 12, 002.

Andriamonje, S., et al. (CAST Collaboration), 2010, J. Cosmol. Astropart. Phys. 03, 032.

Anselm, A., 1985, Yad. Fiz. **42**, 1480.

Aprile, E., et al. (XENON100 Collaboration), 2014, Phys. Rev. D **90**, 062009; **95**, 029904(E) (2017).

Arias, P., D. Cadamuro, M. Goodsell, J. Jaeckel, J. Redondo, and A. Ringwald, **2012**, J. Cosmol. Astropart. Phys. 06, 013.

Arik, E., et al. (CAST Collaboration), 2009, J. Cosmol. Astropart. Phys. 02, 008.

Arik, M., et al. (CAST Collaboration), 2014, Phys. Rev. Lett. **112**, 091302.

Arik, M., et al. (CAST Collaboration), 2015, Phys. Rev. D **92**, 021101.

Armengaud, E., et al., 2013, J. Cosmol. Astropart. Phys. 11, 067.

Armengaud, E., et al. (IAXO Collaboration), 2019, J. Cosmol. Astropart. Phys. 06, 047.

Arvanitaki, A., M. Baryakhtar, and X. Huang, 2015, Phys. Rev. D **91**, 084011.

Arvanitaki, A., S. Dimopoulos, S. Dubovsky, N. Kaloper, and J. March-Russell, 2010, Phys. Rev. D **81**, 123530.

Arvanitaki, A., S. Dimopoulos, and K. Van Tilburg, 2018, Phys. Rev. X **8**, 041001.

Arvanitaki, A., and S. Dubovsky, 2011, Phys. Rev. D **83**, 044026.

Arvanitaki, A., and A. A. Geraci, 2014, Phys. Rev. Lett. **113**, 161801.

Arza, A., and P. Sikivie, 2019, Phys. Rev. Lett. **123**, 131804.

Asztalos, S., et al. (ADMX Collaboration), 2004, Phys. Rev. D **69**, 011101.

Asztalos, S., et al. (ADMX Collaboration), 2010, Phys. Rev. Lett. **104**, 041301.

Asztalos, S., et al. (ADMX Collaboration), 2011, Nucl. Instrum. Methods Phys. Res., Sect. A **656**, 39.

Asztalos, S. J., L. J. Rosenberg, K. van Bibber, P. Sikivie, and K. Zioutas, 2006, Annu. Rev. Nucl. Part. Sci. **56**, 293.

Asztalos, S. J., et al. (ADMX Collaboration), 2001, Phys. Rev. D **64**, 092003.

Asztalos, S. J., et al. (ADMX Collaboration), 2002, Astrophys. J. Lett. **571**, L27.

Avignone, F., R. Creswick, and J. Vergados, 2018, arXiv: 1801.02072.

Avignone, F., R. Creswick, J. Vergados, P. Pirinen, P. Srivastava, and J. Suhonen, 2018, J. Cosmol. Astropart. Phys. 01, 021.

Avignone III, F. T. , 2009, Phys. Rev. D **79**, 035015.

Avignone III, F. T., R. Brodzinski, S. Dimopoulos, G. Starkman, A. Drukier, D. Spergel, G. Gelmini, and B. Lynn, 1987, Phys. Rev. D **35**, 2752.

Avignone III, F. T., et al. (SOLAX Collaboration), 1998, Phys. Rev. Lett. **81**, 5068.

Ayala, A., I. Domínguez, M. Giannotti, A. Mirizzi, and O. Straniero, 2014, Phys. Rev. Lett. **113**, 191302.

Bähre, R., et al., 2013, J. Instrum. **8**, T09001.

Baker, O. K., M. Betz, F. Caspers, J. Jaeckel, A. Lindner, A. Ringwald, Y. Semertzidis, P. Sikivie, and K. Zioutas, 2012, Phys. Rev. D **85**, 035018.

Ballou, R., et al. (OSQAR Collaboration), 2015, Phys. Rev. D **92**, 092002.

Baluni, V., 1979, Phys. Rev. D **19**, 2227.

Banik, N., and P. Sikivie, 2016, Phys. Rev. D **93**, 103509.

Barbieri, R., C. Braggio, G. Carugno, C. Gallo, A. Lombardi, A. Ortolan, R. Pengo, G. Ruoso, and C. Speake, 2017, Phys. Dark Universe **15**, 135.

Barbieri, R., M. Cerdonio, G. Fiorentini, and S. Vitale, 1989, Phys. Lett. B **226**, 357.

Bardeen, W. A., and S.-H. Tye, 1978, Phys. Lett. B **74B**, 229.

Baryakhtar, M., J. Huang, and R. Lasenby, 2018, Phys. Rev. D **98**, 035006.

Bellini, G., *et al.* (Borexino Collaboration), 2012, Phys. Rev. D **85**, 092003.

Berlin, A., R. T. D'Agnolo, S. A. Ellis, C. Nantista, J. Neilson, P. Schuster, S. Tantawi, N. Toro, and K. Zhou, 2020, J. High Energy Phys. 07 088.

Bernabei, R., *et al.*, 2001, Phys. Lett. B **515**, 6.

Bershady, M. A., M. Ressell, and M. S. Turner, 1991, Phys. Rev. Lett. **66**, 1398.

Blinnikov, S., and N. Dunina-Barkovskaya, 1994, Mon. Not. R. Astron. Soc. **266**, 289.

Blout, B., E. Daw, M. Decowski, P. T. Ho, L. Rosenberg, and D. Yu, 2001, Astrophys. J. **546**, 825.

Bogorad, Z., A. Hook, Y. Kahn, and Y. Soreq, 2019, Phys. Rev. Lett. **123**, 021801.

Boutan, C., *et al.* (ADMX Collaboration), 2018, Phys. Rev. Lett. **121**, 261302.

Bradley, R., 1999, Nucl. Phys. B, Proc. Suppl. **72**, 137.

Bradley, R., J. Clarke, D. Kinion, L. Rosenberg, K. van Bibber, S. Matsuki, M. Muck, and P. Sikivie, 2003, Rev. Mod. Phys. **75**, 777.

Braggio, C., *et al.*, 2017, Sci. Rep. **7**, 15168.

Braine, T., *et al.* (ADMX Collaboration), 2020, Phys. Rev. Lett. **124**, 101303.

Brockway, J. W., E. D. Carlson, and G. G. Raffelt, 1996, Phys. Lett. B **383**, 439.

Brubaker, B., L. Zhong, S. Lamoreaux, K. Lehnert, and K. van Bibber, 2017, Phys. Rev. D **96**, 123008.

Brubaker, B., *et al.*, 2017, Phys. Rev. Lett. **118**, 061302.

Brun, P., *et al.* (MADMAX Collaboration), 2019, Eur. Phys. J. C **79**, 186.

Budker, D., P. W. Graham, M. Ledbetter, S. Rajendran, and A. Sushkov, 2014, Phys. Rev. X **4**, 021030.

Caldwell, A., G. Dvali, B. Majorovits, A. Millar, G. Raffelt, J. Redondo, O. Reimann, F. Simon, and F. Steffen (MADMAX Working Group), 2017, Phys. Rev. Lett. **118**, 091801.

Cameron, R., *et al.*, 1993, Phys. Rev. D **47**, 3707.

Carroll, S. M., G. B. Field, and R. Jackiw, 1990, Phys. Rev. D **41**, 1231.

Caspers, F., J. Jaeckel, and A. Ringwald, 2009, J. Instrum. **4**, P11013.

Catelan, M., J. Freitas Pacheco, and J. Horvath, 1996, Astrophys. J. **461**, 231.

Chakrabarty, S. S., Y. Han, A. Gonzalez, and P. Sikivie, 2020, arXiv:2007.10509.

Chaudhuri, S., K. Irwin, P. W. Graham, and J. Mardon, 2018, arXiv:1803.01627.

Chaudhuri, S., K. D. Irwin, P. W. Graham, and J. Mardon, 2019, arXiv:1904.05806.

Cheng, T., and L. Li, 1984, *Gauge Theory of Elementary Particle Physics* (Oxford University Press, New York).

Chigusa, S., T. Moroi, and K. Nakayama, 2020, Phys. Rev. D **101**, 096013.

Chou, A. S., *et al.* [GammeV (T-969) Collaboration], 2008, Phys. Rev. Lett. **100**, 080402.

Chu, P.-H., L. Duffy, Y. Kim, and I. Savukov, 2018, Phys. Rev. D **97**, 072011.

Clarke, J., P. Kronberg, and M. Simard-Normandin, 1980, Mon. Not. R. Astron. Soc. **190**, 205.

Conlon, J. P., F. Day, N. Jennings, S. Krippendorf, and M. Rummel, 2017, J. Cosmol. Astropart. Phys. 07, 005.

Crescini, N., C. Braggio, G. Carugno, P. Falferi, A. Ortolan, and G. Ruoso, 2017, Phys. Lett. B **773**, 677.

Crescini, N., *et al.*, 2018, Eur. Phys. J. C **78**, 703; **78**, 813(E) (2018).

Crescini, N., *et al.* (QUAX Collaboration), 2020, Phys. Rev. Lett. **124**, 171801.

Crewther, R., P. Di Vecchia, G. Veneziano, and E. Witten, 1979, Phys. Lett. **88B**, 123; **91B**, 487(E) (1980).

Crisosto, N., G. Rybka, P. Sikivie, N. Sullivan, D. Tanner, and J. Yang, 2020, Phys. Rev. Lett. **124**, 241101.

Crisosto, N., P. Sikivie, N. Sullivan, and D. Tanner, 2018, Springer Proc. Phys. **211**, 127.

Csaki, C., N. Kaloper, and J. Terning, 2002, Phys. Rev. Lett. **88**, 161302.

Dafni, T., C. A. O'Hare, B. Lakić, J. Galán, F. J. Iguaz, I. G. Irastorza, K. Jakovčic, G. Luzón, J. Redondo, and E. Ruiz Chóliz, 2019, Phys. Rev. D **99**, 035037.

Davoudiasl, H., and P. Huber, 2006, Phys. Rev. Lett. **97**, 141302.

De Angelis, A., O. Mansutti, and M. Roncadelli, 2008, Phys. Lett. B **659**, 847.

De Angelis, A., M. Roncadelli, and O. Mansutti, 2007, Phys. Rev. D **76**, 121301.

De Panfilis, S., A. Melissinos, B. Moskowitz, J. Rogers, Y. Semertzidis, W. Wuensch, H. Halama, A. Prodell, W. Fowler, and F. Nezrick, 1987, Phys. Rev. Lett. **59**, 839.

Derbin, A., S. Bakhlanov, I. Dratchnev, A. Kayunov, and V. Muratova, 2013, Eur. Phys. J. C **73**, 2490.

Derevianko, A., V. Dzuba, V. Flambaum, and M. Pospelov, 2010, Phys. Rev. D **82**, 065006.

DeRocco, W., and A. Hook, 2018, Phys. Rev. D **98**, 035021.

De Rujula, A., and K. Zioutas, 1989, Phys. Lett. B **217**, 354.

Di Luzio, L., M. Giannotti, E. Nardi, and L. Visinelli, 2020, Phys. Rep. **870**, 1.

Dimopoulos, S., G. Starkman, and B. Lynn, 1986, Phys. Lett. **168B**, 145.

Dine, M., P. Draper, L. Stephenson-Haskins, and D. Xu, 2017, Phys. Rev. D **96**, 095001.

Dine, M., and W. Fischler, 1983, Phys. Lett. **120B**, 137.

Dine, M., W. Fischler, and M. Srednicki, 1981, Phys. Lett. **104B**, 199.

Donnelly, T., S. Freedman, R. Lytel, R. Peccei, and M. Schwartz, 1978, Phys. Rev. D **18**, 1607.

Donoghue, J., E. Golowich, and B. R. Holstein, 2014, *Dynamics of the Standard Model*, Vol. 2, Cambridge Monographs on Particle Physics, Nuclear Physics and Cosmology Vol. 35 (Cambridge University Press, Cambridge, England).

Du, N., *et al.* (ADMX Collaboration), 2018, Phys. Rev. Lett. **120**, 151301.

Duffy, L., and P. Sikivie, 2008, Phys. Rev. D **78**, 063508.

Duffy, L., P. Sikivie, D. Tanner, S. J. Asztalos, C. Hagmann, D. Kinion, L. Rosenberg, K. van Bibber, D. Yu, and R. Bradley, 2005, Phys. Rev. Lett. **95**, 091304.

Duffy, L. D., P. Sikivie, D. Tanner, S. J. Asztalos, C. Hagmann, D. Kinion, L. Rosenberg, K. van Bibber, D. Yu, and R. Bradley (ADMX Collaboration), 2006, Phys. Rev. D **74**, 012006.

Ehret, K., *et al.*, 2010, Phys. Lett. B **689**, 149.

Ellis, J. R., and M. K. Gaillard, 1978, Phys. Lett. **74B**, 374.

Ellis, J. R., and M. K. Gaillard, 1979, Nucl. Phys. **B150**, 141.

Ellis, J. R., and K. A. Olive, 1987, Phys. Lett. B **193**, 525.

Erken, O., P. Sikivie, H. Tam, and Q. Yang, 2012, Phys. Rev. D **85**, 063520.

Ficek, F., D. F. J. Kimball, M. Kozlov, N. Leefer, S. Pustelny, and D. Budker, 2017, Phys. Rev. A **95**, 032505.

Flambaum, V., I. Samsonov, H. Tran Tan, and D. Budker, 2018, Phys. Rev. D **98**, 095028.

Flower, G., J. Bourhill, M. Goryachev, and M. E. Tobar, 2019, Phys. Dark Universe **25**, 100306.

Fu, C., *et al.* (PandaX Collaboration), 2017, Phys. Rev. Lett. **119**, 181806.

Fukuda, Y., T. Kohmoto, S. i. Nakajima, and M. Kunitomo, 1996, Prog. Cryst. Growth Charact. Mater. **33**, 363.

Garcon, A., *et al.*, 2018, Quantum Sci. Technol. **3**, 014008.

Georgi, H., H. R. Quinn, and S. Weinberg, 1974, Phys. Rev. Lett. **33**, 451.

Georgi, H., and L. Randall, 1986, Nucl. Phys. **B276**, 241.

Glenday, A. G., C. E. Cramer, D. F. Phillips, and R. L. Walsworth, 2008, Phys. Rev. Lett. **101**, 261801.

Goldman, J., and C. Hoffman, 1978, Phys. Rev. Lett. **40**, 220.

Goryachev, M., B. McAllister, and M. E. Tobar, 2019, Phys. Dark Universe **26**, 100345.

Graham, P. W., and S. Rajendran, 2013, Phys. Rev. D **88**, 035023.

Grifols, J., E. Masso, and R. Toldra, 1996, Phys. Rev. Lett. **77**, 2372.

Guigue, M., D. Jullien, A. Petukhov, and G. Pignol, 2015, Phys. Rev. D **92**, 114001.

Hagmann, C., P. Sikivie, N. Sullivan, and D. Tanner, 1990, Phys. Rev. D **42**, 1297(R).

Hagmann, C., P. Sikivie, N. Sullivan, D. Tanner, and S. Cho, 1990, Rev. Sci. Instrum. **61**, 1076.

Hagmann, C., *et al.* (ADMX Collaboration), 1998, Phys. Rev. Lett. **80**, 2043.

Hagmann, C. A., 1990, Ph.D. thesis (University of Florida).

Hammond, G., C. Speake, C. Trenkel, and A. Pulido Paton, 2007, Phys. Rev. Lett. **98**, 081101.

Harari, D., and P. Sikivie, 1992, Phys. Lett. B **289**, 67.

Harvey, J. A., and S. G. Naculich, 1989, Phys. Lett. B **217**, 231.

Haves, P., and R. Conway, 1975, Mon. Not. R. Astron. Soc. **173**, 53P.

Haxton, W., and K. Lee, 1991, Phys. Rev. Lett. **66**, 2557.

Heisenberg, W., and H. Euler, 1936, Z. Phys. **98**, 714.

Hoedl, S., F. Fleischer, E. Adelberger, and B. Heckel, 2011, Phys. Rev. Lett. **106**, 041801.

Hong, J., *et al.*, 2019, Proc. SPIE Int. Soc. Opt. Eng. **11118**, 1111810.

't Hooft, G., 1976a, Phys. Rev. D **14**, 3432; **18**, 2199(E) (1978).

't Hooft, G., 1976b, Phys. Rev. Lett. **37**, 8.

Hoogeveen, F., 1992, Phys. Lett. B **288**, 195.

Hoogeveen, F., and T. Ziegenhagen, 1991, Nucl. Phys. **B358**, 3.

Hook, A., Y. Kahn, B. R. Safdi, and Z. Sun, 2018, Phys. Rev. Lett. **121**, 241102,.

Horns, D., J. Jaeckel, A. Lindner, A. Lobanov, J. Redondo, and A. Ringwald, 2013, J. Cosmol. Astropart. Phys. 04, 016.

Horns, D., L. Maccione, M. Meyer, A. Mirizzi, D. Montanino, and M. Roncadelli, 2012, Phys. Rev. D **86**, 075024.

Hoskins, J., *et al.*, 2011, Phys. Rev. D **84**, 121302.

Hoskins, J., *et al.*, 2016, Phys. Rev. D **94**, 082001.

Huang, F. P., K. Kadota, T. Sekiguchi, and H. Tashiro, 2018, Phys. Rev. D **97**, 123001.

Huang, M., and P. Sikivie, 1985, Phys. Rev. D **32**, 1560.

Ignatovich, V., and Y. Pokotilovski, 2009, Eur. Phys. J. C **64**, 19.

Inoue, Y., Y. Akimoto, R. Ohta, T. Mizumoto, A. Yamamoto, and M. Minowa, 2008, Phys. Lett. B **668**, 93.

Inoue, Y., T. Namba, S. Moriyama, M. Minowa, Y. Takasu, T. Horiuchi, and A. Yamamoto, 2002, Phys. Lett. B **536**, 18.

Ioannisian, A. N., N. Kazarian, A. J. Millar, and G. G. Raffelt, 2017, J. Cosmol. Astropart. Phys. 09, 005.

Ipser, J., and P. Sikivie, 1983, Phys. Rev. Lett. **50**, 925.

Irastorza, I. G., and J. Redondo, 2018, Prog. Part. Nucl. Phys. **102**, 89.

Itzykson, C., and J. Zuber, 1980, *Quantum Field Theory*, International Series in Pure and Applied Physics (McGraw-Hill, New York).

Jackson, J. D., 1998, *Classical Electrodynamics* (Wiley, New York).

Janish, R., V. Narayan, S. Rajendran, and P. Riggins, 2019, Phys. Rev. D **100**, 015036.

Jeong, J., S. Youn, S. Ahn, C. Kang, and Y. K. Semertzidis, 2018, Astropart. Phys. **97**, 33.

Jeong, J., S. Youn, S. Ahn, J. E. Kim, and Y. K. Semertzidis, 2018, Phys. Lett. B **777**, 412.

Kahn, Y., B. R. Safdi, and J. Thaler, 2016, Phys. Rev. Lett. **117**, 141801.

Kandaswamy, J., P. Salomonson, and J. Schechter, 1978, Phys. Rev. D **17**, 3051.

Kaplan, D. B., 1985, Nucl. Phys. **B260**, 215.

Kim, J., S. Youn, J. Jeong, W. Chung, O. Kwon, and Y. K. Semertzidis, 2020, J. Phys. G **47**, 035203.

Kim, J. E., 1979, Phys. Rev. Lett. **43**, 103.

Kim, J. E., 1987, Phys. Rep. **150**, 1.

Kittel, C., 1968, *Introduction to Solid State Physics* (Wiley, New York).

Krauss, L., J. Moody, F. Wilczek, and D. E. Morris, 1985, Phys. Rev. Lett. **55**, 1797.

Krcmar, M., Z. Krecak, A. Ljubicic, M. Stipcevic, and D. Bradley, 2001, Phys. Rev. D **64**, 115016.

Kuzmin, L. S., A. S. Sobolev, C. Gatti, D. Di Gioacchino, N. Crescini, A. Gordeeva, and E. Il'ichev, 2018, IEEE Trans. Appl. Supercond. **28**, 2400505.

Lamoreaux, S., K. van Bibber, K. Lehnert, and G. Carosi, 2013, Phys. Rev. D **88**, 035020.

Lasenby, R., 2020, Phys. Rev. D **102**, 015008.

Lawson, M., A. J. Millar, M. Pancaldi, E. Vitagliano, and F. Wilczek, 2019, Phys. Rev. Lett. **123**, 141802.

Lazarus, D., G. Smith, R. Cameron, A. Melissinos, G. Ruoso, Y. Semertzidis, and F. Nezrick, 1992, Phys. Rev. Lett. **69**, 2333.

Ledbetter, M. P., M. Romalis, and D. F. Jackson-Kimball, 2013, Phys. Rev. Lett. **110**, 040402.

Lee, J., A. Almasi, and M. Romalis, 2018, Phys. Rev. Lett. **120**, 161801.

Lee, J., H. Winarto, M. Smiciklas, and M. V. Romalis, 2018, arXiv:1811.03614.

Lee, S., S. Ahn, J. Choi, B. Ko, and Y. Semertzidis, 2020, Phys. Rev. Lett. **124**, 101802,.

Ling, F.-S., P. Sikivie, and S. Wick, 2004, Phys. Rev. D **70**, 123503.

Liu, S., *et al.* (CDEX Collaboration), 2017, Phys. Rev. D **95**, 052006,.

Ljubicic, A., D. Kekez, Z. Krecak, and T. Ljubicic, 2004, Phys. Lett. B **599**, 143.

Luo, P., J. Ding, J. Wang, and X. Ren, 2017, Phys. Rev. D **96**, 055028.

Maiani, L., R. Petronzio, and E. Zavattini, 1986, Phys. Lett. B **175**, 359.

Majewski, S. R., M. Skrutskie, M. D. Weinberg, and J. C. Ostheimer, 2003, Astrophys. J. **599**, 1082.

Malnou, M., D. Palken, B. Brubaker, L. R. Vale, G. C. Hilton, and K. Lehnert, 2019, Phys. Rev. X **9**, 021023.

Marsh, D. J. E., 2016, Phys. Rep. **643**, 1.

Matsuki, S., and K. Yamamoto, 1991, Phys. Lett. B **263**, 523.

McAllister, B. T., G. Flower, E. N. Ivanov, M. Goryachev, J. Bourhill, and M. E. Tobar, 2017, Phys. Dark Universe **18**, 67.

McAllister, B. T., G. Flower, L. E. Tobar, and M. E. Tobar, 2018, Phys. Rev. Applied **9**, 014028.

McAllister, B. T., S. R. Parker, and M. E. Tobar, 2016, Phys. Rev. D **94**, 042001.

McAllister, B. T., Y. Shen, G. R. Flower, S. R. Parker, and M. E. Tobar, 2017, J. Appl. Phys. **122**, 144501.

Melcón, A. A., *et al.*, 2018, J. Cosmol. Astropart. Phys. 05, 040.

Melissinos, A. C., 2009, Phys. Rev. Lett. **102**, 202001.

Miceli, L., 2015, in *Proceedings of the 11th Patras Workshop on Axions, WIMPs and WISPs, Zaragoza, Spain, 2015*, edited by I. G. Irastorza, J. Redondo, J. M. Carmona, S. Cebrian, and T. Dafni, pp. 164–168, https://inspirehep.net/files/25e7017965f997d8e6f27ad0696f473b.

Millar, A. J., J. Redondo, and F. D. Steffen, 2017, J. Cosmol. Astropart. Phys. 10, 006; 05 (2018) E02.

Moody, J., and F. Wilczek, 1984, Phys. Rev. D **30**, 130.

Morales, A., *et al.* (COSME Collaboration), 2002, Astropart. Phys. **16**, 325.

Moriyama, S., 1995, Phys. Rev. Lett. **75**, 3222,.

Moriyama, S., M. Minowa, T. Namba, Y. Inoue, Y. Takasu, and A. Yamamoto, 1998, Phys. Lett. B **434**, 147.

Morris, D. E., 1984 (unpublished).

Morris, D. E., 1986, Phys. Rev. D **34**, 843.

Muck, M., M.-O. André, J. Clarke, J. Gail, and C. Heiden, 1998, Appl. Phys. Lett. **72**, 2885.

Muck, M., C. Welzel, and J. Clarke, 2003, Appl. Phys. Lett. **82**, 3266.

Mueller, G., P. Sikivie, D. Tanner, and K. van Bibber, 2009, Phys. Rev. D **80**, 072004.

Naculich, S. G., 1988, Nucl. Phys. **B296**, 837.

Natarajan, A., and P. Sikivie, 2005, Phys. Rev. D **72**, 083513.

Newberg, H. J., *et al.* (SDSS Collaboration), 2002, Astrophys. J. **569**, 245.

Ni, W.-T., S.-S. Pan, H.-C. Yeh, L.-S. Hou, and J.-L. Wan, 1999, Phys. Rev. Lett. **82**, 2439.

Nyquist, H., 1928, Phys. Rev. **32**, 110.

Obata, I., T. Fujita, and Y. Michimura, 2018, Phys. Rev. Lett. **121**, 161301.

Ogawa, I., S. Matsuki, and K. Yamamoto, 1996, Phys. Rev. D **53**, 1740.

Ouellet, J. L., *et al.*, 2019a, Phys. Rev. D **99**, 052012.

Ouellet, J. L., *et al.*, 2019b, Phys. Rev. Lett. **122**, 121802,.

Paschos, E., and K. Zioutas, 1994, Phys. Lett. B **323**, 367.

Payez, A., C. Evoli, T. Fischer, M. Giannotti, A. Mirizzi, and A. Ringwald, 2015, J. Cosmol. Astropart. Phys. 02, 006.

Peccei, R., and H. R. Quinn, 1977a, Phys. Rev. D **16**, 1791.

Peccei, R., and H. R. Quinn, 1977b, Phys. Rev. Lett. **38**, 1440.

Pendlebury, J. M., *et al.*, 2015, Phys. Rev. D **92**, 092003.

Petrakou, E. (CAPP/IBS Collaboration), 2017, EPJ Web Conf. **164**, 01012.

Pi, S.-Y., 1984, Phys. Rev. Lett. **52**, 1725.

Preskill, J., M. B. Wise, and F. Wilczek, 1983, Phys. Lett. **120B**, 127.

Pugnat, P., *et al.* (OSQAR Collaboration), 2008, Phys. Rev. D **78**, 092003.

Raffelt, G., and D. Seckel, 1988, Phys. Rev. Lett. **60**, 1793.

Raffelt, G., and L. Stodolsky, 1988, Phys. Rev. D **37**, 1237.

Raffelt, G., and A. Weiss, 1995, Phys. Rev. D **51**, 1495.

Raffelt, G. G., 1986, Phys. Lett. **166B**, 402.

Raffelt, G. G., 1990, Phys. Rep. **198**, 1.

Raffelt, G. G., 2008, Lect. Notes Phys. **741**, 51.

Redondo, J., 2013, J. Cosmol. Astropart. Phys. 12, 008.

Ressell, M., 1991, Phys. Rev. D **44**, 3001.

Ritter, R., L. Winkler, and G. Gillies, 1993, Phys. Rev. Lett. **70**, 701.

Robilliard, C., R. Battesti, M. Fouche, J. Mauchain, A.-M. Sautivet, F. Amiranoff, and C. Rizzo, 2007, Phys. Rev. Lett. **99**, 190403.

Rosenberg, L., and K. van Bibber, 2000, Phys. Rep. **325**, 1.

Ruoso, G., *et al.*, 1992, Z. Phys. C **56**, 505.

Rybka, G., A. Wagner, A. Brill, K. Ramos, R. Percival, and K. Patel, 2015, Phys. Rev. D **91**, 011701.

Sanchez-Conde, M., D. Paneque, E. Bloom, F. Prada, and A. Dominguez, 2009, Phys. Rev. D **79**, 123511.

Santamaria, L., C. Braggio, G. Carugno, V. D. Sarno, P. Maddaloni, and G. Ruoso, 2015, New J. Phys. **17**, 113025.

Semertzidis, Y. K., *et al.*, 2019, arXiv:1910.11591.

Serebrov, A., *et al.*, 2010, JETP Lett. **91**, 6.

Shakeri, S., D. J. Marsh, and S.-S. Xue, 2020, arXiv:2002.06123.

Shifman, M. A., A. Vainshtein, and V. I. Zakharov, 1980, Nucl. Phys. **B166**, 493.

Sikivie, P., 1983, Phys. Rev. Lett. **51**, 1415; **52**, 695(E) (1984).

Sikivie, P., 1984, Phys. Lett. **137B**, 353.

Sikivie, P., 1985, Phys. Rev. D **32**, 2988; **36**, 974(E) (1987).

Sikivie, P., 1986, in *Proceedings of the 17th International Seminar on Theoretical Physics and Cosmology, Peniscola, Spain, 1986*, edited by E. Alvarez, R. D. Dominguez Tenreiro, J. M. Ibanez Cabanell, and M. Quiros, pp. 143–169, https://lib-extopc.kek.jp/preprints/PDF/1987/8704/8704057.pdf.

Sikivie, P., 1988, Phys. Rev. Lett. **61**, 783.

Sikivie, P., 2003, Phys. Lett. B **567**, 1.

Sikivie, P., 2008, Lect. Notes Phys. **741**, 19.

Sikivie, P., 2010, arXiv:1009.0762.

Sikivie, P., 2011, Phys. Lett. B **695**, 22.

Sikivie, P., 2014, Phys. Rev. Lett. **113**, 201301; **125**, 029901(E) (2020).

Sikivie, P., and J. R. Ipser, 1992, Phys. Lett. B **291**, 288.

Sikivie, P., N. Sullivan, and D. Tanner, 2014, Phys. Rev. Lett. **112**, 131301.

Sikivie, P., D. Tanner, and K. van Bibber, 2007, Phys. Rev. Lett. **98**, 172002.

Sikivie, P., D. Tanner, and Y. Wang, 1994, Phys. Rev. D **50**, 4744.

Sikivie, P., I. Tkachev, and Y. Wang, 1995, Phys. Rev. Lett. **75**, 2911.

Sikivie, P., I. Tkachev, and Y. Wang, 1997, Phys. Rev. D **56**, 1863.

Sikivie, P., and Q. Yang, 2009, Phys. Rev. Lett. **103**, 111301.

Silva-Feaver, M., *et al.*, 2017, IEEE Trans. Appl. Supercond. **27**, 1400204.

Srednicki, M., 1985, Nucl. Phys. **B260**, 689.

Stadnik, Y., V. Dzuba, and V. Flambaum, 2018, Phys. Rev. Lett. **120**, 013202.

Stadnik, Y., and V. Flambaum, 2015, Eur. Phys. J. C **75**, 110.

Stern, I., A. Chisholm, J. Hoskins, P. Sikivie, N. Sullivan, D. Tanner, G. Carosi, and K. van Bibber, 2015, Rev. Sci. Instrum. **86**, 123305.

Svrcek, P., and E. Witten, 2006, J. High Energy Phys. 06, 051.

Tada, M., Y. Kishimoto, K. Kominato, M. Shibata, H. Funahashi, K. Yamamoto, A. Masaike, and S. Matsuki, 1999, Nucl. Phys. B, Proc. Suppl. **72**, 164.

Terrano, W., E. Adelberger, J. Lee, and B. Heckel, 2015, Phys. Rev. Lett. **115**, 201801.

Thomson, C. A., B. T. McAllister, M. Goryachev, E. N. Ivanov, and M. E. Tobar, 2019, arXiv:1912.07751.

Treiman, S., and F. Wilczek, 1978, Phys. Lett. **74B**, 381.

Tullney, K., *et al.*, 2013, Phys. Rev. Lett. **111**, 100801.

Turner, M. S., 1986, Phys. Rev. D **33**, 889.

Turner, M. S., 1988, Phys. Rev. Lett. **60**, 1797.

Turner, M. S., 1990, Phys. Rep. **197**, 67.

Vafa, C., and E. Witten, 1984, Phys. Rev. Lett. **53**, 535.

van Bibber, K., and G. Carosi, 2013, in Proceedings of the 8th Patras Workshop on Axions, WIMPs and WISPs, Chicago, 2013 (unpublished) [arXiv:1304.7803].

van Bibber, K., P. McIntyre, D. Morris, and G. Raffelt, 1989, Phys. Rev. D **39**, 2089.

Van Bibber, K., N. Dagdeviren, S. Koonin, A. Kerman, and H. Nelson, 1987, Phys. Rev. Lett. **59**, 759.

Vasilakis, G., J. Brown, T. Kornack, and M. Romalis, 2009, Phys. Rev. Lett. **103**, 261801.

Viaux, N., M. Catelan, P. B. Stetson, G. Raffelt, J. Redondo, A. A. R. Valcarce, and A. Weiss, 2013, Phys. Rev. Lett. **111**, 231301.

Vorobev, P., A. Kakhidze, and I. Kolokolov, 1995, Phys. At. Nucl. **58**, 959.

Wang, Y., *et al.* (CDEX Collaboration), 2020, Phys. Rev. D **101**, 052003,.

Weinberg, S., 1978, Phys. Rev. Lett. **40**, 223.

Wilczek, F., 1978, Phys. Rev. Lett. **40**, 279.

Wuensch, W., S. De Panfilis-Wuensch, Y. Semertzidis, J. Rogers, A. Melissinos, H. Halama, B. Moskowitz, A. Prodell, W. Fowler, and F. Nezrick, 1989, Phys. Rev. D **40**, 3153.

Youdin, A., D. Krause, K. Jagannathan, L. Hunter, and S. Lamoreaux, 1996, Phys. Rev. Lett. **77**, 2170.

Zarei, M., S. Shakeri, M. Abdi, D. J. Marsh, and S. Matarrese, 2019, arXiv:1910.09973.

Zavattini, E., *et al.* (PVLAS Collaboration), 2006, Phys. Rev. Lett. **96**, 110406; **99**, 129901(E) (2007).

Zavattini, E., *et al.* (PVLAS Collaboration), 2008, Phys. Rev. D **77**, 032006.

Zhitnitsky, A., 1980, Sov. J. Nucl. Phys. **31**, 260.

Zhitnitsky, A., and Y. Skovpen, 1979, Sov. J. Nucl. Phys. **29**, 513.

Zhong, L., *et al.* (HAYSTAC Collaboration), 2018, Phys. Rev. D **97**, 092001.

Zioutas, K., *et al.* (CAST Collaboration), 2005, Phys. Rev. Lett. **94**, 121301.